General Disclaimer

One or more of the Following Statements may affect this Document

- This document has been reproduced from the best copy furnished by the organizational source. It is being released in the interest of making available as much information as possible.

- This document may contain data, which exceeds the sheet parameters. It was furnished in this condition by the organizational source and is the best copy available.

- This document may contain tone-on-tone or color graphs, charts and/or pictures, which have been reproduced in black and white.

- This document is paginated as submitted by the original source.

- Portions of this document are not fully legible due to the historical nature of some of the material. However, it is the best reproduction available from the original submission.

CR-152262

RM-684

AN ANALYSIS OF WATER IN GALACTIC INFRARED SOURCES USING THE NASA LEAR AIRBORNE OBSERVATORY

March 1979

(NASA-CR-152262) AN ANALYSIS OF WATER IN GALACTIC INFRARED SOURCES USING THE NASA LEAR AIRBORNE OBSERVATORY Final Report, 2 Jan. 1975 - 31 Mar. 1978 (Grumman Aerospace Corp.) 81 p HC A05/MF A01 CSCL 03A G3/89

N79-21965

Unclas 19589

Grumman Research Department Memorandum RM-684

AN ANALYSIS OF WATER IN GALACTIC INFRARED SOURCES USING THE NASA LEAR AIRBORNE OBSERVATORY

by

Lewis L. Smith
Principal Investigator

and

Theodore Hilgeman
Co-Investigator

Supported by NASA Contract
NAS 2-8664. Period of investigation
is from 2 January 1975 to 31 March 1978

Prepared for

NASA-Ames Research Center

March 1979

Richard Scheuing
Director of Research

ABSTRACT

This is the final report for NASA Contract NAS 2-8664, "An Analysis of Water in Galactic Infrared Sources Using the NASA Lear Airborne Observatory."

We have completed a very successful program using the Grumman interferometer system on the NASA Lear Jet Airborne Observatory. Following a description of the instrumentation and data reduction procedures, a review is presented of the objects observed (standard stars, M stars, a nebula, planets, and the moon). The observing parameters are listed for each flight date. The spectra obtained from these data flights are presented, grouped by class of object. A brief discussion is presented of how these spectra can be utilized.

A number of presentations and publications have already resulted from this contract and are listed in this report.

CONTENTS

ILLUSTRATIONS

INTRODUCTION

This is the final report for NASA Contract NAS 2-8664, "Analysis of Water in Galactic Infrared Sources Using the NASA Lear Airborne Observatory," from 2 January 1975 to 31 March 1978. We describe the instrumentation used, the observational data obtained, and our analyses to date as well as the potential for future work.

Observational data were obtained on every scheduled flight, and met or exceeded the contract requirements. In addition, an order of magnitude better signal-to-noise ratio (S/N), was obtained than originally anticipated allowing the full resolution capability of the system to be realized. We report here in detail on those spectra with high S/N with all other spectra being available on request in a tape format. We have analyzed some of the surprisingly large quantity of excellent data, presented this material orally at meetings in the scientific community and published the detailed results in the open literature. (See Publications and Presentations section.)

The objects observed are standard stars, M stars, a nebula, planets, and the moon. The M stars have large amounts of water in their atmosphere and can provide information about the evolution of water in the galaxy. The emission lines in the nebula (M 42 in Orion) are useful in determining the reddening and dust properties in the ionized region. The planetary observations reveal information on the physical properties of the atmosphere and surface, and the lunar observations observed through the earth's atmosphere provide information on the chemical composition of the stratosphere. The standard stars provide calibration checks on the above objects.

INSTRUMENTATION

In the field of infrared astronomy the quality of the instrumentation used has always been a strong factor in determining the success of an experiment. This requirement is especially strong for airborne infrared astronomy. We report here on a general description of the Grumman Michelson interferometer instrumentation, and in particular, the design of the optics, and the use of advanced data reduction procedures.

General Instrumentation

The Michelson interferometer remains the ideal instrument to be used for the observation of water vapor in M stars and the interstellar medium. Its large throughput (no slits) and multiplexing ability (all wavelengths measured simultaneously) allows maximum efficiency when observing faint objects (K mag 0) at good wavelength resolution (2 cm^{-1}) over a large bandpass (1.5-3.5 μm). An entire spectrum is obtained in one 2-second scan with the S/N

improved by means of co-adding hundreds of scans. Guiding problems are thereby reduced over those required by a scanning spectrometer.

The Lear Airborne Observatory, flying at 13.7 km (above the tropopause), reduces the overhead precipitable water vapor to less than 10 μm compared to several mm over a ground based observatory. The availability of frequent observing flights with the Lear Jet allows us to observe how the properties of the M stars vary with phase.

The configuration we use consists of a NASA heliostat and a vibration-isolated 30-cm, f/23 telescope hard-mounted to the interferometer assembly. Figure 1 shows a photograph of the system mounted in the NASA Lear Jet. On the left is the heliostat mirror which compensates for the airplane motions. The starlight comes in through the infrared transmitting cabin window (not shown) and is reflected off the heliostat into the telescope shown in the center and extending to the right. Further to the right and lower in the picture is the mounting platform containing foreoptics, dewars, and the interferometer. Figure 2 shows this same optical system schematically with more detail on the light path through the foreoptics and interferometer. The foreoptics is of a symmetric, dual beam type; only one side of the light path is shown traced to the detectors. The telescope is a folded Dall-Kirkham type designed by us to give a field of observation of 6.3 arc-minutes. This wide field is a necessary requirement to observe the extended object in our program, M42 (the Orion Nebula). The Grumman interferometer system operates in a double beam, double detector configuration to give automatic cancellation of the emitted light due to the sky, telescope, and interferometer. The detectors are nitrogen-cooled 1/2 mm InSb cells with cold filter limited response out to 3.5 μm, where the GE 105 window effectively stops transmitting. The interferometer is set to run at any resolution down to 2 cm^{-1}, which is the maximum possible with an f/23 beam. The telescope interferometer system floats on a foam pad resting on a plate bolted to the baggage compartment floor. The system has been developed to the point where both mechanical and electrical interference from the aircraft have been overcome.

Our guiding telescope was initially capable of locating objects as faint as V = 10. This guider has been upgraded by the addition of an image intensifier. The visual magnitude limit, since we are looking through the main telescope, is now V = 12, which was sufficient for all our observations except for a few of the M stars at minimum phase. For all these observations offset guiding was used.

Data from the interferometer were recorded on a instrumentation grade analog tape recorder and digitized on the ground after every flight. The digitization and co-adding was done on the Grumman Research Department's Portable Data Acquisition System which also allowed data to be sent by phone link back to the Department's 16K word computer. A

complete full resolution spectrum was computed and sent back to us at Ames for initial evaluation. We were then able to use this information in planning the observations for the next flight. For example, the interferometer mirror travel (which determines spectral resolution), and total observing time (which determines S/N) occasionally had to be changed based on previous flight data. One of the strong limitations of IR interferometry in the past has been the inability to look at the spectrum in "real time." Usually, the astronomer only sees a spectrum after he has left the observatory and finished his series of measurements. Our data system and the necessary computer programs are developed and have been used successfully for our four flight series.

Optical Design

An important source of progress in our optics laboratory has been use of a computer optical design capability, allowing us to design foreoptics to mate the interferometer to various telescopes in a way that is optimum for the type of object to be observed. Figure 3 shows a typical output from this program in which it was desired to fit the interferometer to an f/23 telescope with a 6.3 arc-minute field of view. In this case, available room was also tightly constrained so that the beam had to be folded several times. Figure 4 shows a picture of this foreoptics system in our laboratory in preparation for testing with our interferometer and detectors. In this system, which is the one eventually used in the Lear, we have also included remotely adjustable alignment mirrors and focal plane guiding optics for ease of operation in an aircraft. We have used this system to make low resolution observations from the ground at our own laboratory, using a 30 cm highly folded telescope we designed and built at Grumman. Figure 5 shows an example of our results on a humid night. In addition to the atmospheric absorption by CO_2, one can see the very strong water absorption features which confuse groundbased astronomical observations of water.

Data Reduction Procedures

After every flight the tape recorder was taken from the plane to the computing facility brought to the Ames Research Center. The tapes were first played through, and all verbal comments were transcribed along with a relative time code which was recorded on the tape prior to each flight. This code allows reliable repeat access to any region of the data and was found to be much more accurate than the conventional tape recorder foot counter.

The tape recorder data channel was connected to a Hewlett Packard (HP) 5465A A/D converter and the white light (start) and HeNe laser (sampling) channels were connected to a GAC-designed interface electronics unit which generates synchronized pulses and sends them to the A/D unit. Synchronization with the desired data is thus assured independent of any tape recorder or interfeometer speed fluctuations.

A Texas Instrument Silent 700 Terminal with dual cassette reader was connected directly to the HP 21MX computer (a minicomputer) and the 21MX programs BABL8 and LEWDAL were loaded into the computer. These programs (stored on tape cassettes) were previously generated by the Grumman Research Department and allow the HP 21MX to interact with the larger time-sharing HP3000 computer located in the Research Department Computing Center in Bethpage, New York. From discussions with HP, this represents the first successful attempt of a direct link between an HP3000 and an HP 21MX.

A junction switch provides a TI terminal-HP3000 or HP 21MX-HP3000 connection through the phone lines. This transcontinental computer linkup has worked successfully and allows each night's data to be examined the next day. In the Jan/Feb 1976 series of flights, after the first 5 flights had demonstrated the good quality of the data we were obtaining, we decided to increase the spectral resolution from 100 to 13.3 cm^{-1}. Without the ability to see the finished spectra, we would have been more conservative in changing our resolution.

A BASIC A/D program, which determines the number of interferogram scans to be co-added and the number of points to be digitized in each scan, is transmitted from the HP3000 in Bethpage to the HP 21MX at Ames. The data tape is started at the desired scan and the digitization proceeds. Scans with the star in one aperture are co-added and the result subtracted from the co-added scans with the star in the other aperture. In this way the residual background from the sky, airplane, telescope, and interferometer is considerably reduced. The individual scans are visually monitored on an oscilloscope and any that are considered irregular can be knocked out of the co-adding process through a switch on the HP 21MX. After co-adding, the resultant digital interferogram is displayed on the HP 5460A display unit. If the interferogram has sufficient S/N it is transmitted in a packed format over the phone lines to the HP3000. The transmission takes about 4 minutes for 7100 points at 1200 BAUD. If for any reason a "glitch" develops in the transmission due to noise on the long distance lines, the data can be retrieved by the computer and retransmitted without having to redigitize the data.

All operations on the data are now done by the HP 3000 through the TI terminal. The data in the HP 3000 is unpacked (symbols converted to digital numbers) and the region near the interferogram white light point is transmitted back and plotted on the terminal at Ames. To maximize observational efficiency, the interferogram is generated single-sided, i.e., the white light point is to one side of the data. This increases the S/N by $\sqrt{2}$ for a given observing time, but the interferogram needs to be phase corrected before the Fourier

transform can be taken. The phase correction technique used is that of Forman et al (1966) and the correction program PHASE is listed in the Appendix.

This program symmetrizes the interferogram about the white light point; hence, a cosine transform can be done on the data. A fast cosine transform program HFFT (see Appendix) using the Cooley-Tukey method has been developed at GAC which is extremely efficient in computer core storage, i.e., the transform of 8192 points only needs 8200 storage locations. This program also smooths the spectrum with a Hamming function (Blackman and Tukey, 1958) and interpolates for four points between each pair of output points for ease in line identification. To our knowledge, no fast cosine transform program has previously been published which is even within a factor of two of the storage efficiency of this program.

The spectral resolution is given by

$$\Delta\nu = 1.815 * \left(\frac{7901.14}{N}\right) \text{ cm}^{-1}$$

where N is the number of data points from the white light point, 7901.14 cm^{-1} is the Nyquist frequency when the He-Ne laser line at 0.63282 μm is used as the interferogram digitizing clock (7901.14 cm^{-1} = 1/ [2 x .63282 x 10^{-4} cm]) and 1.815 is the ratio of the full-width at half maximum (FWHM) of the Hamming function to the frequency separation of the output spectral points (7901.14/N). This frequency separation also equals the first zero of the sinc function (sin(x)/x) which is the inherent apodization of the spectrum with no smoothing. The familiar "ringing" phenomenon is suppressed by convolving the spectrum with the Hamming function (Bell, 1972).

Selected regions of the complete spectrum, i.e., CO_2 bands at 3700 cm^{-1}, are transmitted back to the TI terminal and plotted, and the S/N can be examined to see if it is sufficient. Since all the reduction procedures just described can be done after each flight, necessary changes to the equipment or experimental procedures can be made for subsequent flights. This real time look at the finished spectra has proven invaluable to the success of our program. Upon completion of the flight series and return home, all spectra are plotted on a Tektronix 4014 Graphics terminal and a hard copy is made.

OBSERVATIONS

An observational data summary is presented in Tables 1A and 1B for the 36 flights conducted in 1976 and 1977. Column 1 is the flight number, 2 is the flight date in U.T., 3 lists the objects observed, 4, 5 and 6 are the interferometer settings (relative), 7 is the data filter in Hz, 8 is the amplifier gain in db with the first value referring to the first object, etc., 9 identifies spectra shown in the report, and 10 lists particular comments

explained at the bottom of Table 1B. All observations used a 6.3 arc-min aperture except for observations of the moon after Flight 17.

The primary goal of our program is its scientific return. The spectra shown are the first step in obtaining this return, and are in compliance with the requirements of the contract work statement. A brief discussion of some of the results follows. A list of spectra is given in Table 2 arranged by class of object-standard (non-variable) stars, M stars, nebula, planets, and stratospheric observations. Column 1 is the object observed, 2 is the flight number, 3 is the date in U.T., 4 is the number of scans, 5 is the spectral resolution in cm^{-1} using Hamming apodization, 6 is the file name used for identification purposes by the computer, and 7 is the figure number in this report.

For observations of the moon (diameter ~ 30 arc-minutes), two separate apertures (labeled L and R) were used and these are so labeled in Table 2 and in the figure.

The wavenumber range shown in all spectra is 2800-6000 cm^{-1} with the limits being determined by the optical filter in front of the InSb detectors.

The captions on all figures identify the object, the date of observation (U.T.), and the resolution in cm^{-1} defined as the full-width at half maximum of the Hamming apodization function. For some of the spectra the resolution has been degraded from the maximum measured values to improve the S/N value.

Per the work statement, these spectra are shown in relative units uncorrected for frequency shift, instrument response, and residual telluric absorption. As such their primary ability is for spectroscopic identification of molecular features. However, we have reduced a number of selected spectra further for purposes of publication. An example of the technique used to reduce these spectra to absolute fluxes in Janskys ($1\ J_y = 10^{-26} W/m^2/Hz$) and true (laboratory) frequencies is discussed later in this report along with several samples of spectra so corrected.

DISCUSSION OF SPECTRA

The results of the observations presented in the previous section are now discussed according to class of object-standard stars, M stars, nebula, planets, and stratospheric observations. A brief discussion is given on important features seen in the spectra and on their significance. This is followed by examples of reduction to absolute flux.

Standard Stars

The standard (non-variable) stellar spectra are shown in Figures 6 - 23 for α Ori, α Tau, α Boo, μ Cep, α Lyr and α CMa. The only stellar features easily seen are the first

TABLE 1A 1976 OBSERVATIONAL DATA

Relative Interferometer Settings

(1) No.	(2) Date (UT)	(3) Object	(4) Sweep Length	(5) Velocity	(6) Offset	(7) Data Filter (Hz)	(8) Ampl Gain (db)	(9) Spectra	(10) Comments
1	27 Jan	Moon, Venus	0.010	100 slow	846.5	50-160	15,40		A
2	28 Jan	α C Ma, α Ori	0.010	100 s	846.5	50-160	35,35		A
3	29 Jan	RX Boo, α Tau	0.010	100 s	846.5	50-160	30,30		
4	30 Jan	μCep	0.010	100 s	846.5	50-160	30		
5	3 Feb	αC Ma, αOri	0.010	100 s	832	50-160	30,25		
6	5 Feb	αOri	0.040	195 fast	750	100-315	35	α Ori	
7	6 Feb	RX Boo, αC Ma, α Tau	0.040	195 f	750	100-315	45,45,40	RX Boo, α Tau	
8	10 Feb	α C Ma, Moon	0.040	195 f	750	100-315	45,10	Moon	
9	11 Feb	Mars, Moon	0.040	195 f	750	100-315	50,10	Mars, Moon	
10	12 Feb	Jupiter, Mira	0.040	195 f	750	100-315	40,40	Mira	
11	24 Aug	α Boo	0.020	128.5 f	426	40-160	35		A
12	25 Aug	α Boo, RX Boo	0.270	370 f	120	250-1000	35,35		
13	26 Aug	α Boo, RX Boo	0.270	370 f	120	250-1000	40,40		
14	27 Aug	α Boo, RX Boo	0.270	370 f	120	250-1000	45,45	α Boo, RX Boo	
15	31 Aug	α Lyr, M42	0.020	128.5 f	426	40-160	45,45		
16	1 Sept	U Ori, α Ori	0.270	370 f	120	250-1000	55,45	α Ori	
17	3 Sept	Moon	0.270	370 f	120	250-1000	15,45	Moon	
18	8 Sept	α Lyr, M42	0.047	185 f	391	80-315	45,45		B
19	9 Sept	α Lyr, M42	0.055	185 f	384	80-315	45,45	α Lyr, M42	B
20	10 Sept	α Boo, Moon	0.270	370 f	123	250-1000	45,25	Moon	B,C

TABLE 1B 1977 OBSERVATIONAL DATA (Cont)

Relative Interferometer Settings

(1) No.	(2) Date (UT)	(3) Object	(4) Sweep Length	(5) Velocity	(6) Offset	(7) Data Filter (Hz)	(8) Ampl Gain (db)	(9) Spectra	(10) Comments
21	8 Feb	α CMa, α Ori	055	185 f	384	80-315	50,40	α CMa, α Ori	
22	9 Feb	α CMa,	055	185 f	384	80-315	45	α CMa	
		Moon	270	370 f	123	250-1000	20	Moon	C
23	10 Feb	μ Cep, Mira	055	185 f	384	80-315	45,40	μ Cep, Mira	
24	11 Feb	α CMa	055	185 f	384	80-315	45	α CMa	
25	17 Feb	RLeo, Venus	055	185 f	384	80-315	45,30	RLeo, Venus	
26	18 Feb	RLeo	055	185 f	384	80-315	45	RLeo	
27	12 Oct	UOri, α Ori	055	185 f	384	80-315	40,35	α Ori	D
28	13 Oct	UOri, α Ori	055	185 f	384	80-315	50,40	α Ori	D
29	14 Oct	UHer, Mira	055	185 f	384	80-315	45,45	Mira	D
30	18 Oct	RLeo	020	228.5 f	429.5	100-315	40	RLeo	D
		μ Cep	055	185 f	384	125-315	40	μ Cep	D
31	19 Oct	UHer	020	228.5 f	429.5	100-315	50	UHer	D
32	20 Oct	Moon	270	370 f	123	250-1000	30	Moon	C, D
		RAql	020	228.5 f	429.5	100-315	40	R Aql	D
33	21 Oct	UHer	020	228.5 f	429.5	100-315	45		D
		Mira	055	185 f	384	125-315	45		D
34	26 Oct	α Ori	020	228.5 f	429.5	100-315	45	α Ori	D
35	27 Oct	α Ori, M 42	020	228.5 f	430	80-250	40,45	α Ori, M42	D
36	28 Oct	Mars	055	185 f	385	125-315	50	Mars	D
		α CMa	020	228.5 f	430	80-250	45	α CMa	D

Comments:

A. Dewar D 11 (rear) only

B. Blocking filter with long wavelength cutoff of 3.15 μm used. All other flights used filter with cutoff of 3.55 μm.

C. One arc-minute limiting aperture placed in front of Dewar D 10 (front) for moon observation to increase spectral Resolution. Dewar D 11 (rear) was disconnected.

D. Observations were conducted using a quartz window (S/N 016) which contained water of hydration bands.

TABLE 2 LIST OF SPECTRA - STANDARD STARS

(1) Object	(2) Flt	(3) Date (UT)	(4) No. Scans	(5) Resol. (cm^{-1})	(6) File Name	(7) Fig. No.
α Ori	6	5 Feb 1976	64	13.3	AORI6SP	6a, b
α Ori	16	1 Sep 1976	170	1.8	AORI16SP	7a, b, c, d
α Ori	16	1 Sep 1976	100	2.1	AORI16S1	8a, b, c, d
α Ori	21	8 Feb 1977	250	9.9	AORI21SP	9a, b
α Ori	27	12 Oct 1977	200	9.9	AORI27S1	10a, b
α Ori	28	13 Oct 1977	140	9.9	AORI28SP	11a, b
α Ori	34	26 Oct 1977	100	37.7	AORI34SP	12
α Ori	35	27 Oct 1977	150	37.7	AORI35SP	13
α Tau	7	6 Feb 1976	140	13.3	ATAU7SP	14a, b
α Boo	14	27 Aug 1976	170	1.8	ABOO14S1	15a, b, c, d
α Boo	14	27 Aug 1976	100	2.1	ABOO14SP	16a, b, c, d
μ Cep	23	10 Feb 1977	200	29.9	MCEP23S2	17
μ Cep	30	18 Oct 1977	100	29.9	MCEP30SP	18
α Lyr	19	9 Sep 1976	500	56.0	ALY19BSP	19
α CMa	21	8 Feb 1977	180	29.9	ACM21S1	20
α CMa	22	9 Feb 1977	200	29.9	ACM22S2	21
α CMa	24	11 Feb 1977	120	29.9	ACM24S1	22
α CMa	36	18 Oct 1977	400	37.7	ACM36SP	23
			M STARS			
RX Boo	7	6 Feb 1976	160	29.9	RBOO7SP	24
RX Boo	14	27 Aug 1976	200	29.9	RBOO14S2	25
Mira	10	12 Feb 1976	290	13.3	MIRA10SP	26a, b
Mira	23	10 Feb 1977	300	9.9	MIRA33SP	27a, b
Mira	23	10 Feb 1977	150	13.3	MIRA23S1	28a, b
Mira	29	14 Oct 1977	100	29.9	MIRA29SP	29
R Leo	25	17 Feb 1977	100	9.9	RLEO25SP	30a, b
R Leo	26	18 Feb 1977	380	9.9	RLEO26S1	31a, b
R Leo	26	18 Feb 1977	200	9.9	RLEO26S2	32a, b
R Leo	26	18 Feb 1977	300	13.3	RLEO26S3	33a, b

TABLE 2 (Cont)

(1) Object	(2) Flt	(3) Date (UT)	(4) No. Scans	(5) Resol (cm^{-1})	(6) File Name	(7) Fig. No.
			M STARS (Cont)			
R Leo	30	18 Oct 1977	350	37.7	RLEO30SP	34
U Her	31	19 Oct 1977	150	37.5	UHER31S1	35
R Aql	32	20 Oct 1977	350	37.3	RAQL32SP	36
			NEBULA			
M 42	19	9 Sep 1976	500	56.0	M4219ASP	37
M 42	19	9 Sep 1976	500	56.0	M4219AB	38
M 42	35	27 Oct 1977	300	56.0	M4235S1	39
			PLANETS			
Venus	25	17 Feb 1977	250	9.9	VEN25SP	40a, b
Mars	9	11 Feb 1976	288	13.3	MARS9SP	41a, b
Mars	36	28 Oct 1977	100	29.9	MARS36S1	42
			STRATOSPHERIC OBSERVATIONS			
Moon (L)	8	10 Feb 1976	30	13.3	MOON8LSP	43a, b
Moon (R)	8	10 Feb 1976	15	13.3	MOON8RSP	44a, b
Moon (L)	9	11 Feb 1976	15	13.3	MOON9LSP	45a, b
Moon (R)	9	11 Feb 1976	15	13.3	MOON9RSP	46a, b
Moon (L)	17	3 Sep 1976	40	1.8	MOON17L	47a, c, e, g
Moon (R)	17	3 Sep 1976	50	1.8	MOON17R	47b, d, f, h
Moon (L)	20	10 Sep 1976	15	2.1	MOON20L1	48a, c, e, g
Moon (R)	20	10 Sep 1976	15	2.1	MOON20R1	48b, d, f, h
Moon (L)	22	9 Feb 1977	18	2.1	MOON22L1	49a, c, e, g
Moon (R)	22	9 Feb 1977	26	2.1	MOON22R1	49b, d, f, h
Moon (R)	32	20 Oct 1977	100	1.8	MOON32R	50a, b, c, d

overtone bands of $^{12}C^{16}0$ and $^{13}C^{16}0$ (4000-4360 cm^{-1}) for the four late type stars. Other stellar features are much weaker. The spike in the α Lyr spectrum (Fig. 19) at 3250 cm^{-1} is a result of uncancelled background. The α CMa spectra (Fig. 20-23) are noisy but provide a check on our calibration techniques.

M Stars

The M (variable) stars are shown in Figures 24-36 for RX Boo, Mira, R Leo, U Her and R Aql. Strong, broad steam bands centered at 3700 and 5300 cm^{-1}, as well as the first overtone bands of $^{12}C^{16}0$ and $^{13}C^{16}0$ (4000-4360 cm^{-1}) are seen in all stars.

Using the best available stellar model atmospheres and a line parameter atlas of high temperature steam, information about the temperature, water abundance, and surface gravity of the stars can be extracted.

Nebula

The bright nebula M42 in Orion is shown in relative units in Figures 37 and 39 and in Janskys in Fig. 38. The absolute curve for M42 was obtained by dividing the relative M42 curve (Fig. 37) by α Lyr taken the same night and at the same air mass (Fig. 19) and then multiplying by the known flux of α Lyr. The K magnitude at 4545 cm^{-1} (2.2 μm) is +1.7 with a 6.3 arc-min FOV centered on θ_1 Ori. The M42 data of Flt. 35 (Fig. 39) is noisy and was not reduced to absolute units as no suitable calibration object was observed during that flight series (Oct. 1977). The strong hydrogen emission lines of Paschen α (5333 cm^{-1}), Brackett β (3809 cm^{-1}) and possibly Brackett γ (4618 cm^{-1}) are seen and identified in the figures.

Planets

The two planets Venus and Mars are shown in Figures 40-42. Strong CO_2 bands at 4850, 4980, and 5110 cm^{-1} and the wing of the very strong band at 3750 cm^{-1} is seen on both planets, with Venus showing additional bands at 4600 and 5300 cm^{-1}.

Modeling of the Martian atmosphere permits the extraction of Martian soil reflectance in the CO_2 bands centered at 3657 cm^{-1}. We have concluded that the Martian soil surface near-infrared optical properties are consistent with a soil composition similar to montmorillonite or limonite, mixed with a basalt Egan et al, 1978). Also, it was found that the non-dust storm aerosol conditions existing in the Martian atmosphere can influence CO_2 line shapes and, hence, the average transmission. Thus, planetary spectroscopic studies dealing with phenomena such as radiation transport, atmospheric circulation, weather, and composition should take aerosol effects into account (Egan et al, 1977).

Stratospheric Observations

The physical properties of the stratosphere can be probed using the Moon as a source as was done for six flights (Fig. 43-50) over the two-year period 1976-1977. Methane (3018 cm^{-1}), CO_2 (3500-3800 cm^{-1}), H_2O (3750-4000 cm^{-1}) and other molecules can be identified from the spectra. The total column density of methane was found to be 5.8×10^{18} molecules/cm^2 above 14 km on 20 October 1977 (Smith and Hilgeman, 1978). This is equivalent to a mean mixing ratio of 1.9 ppmv, a value about 30% higher than other investigators have found for for the daytime stratosphere. Figures 43-47 were obtained with a beam size of 6.3 arc-min which has a limiting resolution of 10 cm^{-1}. The resolution shown on Fig. 47 (R=1.8 cm^{-1}) is not the actual resolution but what would be obtained if the beam size were reduced. Figures 48-50 were measured with a beam of 1 arc-min which corresponds to a limiting resolution of 2 cm^{-1}. A blocking filter with long wavelength cutoff of 3.15 μm (3170 cm^{-1}) was used on Flt. 20 (Fig. 48) preventing the strong CH_4 bands centered at 3018 cm^{-1} from appearing. This cutoff filter was used for the M42 data of Flt. 19 (Figs. 37 and 38) and could not be replaced in time for Flt. 20.

Examples of Reduction to Absolute Flux

A discussion will now be given for converting the above spectra which are shown in relative units to absolute flux in Janskys (1 Jy=10^{-26} $W/m^2/Hz$) and true (laboratory) frequencies. The frequency can be corrected for by measuring lines of known frequency in the observed spectra, i.e. telluric H_2O and CH_4 and plotting [ν (true) - ν (meas)] vs ν (meas).

This is done for the α Ori spectrum of Flt. 21 (Fig. 9) and the Moon spectrum of Flt. 22 (File M00N22L1, Fig. 49) both at a resolution of 9.9 cm^{-1}. The results are shown in Fig. 51 where it is seen that the change between ν (true) and ν (meas) is about one-half of a resolution element (5 cm^{-1}). The least square best fits from Fig. 51 are now applied to the spectra of α Ori and the Moon to correct the frequencies.

The spectrum of α Ori can now be divided by that of the Moon where the lunar spectrum is assumed to have both a thermal component (303°K) and a reflected component (6000°K, albedo .01). The absolute flux of α Ori is normalized to 2.59×10^4 Jy at 4545 cm^{-1} (K mag = -4.0) and is shown in Fig. 52. The strong depression of the continuum from 4000-4400 cm^{-1} is caused by the first overtone brand of CO. Ideally, both the response of the telescope-interferometer system as well as the effect of the telluric absorption lines should divide out. Inspection of Fig. 52 shows residual CO_2 bands in the region 4800-5200 cm^{-1}, as well as strong absorption in the 3550-3800 cm^{-1} region which has been blocked out. The noise in the spectrum from 5200-5800 cm^{-1} is produced by the small value of the flux of both α Ori and the Moon in this region.

Figure 53 shows the results of a similar reduction for α Tau observed on 6 Feb 1976 (Flt 7) with spectral resolution 13.3 cm^{-1}. The region of the hot CO bands is shown with resolution 7.3 cm^{-1} (sinc apodization). Line identification is facilitated with sinc apodization, though the line shapes are distorted. The first overtone bands of $^{12}C^{16}O$ and $^{13}C^{16}O$ are shown.

Mars is shown in absolute units in Fig. 54 for 11 Feb 1976 (Flt 9) with resolution 13.3 cm^{-1}. The CO_2 bands at 4800-5100 cm^{-1}, H_2O bands at 3800-4000 cm^{-1} and water of hydration bands 2900-3750 cm^{-1} are shown. A line by line atmospheric modeling program has provided an analysis of these bands (Egan, et al, 1977, 1978). This modeling is necessary as the vibration-rotation lines of CO_2 are saturated in both the telluric and Martian spectra, and therefore add in a nonlinear way.

Figure 55 is a spectrum of Mira (o Cet) for 12 Feb 1976 (Flt. 10) with resolution 13.3 cm^{-1} (solid lines). A theoretical model by Auman (1969) (dashed curve) with Te = $2000^{o}K$, log g = -2 has been fit to the observed data and shows good agreement with the hot steam bands centered at 3700 and 5300 cm^{-1}, but has too much flux in the region 3900-4500 cm^{-1}. This is to be expected as no CO band absorption was included in the model.

SUMMARY

During the period reported on, we built our optical system, developed a new and unique computer capability, and successfully took data on every flight scheduled. The data taken represent a scientific return an order of magnitude better than anticipated and should provide a fertile source for theoretical analysis for years to come.

The excellent performance of the optical system served to validate our computer-aided optical design capability and demonstrated the predicted wavelength resolution limit of 2.1 cm^{-1}. In addition, the image quality for visual acquisition and guidance has been sufficient to enable us to observe stars down to V = 12 magnitude, an important consideration for some of the very red stars we have measured.

Our new computer capability has proven its worth by allowing us to make flight program decisions between each flight. The flexibility of its design became apparent when we had to reconfigure it to handle an order of magnitude greater data load than we had originally anticipated.

Another important measure of performance is reliability, and this is especially true for limited observing time programs. We were ready to take data for each scheduled flight, thus avoiding any wasted flight time. Our data improved with each flight in a series (see Table 1) as we became aware of the potential of our equipment and kept "pushing" it

further. Surprisingly little modification to our basic design was needed to achieve the order of magnitude improvement we eventually obtained.

We have presented some of the better spectra obtained, illustrating spectra of standard stars, M stars, a nebula, planets and the moon. The spectra show an unprecedented capability to view at good spectral resolution through the hitherto opaque (near-IR) water bands. Water has been seen in the M stars, and in the surface of Mars. The full significance of these observations will take time to develop, but we have clearly demonstrated the capability to acquire data never seen before.

ACKNOWLEDGEMENTS

We would like to thank the following NASA personnel whose advice, encouragement, and generous help greatly contributed to the success of this program; Dr. Nancy Boggess, Chairperson, Management Operations Working Group for Airborne Astronomy, NASA Headquarters; Robert Cameron, Chief, Medium Altitude Mission Branch, Ames Research Center; Robert Mason, Lear Jet Program Manager, Ames Research Center; and Charles Duller, Lear Jet Assistant Mission Manager, Ames Research Center.

The following Grumman personnel provided the necessary support and gave generously of their time; J. Augustine, W. Egan, J. Krassner, and R. Reed. Helpful discussions on several aspects of this work were held with M. D'Agostino.

REFERENCES

Auman, J.R. Jr., "Model Atmospheres of Late Type Stars," Astroph. J. 157, 799, 1969.

Bell, R.J., Introductory Fourier Transform Spectroscopy, Academic Press, New York, 1972.

Blackman, R.B., and Tukey, J.W., The Measurement of Power Spectra, Dover Publication, Inc., New York, 1958.

Egan, W., Fischbein, W., Hilgeman, T., and Smith, L., "High Resolution Martian Atmosphere Modeling Between 2800 and 5600 cm^{-1}," presented at Ninth Annual Meeting of the Division of Planetary Sciences of the American Astronomical Society, Boston, October 27-30, 1977,; published in Bulletin of American Astronomical Society, Vol. 9, No. 4, Part 1, p. 514, 1977.

Egan, W.G., Hilgeman, T. and Smith, L.L., "Comparison between Infrared Martian Disk Spectra and Optical Properties of Terrestrial Analogs," Icarus, Vol. 35, pp. 209-226, 1978.

Forman, M.L., Steel, W.H., and Vanasse, G.A., "Correction of Asymmetric Interferograms Obtained in Fourier Spectroscopy," J. Opt. Soc. Amer. 56, 59, 1966.

Smith, L.L. and Hilgeman, T., "Nightime Observations of Stratospheric Methane", presented at the Topical Meeting on Atmospheric Spectroscopy, Opt Soc of Amer, Keystone, Colorado, 30 Aug-Sept 1, 1978.

PUBLICATIONS AND PRESENTATIONS

1. Egan, W., Fischbein, W., Hilgeman, T., and Smith, L., "Martian Atmosphere Modeling Between 0.4 and 3.5 Micron: Comparison of Theory and Experiment," Proceedings, Symposium on Planetary Atmospheres, Ottawa, Canada, 16-19 August 1977.

2. Egan, W., Fischbein, W., Hilgeman, T., and Smith, L., "High Resolution Martian Atmosphere Modeling Between 2800 and 5600 cm^{-1}," presented at Ninth Annual Meeting of the Division of Planetary Sciences of the American Astronomical Society, Boston, October 27-30, 1977,; published in Bulletin of American Astronomical Society, Vol. 9, No. 4, Part 1, p. 514, 1977.

3. Egan, W.G., Hilgeman, T. and Smith, L.L., Comparison between Infrared Martian Disk Spectra and Optical Properties of Terrestrial Analogs", Icarus, Vol. 35, pp. 209-226, 1978.

4. Hilgeman, T. and Smith, L., "Infrared Interferometry of Astronomical Objects Using Airborne 12-Inch Telescope on Lear Jet," Grumman Research Department Report RE-531, November 1976.

5. Krassner, J., "Limits to Kuiper Airborne Observatory Near Infrared Sensitivity", Grumman Aerospace Corporation, Research Memorandum RM-672, November 1978.

6. Smith, L., "Mira-Type Variables Observed in the Infrared at an Altitude of 13.7 km," Paper presented at 65th Meeting of the American Association of Variable Star Observers, Smith College, Northampton, Mass., 15-17 October 1976.

7. Smith, L., "Infrared Spectra (2900-5600 cm^{-1}) of Stars and Planets," News Letter of the Astronomical Society of New York, Vol. 1, p. 20, 1976.

8. Smith, L. and Hilgeman, T., "Infrared Spectra (2900-5600 cm^{-1}) of Late Type Stars," Bull. of Amer. Astron. Soc., Vol. 8, p. 428, 1976.

9. Smith, L., "The Use of the Maximum Entropy Transformation in the Analyses of IR Astronomical Spectral," Paper presented at the Soc. of Photographic Scient. and Engin., International Conf. on Image Analysis and Evaluation, Toronto, Ontario, 19-23 July 1976.

10. Smith, L. and Hilgeman, T., "Airborne Infrared Spectra (2900-5600 cm^{-1}) of Stars and Planets," Symposium on Recent Results in Infrared Astrophysics, NASA TM X-73, 190, Ames Research Center, Moffett Field, California, January, 1977.

11. Smith, L., Hilgeman, T. and Egan, W., "Mass Loss of Water Vapor From M Stars," Bull. of Amer. Astron. Soc., Vol. 9, p. 346, 1977.

12. Smith, L. and Hilgeman, T. "Astronomical IR Interferometry at a Remote Site," paper presented at 1977 International Conference on Fourier Transform Infrared Spectroscopy, University of South Carolina, Columbia, S.C., 20-24 June 1977.

13. Smith, L. L., "Comparison of Measured Hot Steam with AFGL Line Parameter Atlas", presented at the Annual Review Conference on Atmospheric Transmission Models", AFGL, Hanscom Field, Mass., 17-18 May, 1978.

14. Smith, L. L. and Hilgeman, T., "Airborne Infrared Interferometer Observations and Analysis of Stratospheric Trace Constituents", presented at 1978 Spring Meeting of Amer. Geophys. Union, Miami Beach, 17-21 April 1978.

15. Smith, L. L. and Hilgeman, T., "Nightime Observations of Stratospheric Methane", presented at the Topical Meeting on Atmospheric Spectroscopy, Opt Soc of Amer, Keystone, Colorado, 30 Aug-Sept 1, 1978.

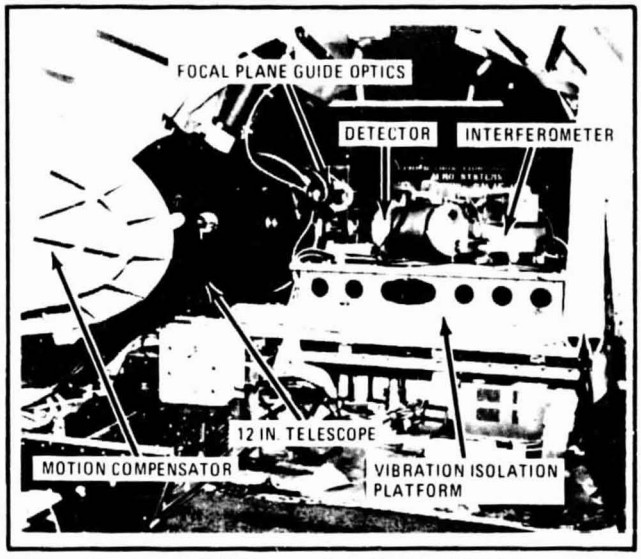

Fig. 1 Grumman FTS System Installed in NASA Lear Jet. Grumman Designed and Constructed Interferometer and Telescope System Shown as It Appeared After Flight Qualification Tests. Telescope Looks Through the Airplane Window (Not Shown) by Means of a Reflection Off the Airplane Motion Compensator. Entire Optical System Sits on a Vibration Isolated Platform

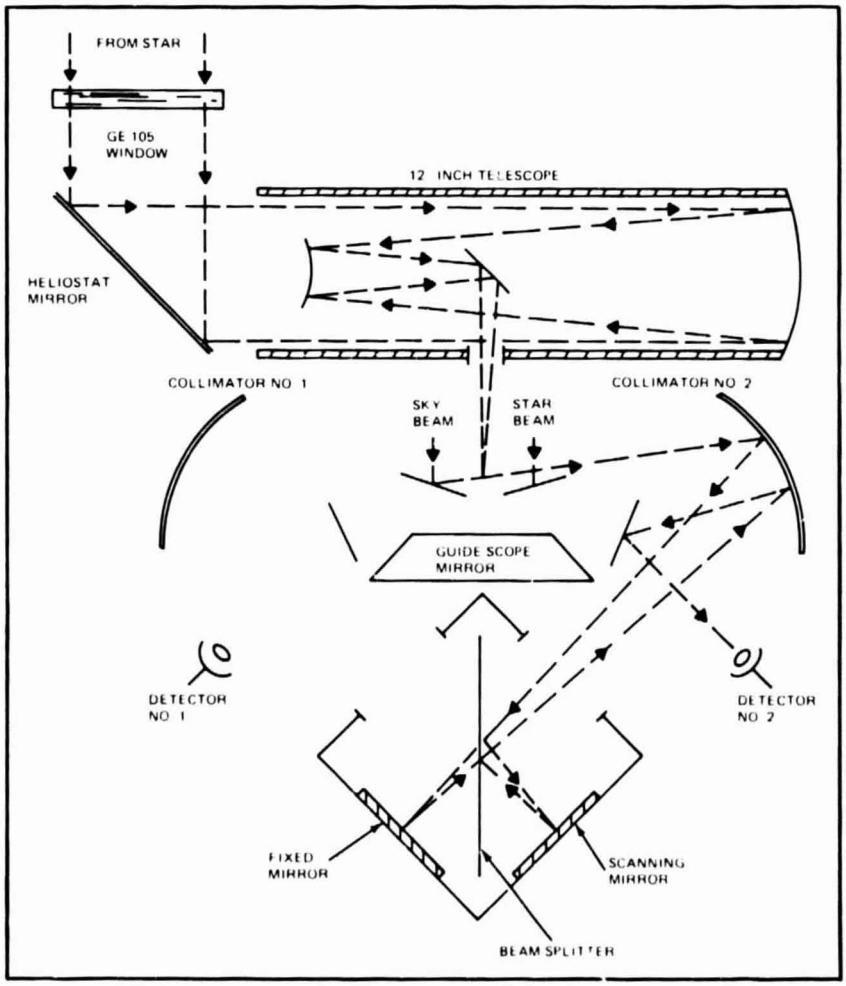

Fig. 2 Schematic Optical System of Telescope and Interferometer as Installed in NASA Lear Airborne Observatory

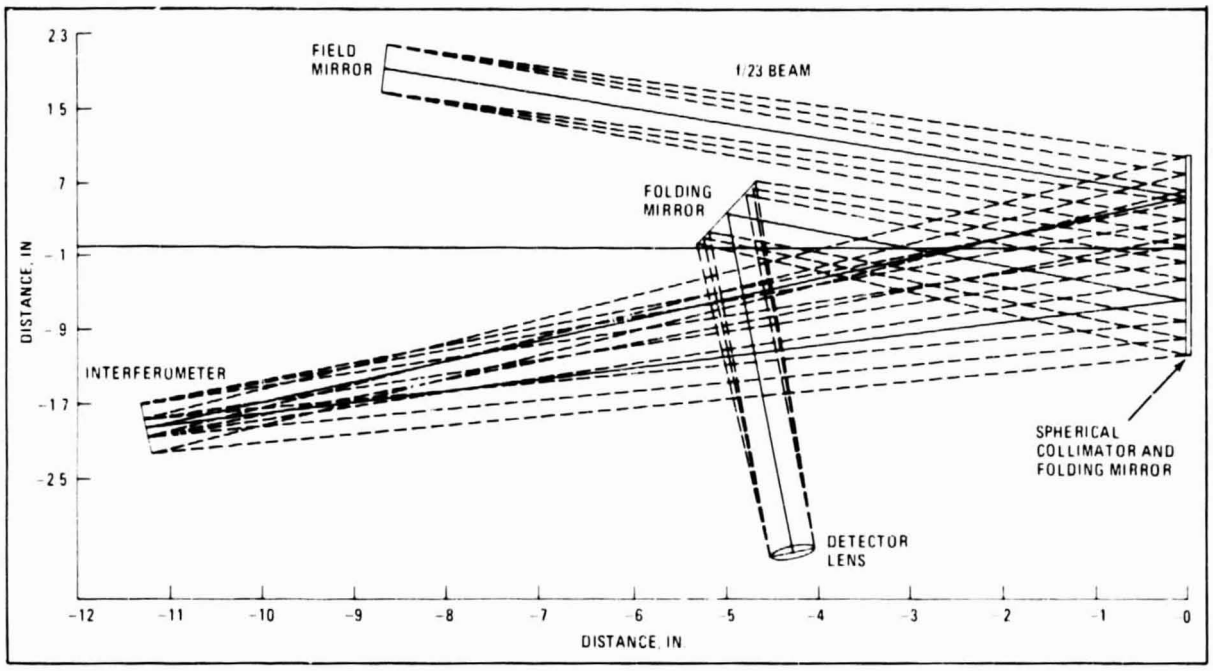

Fig. 3 Optical Design Ray Trace Diagram Shows Path of Travel of Extreme and Center Rays of f/23 Beam as They are Reflected from a Field Mirror, a Collimating Mirror, the Interferometer, a Focusing Mirror, and a Folding Mirror to Reach the Detector Lens. Abscissa and Ordinate are Distances in Inches (Different Scales). Computer Aided Optical Design of This Type Allows Simulation of Proposed Systems Before they are Built

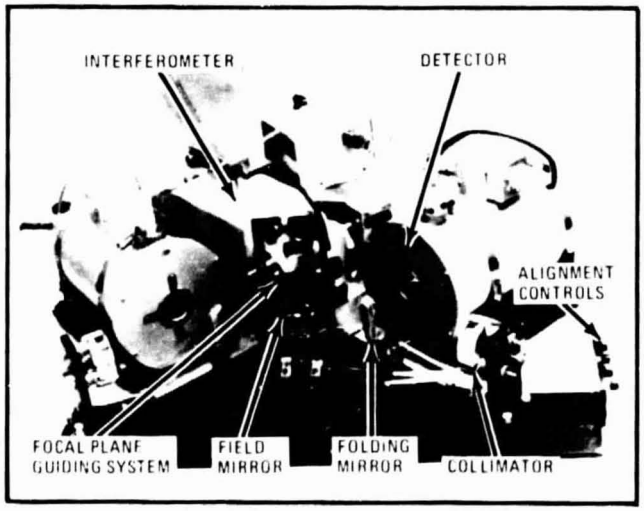

Fig. 4 Completed System Ready for Testing. The Grumman Designed and Built Optical System Indicated in Figure 3 is Shown Here in a Completed State Ready for Laboratory Testing

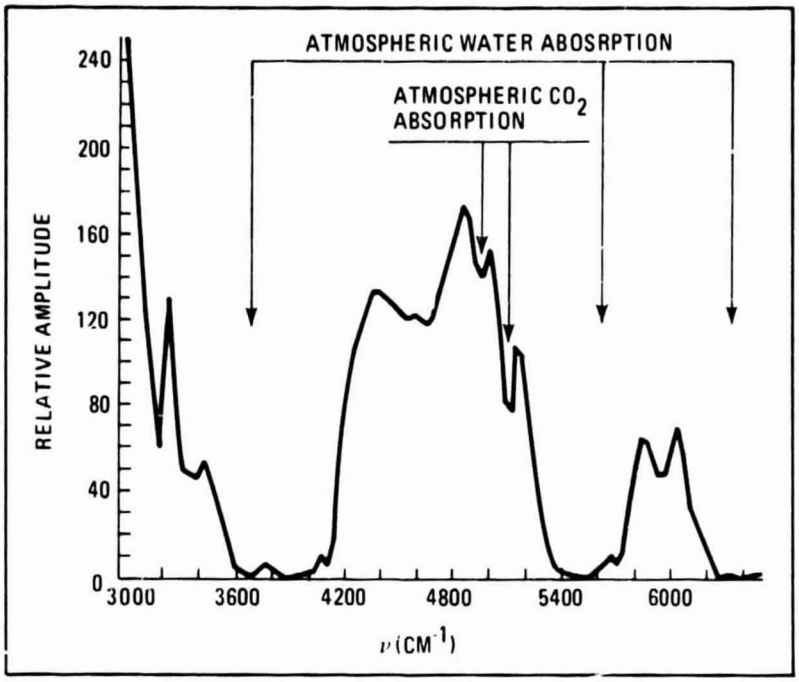

Fig. 5 Lunar Spectrum Taken from Ground at Grumman. Test Spectrum Shows Earth's Atmospheric Absorption Features Due to CO_2 and Water. Plot Shows Intensity of Lunar Signal (Uncorrected for System Response) Versus Wavenumber in Inverse cm. Strong Water Absorption Makes Ground-based Astronomical Observations of Water Difficult

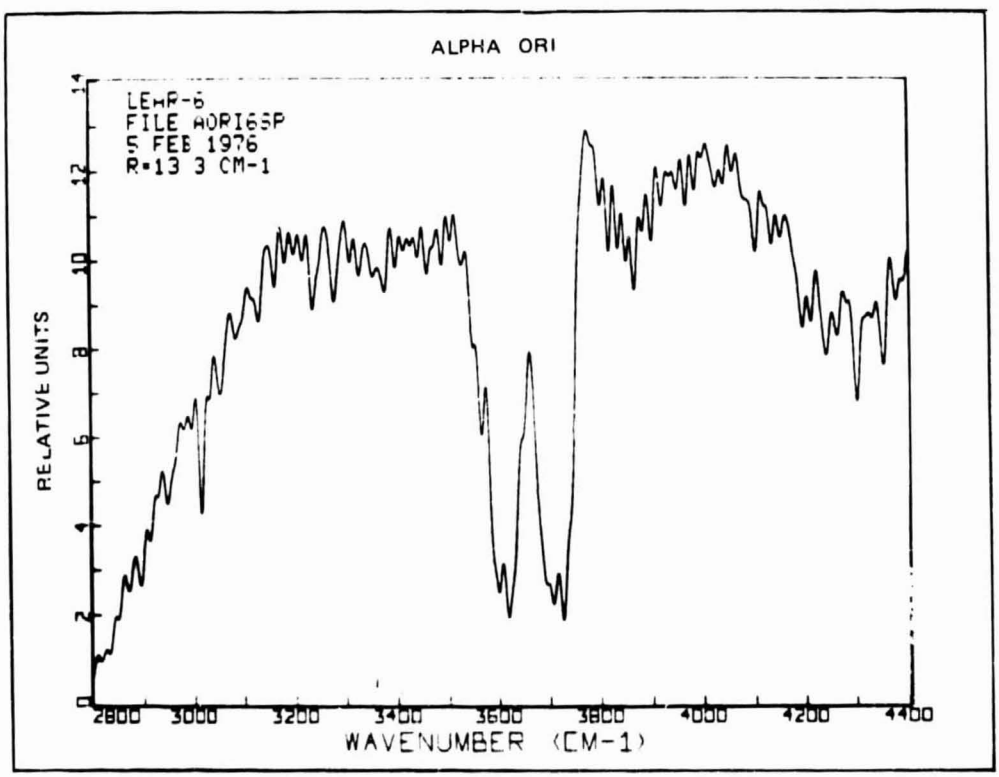

Fig. 6a Spectrum of Alpha Ori on 5 Feb 1976 in 2800-4400 cm^{-1} Region at 13.3 cm^{-1} Resolution.

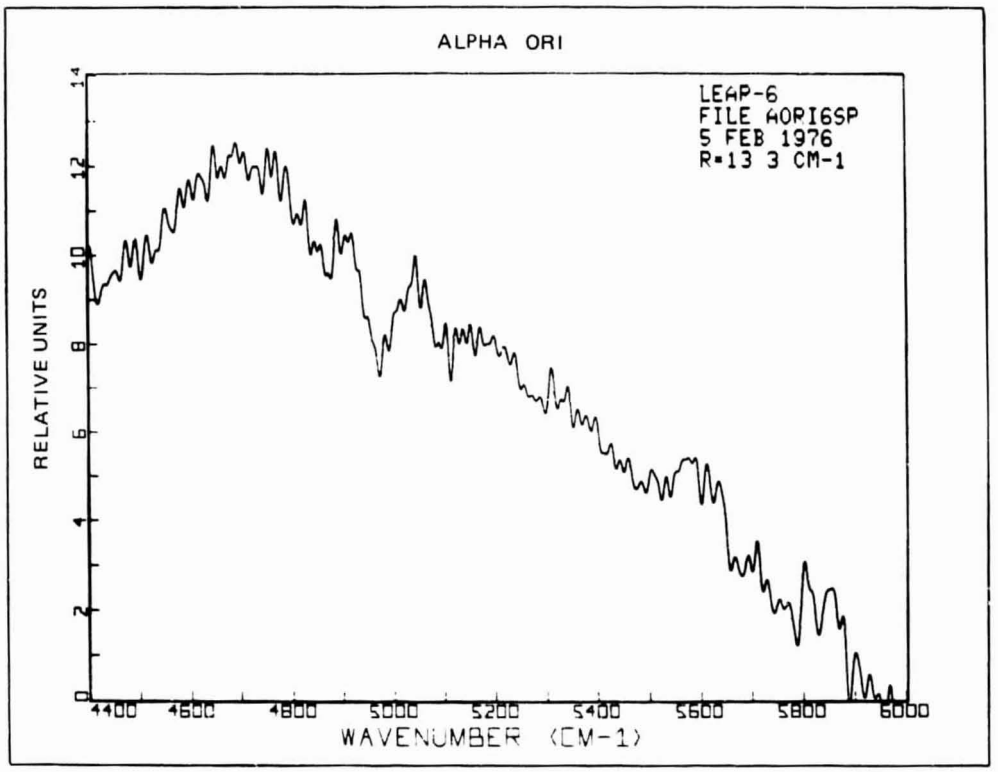

Fig. 6b Spectrum of Alpha Ori on 5 Feb 1976 in 4400-6000 cm^{-1} Region at 13.3 cm^{-1} Resolution.

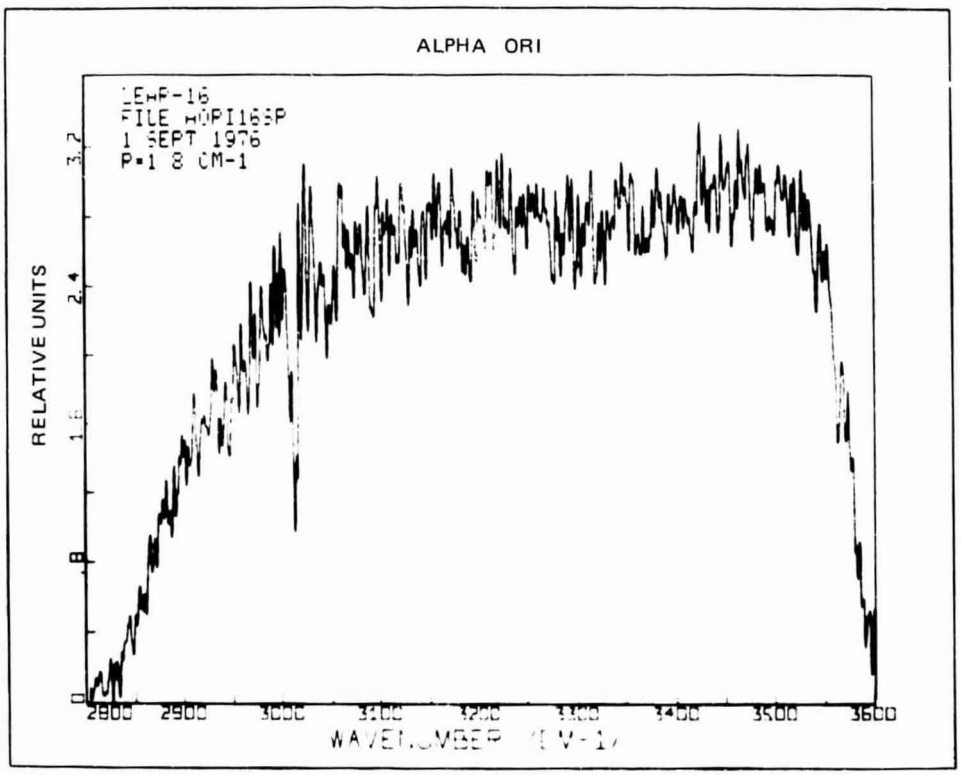

Fig. 7a Spectrum of Alpha Ori on 1 Sept 1976 in 2800-3600 cm^{-1} Region at 1.8 cm^{-1} Resolution.

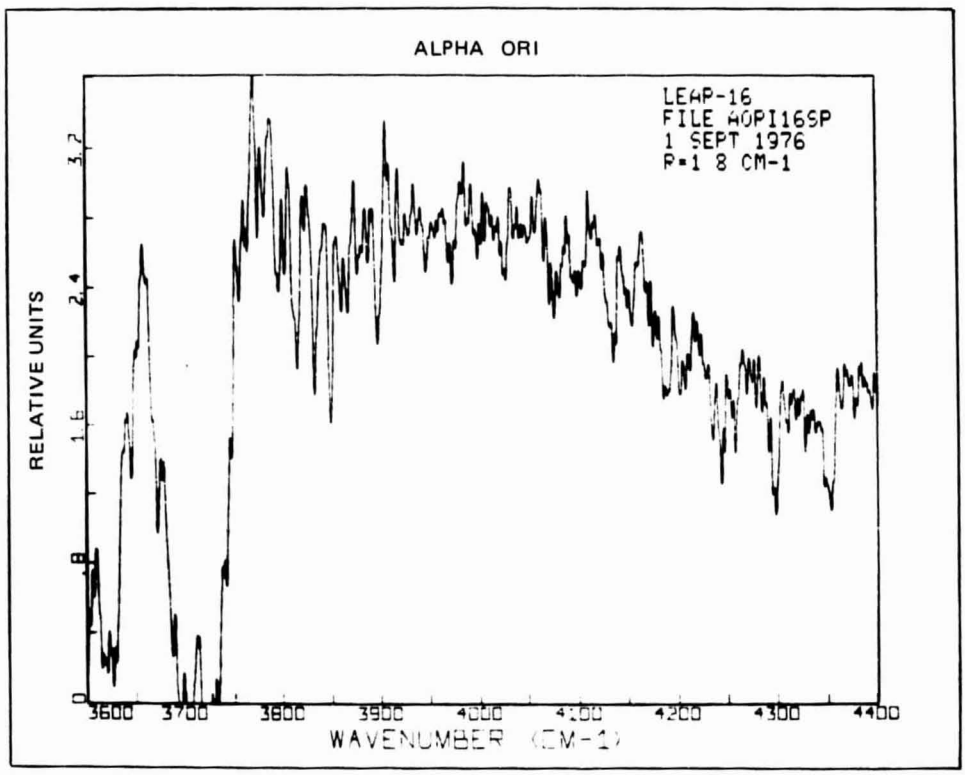

Fig. 7b Spectrum of Alpha Ori on 1 Sept 1976 in 3600-4400 cm^{-1} Region at 1.8 cm^{-1} Resolution.

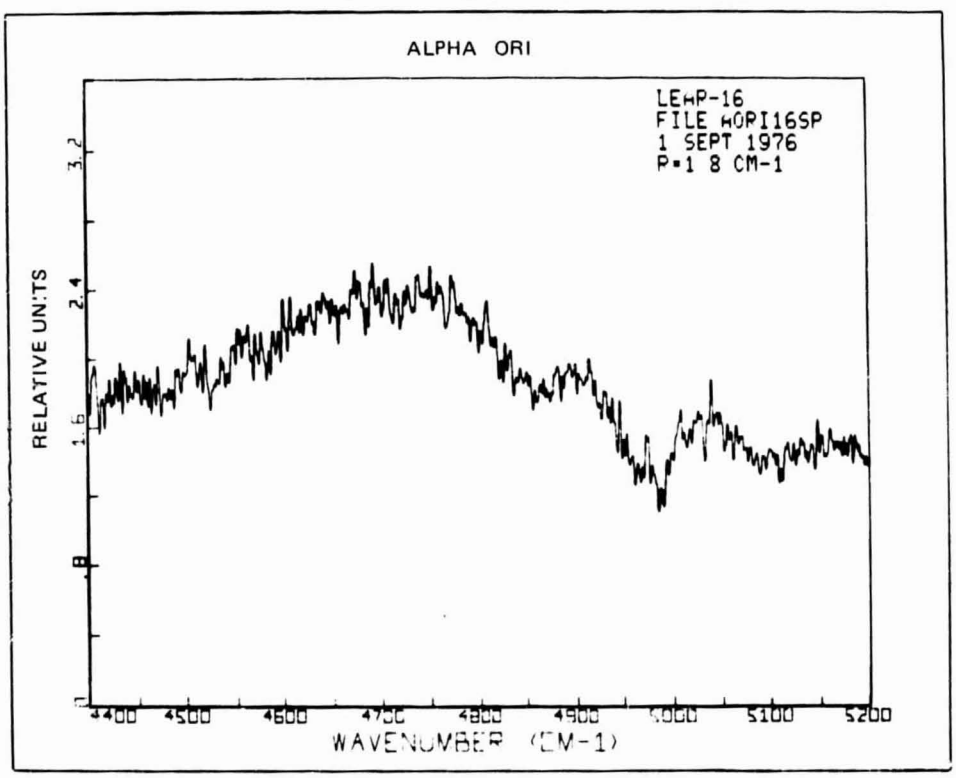

Fig. 7c Spectrum of Alpha Ori on 1 Sept 1976 in 4400-5200 cm^{-1} Region at 1.8 cm^{-1} Resolution.

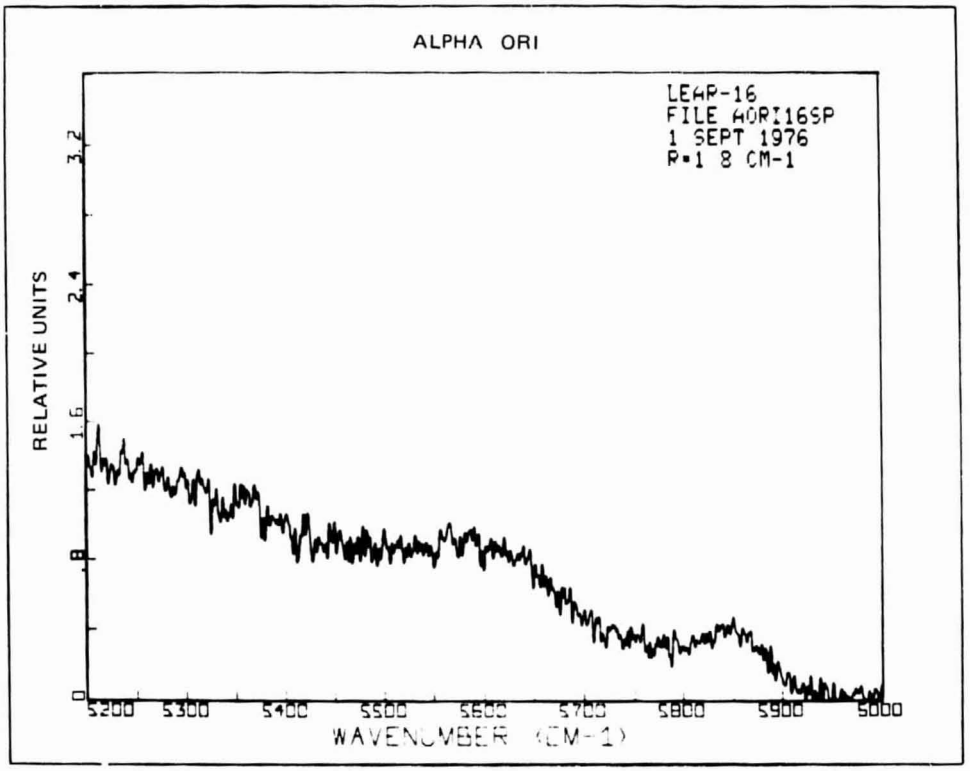

Fig. 7d Spectrum of Alpha Ori on 1 Sept 1976 in 5200-6000 Region at 1.8 cm^{-1} Resolution.

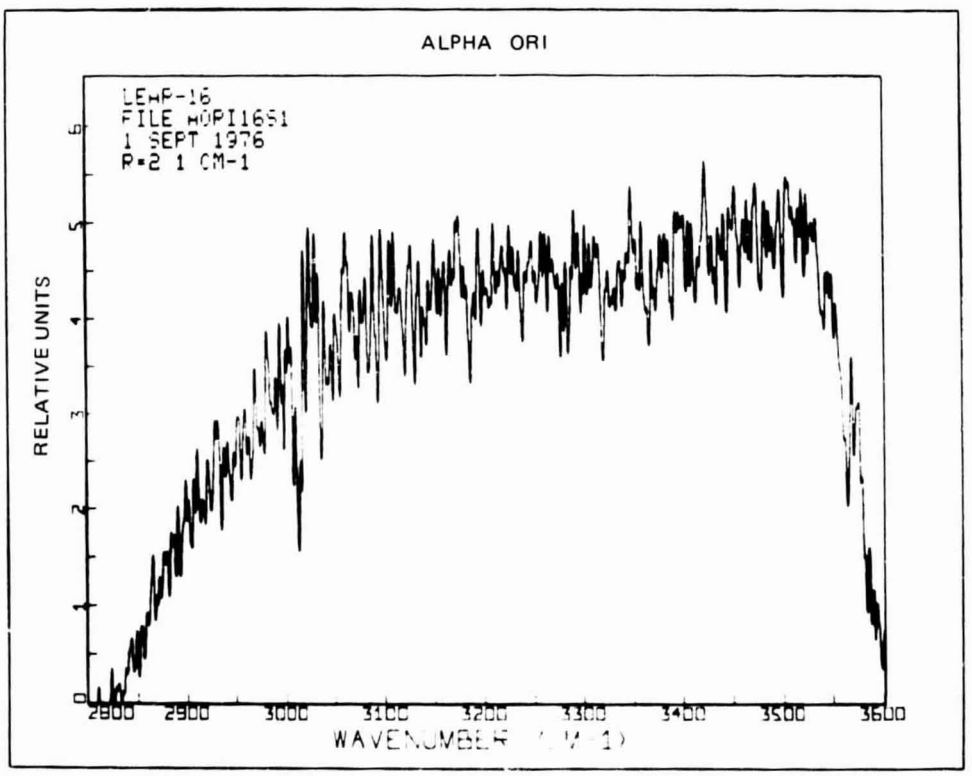

Fig. 8a Spectrum of Alpha Ori on 1 Sept 1976 in 2800-3600 cm^{-1} Region at 2.1 cm^{-1} Resolution.

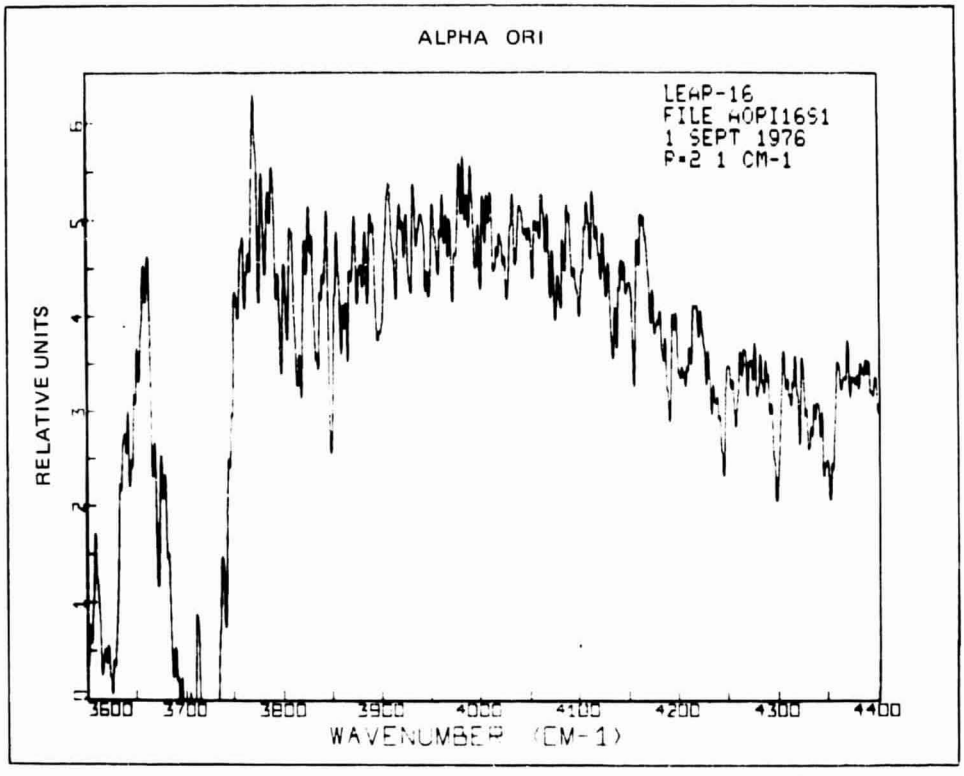

Fig. 8b Spectrum of Alpha Ori on 1 Sept 1976 in 3600-4400 cm^{-1} Region at 2.1 cm^{-1} Resolution.

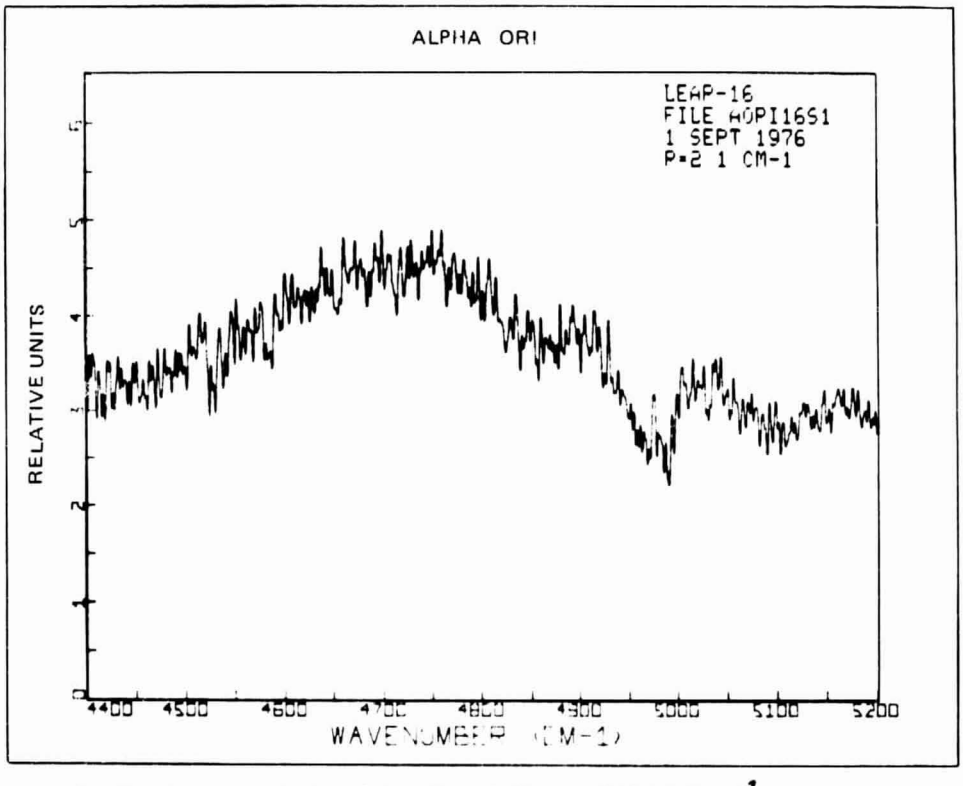

Fig. 8c Spectrum of Alpha Ori on 1 Sept 1976 in 4400-5200 cm^{-1} Region at 2.1 cm^{-1} Resolution.

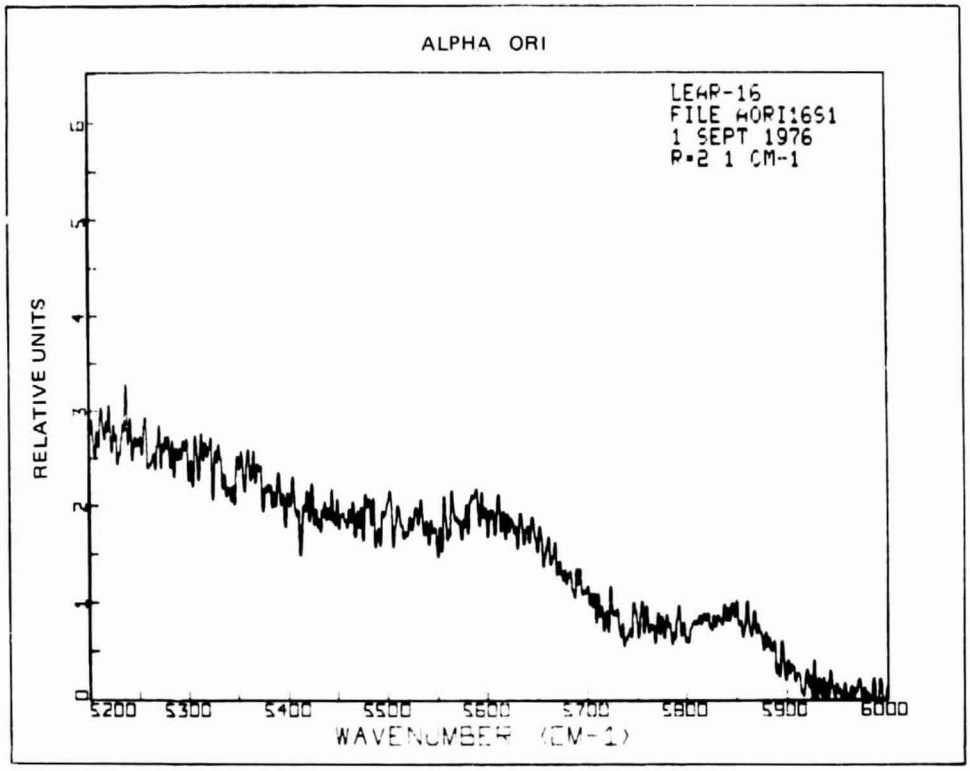

Fig. 8d Spectrum of Alpha Ori on 1 Sept 1976 in 5200-6000 cm^{-1} Region at 2.1 cm^{-1} Resolution.

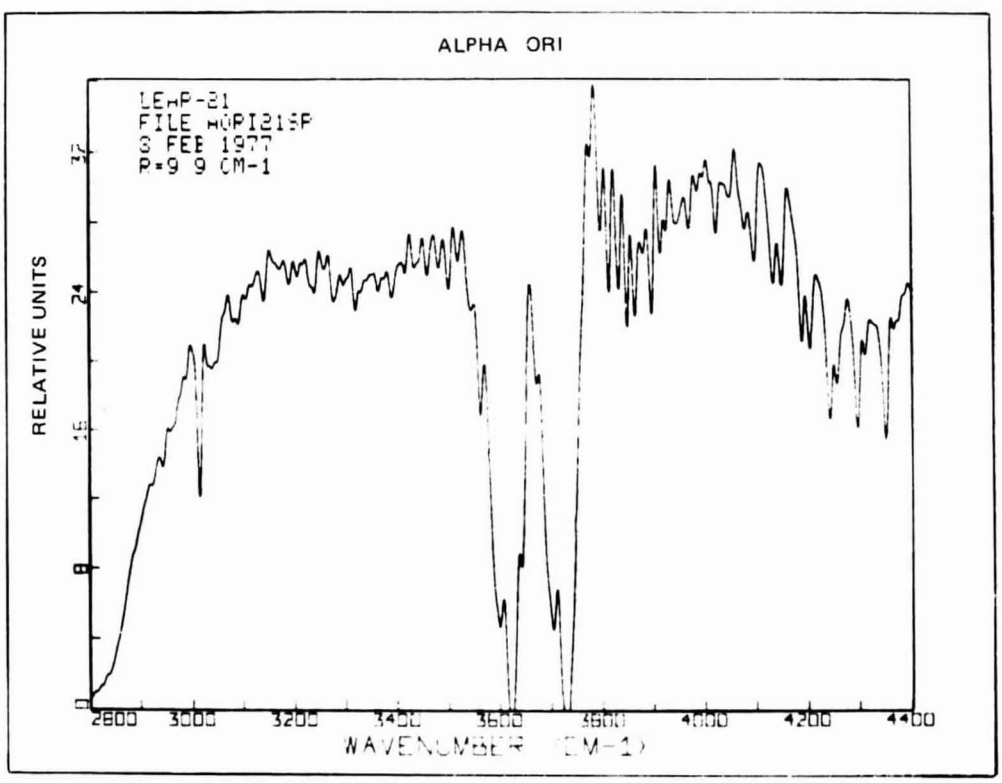

Fig. 9a Spectrum of Alpha Ori on 8 Feb 1977 in 2800-4400 cm^{-1} Region at 9.9 cm^{-1} Resolution.

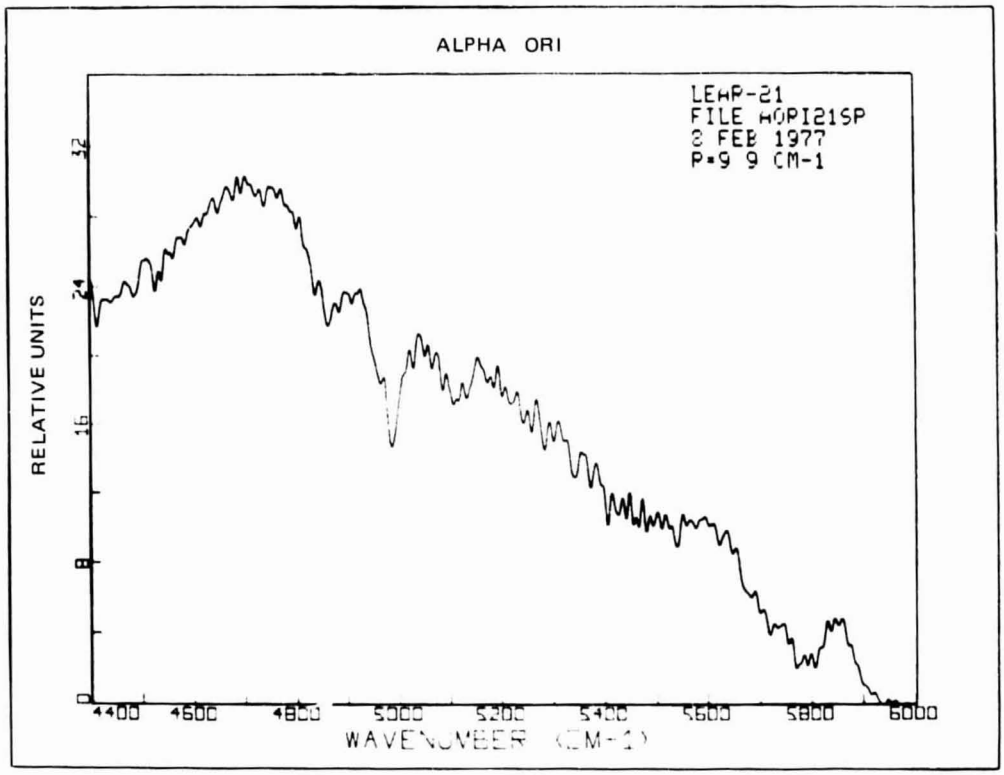

Fig. 9b Spectrum of Alpha Ori on 8 Feb 1977 in 4400-6000 cm^{-1} Region at 9.9 cm^{-1} Resolution.

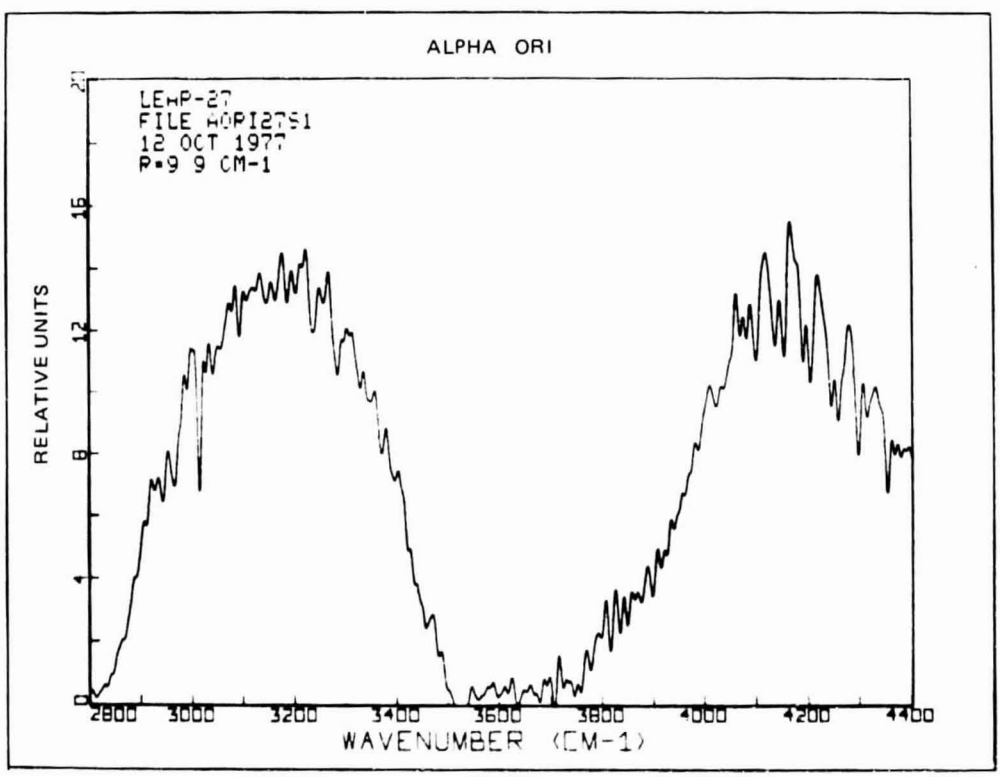

Fig. 10a Spectrum of Alpha Ori on 12 Oct 1977 in 2800-4400 cm^{-1} Region at 9.9 cm^{-1} Resolution.

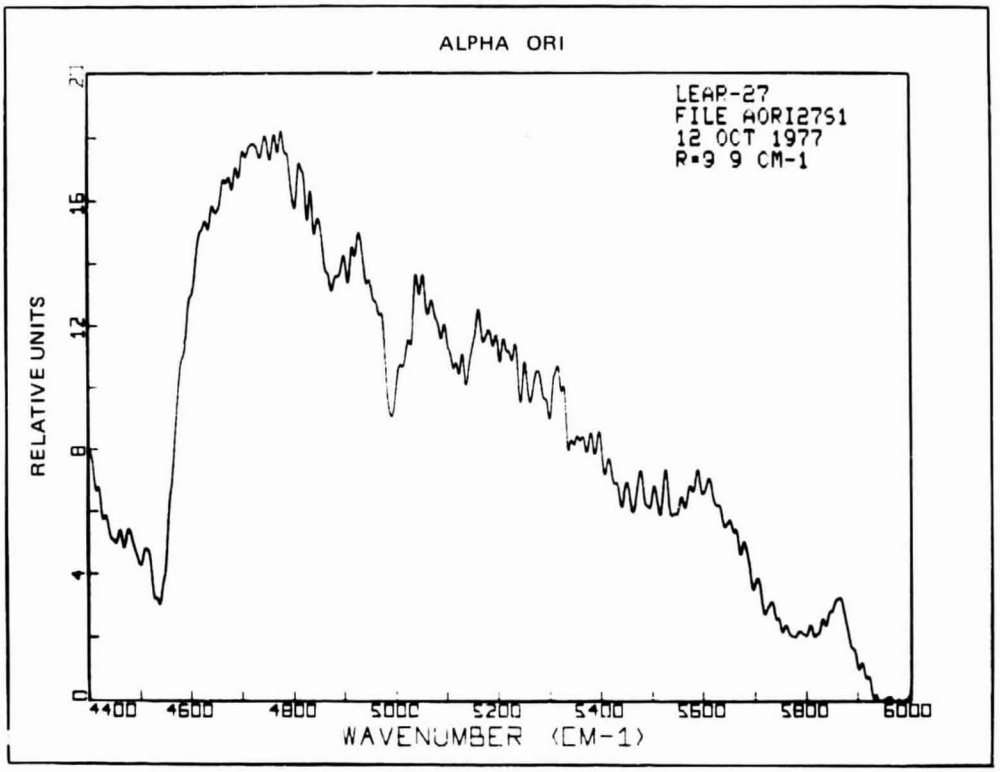

Fig. 10b Spectrum of Alpha Ori on 12 Oct 1977 in 4400-6000 cm^{-1} Region at 9.9 cm^{-1} Resolution.

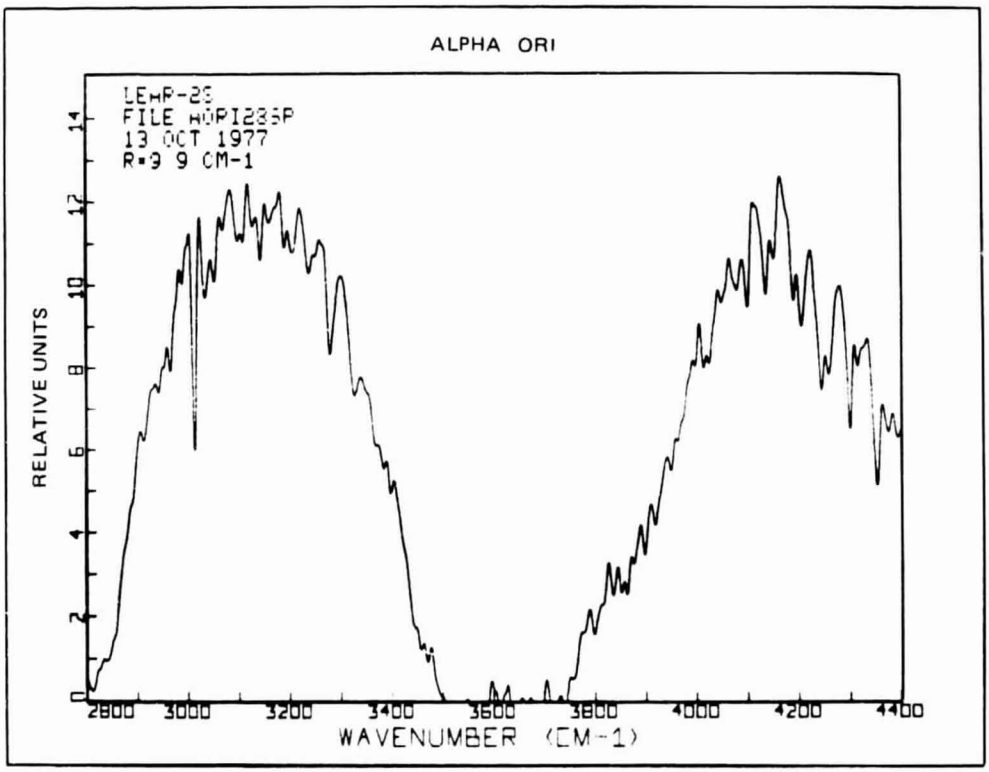

Fig. 11a Spectrum of Alpha Ori on 13 Oct 1977 in 2800-4400 cm^{-1} Region at 9.9 cm^{-1} Resolution.

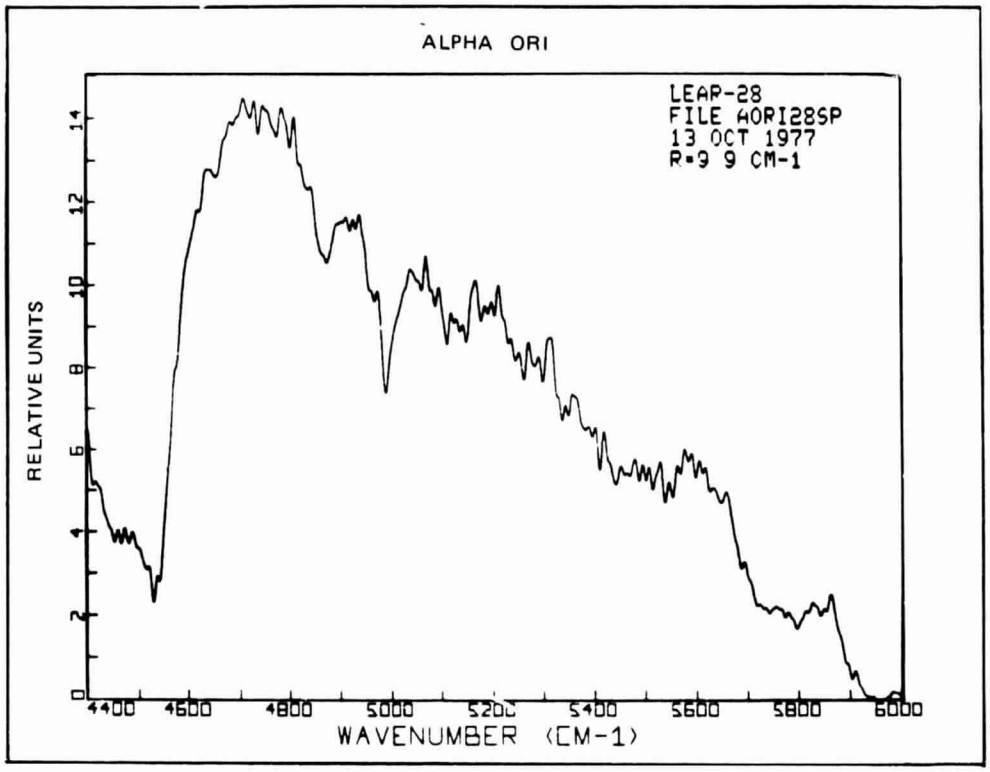

Fig. 11b Spectrum of Alpha Ori on 13 Oct 1977 in 4400-6000 cm^{-1} Region at 9.9 cm^{-1} Resolution.

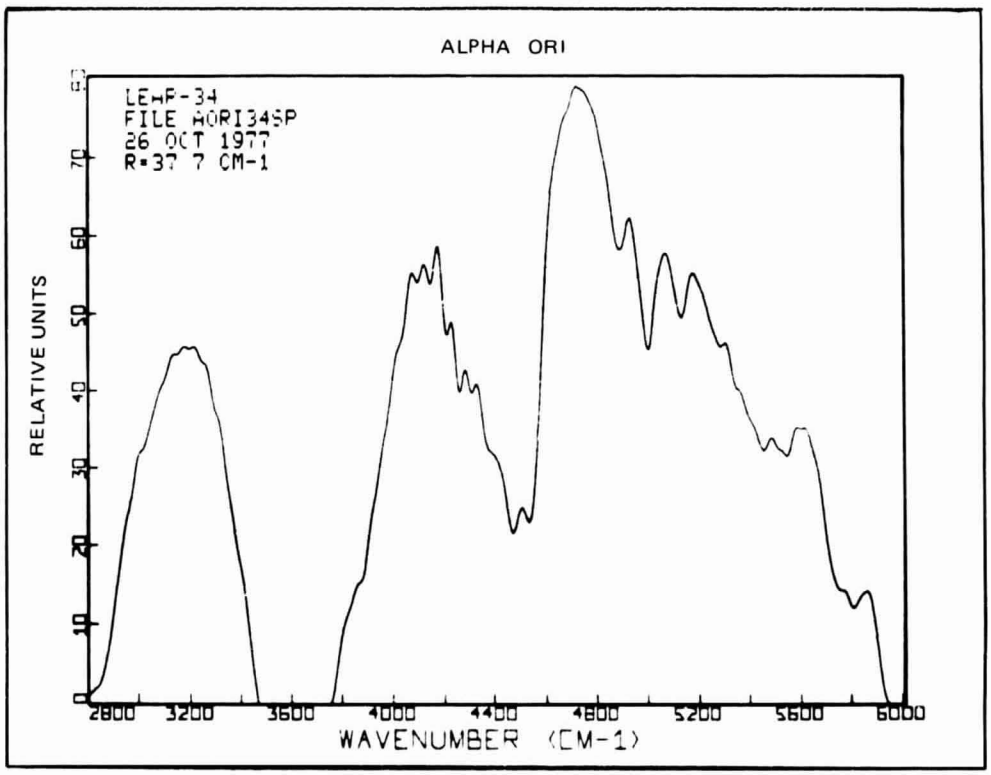

Fig. 12 Spectrum of Alpha Ori on 26 Oct 1977 in 2800-6000 cm^{-1} Region at 37.7 cm^{-1} Resolution.

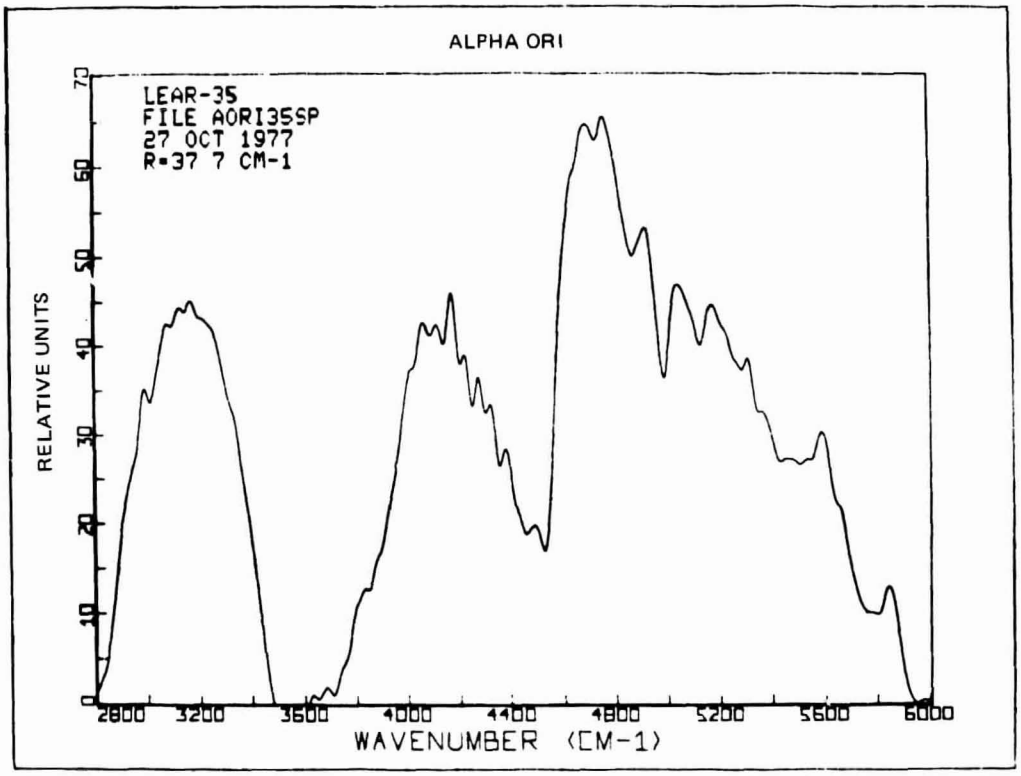

Fig. 13 Spectrum of Alpha Ori on 27 Oct 1977 in 2800-6000 cm^{-1} Region at 37.7 cm^{-1} Resolution.

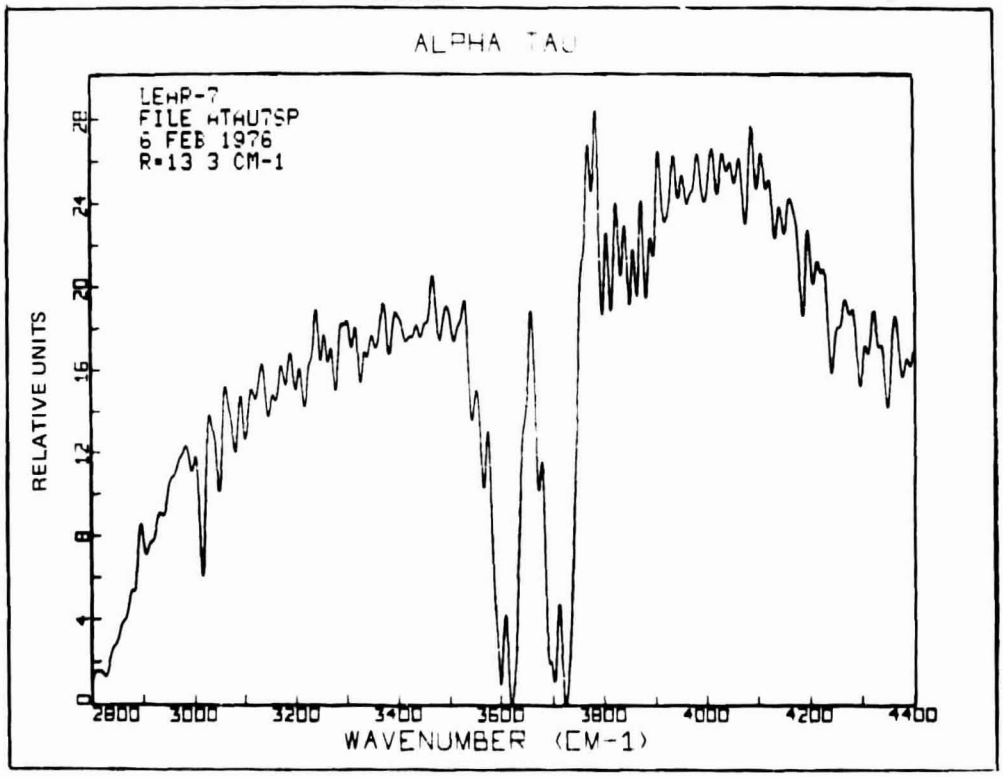

Fig. 14a Spectrum of Alpha Tau on 6 Feb 1976 in 2800-4400 cm^{-1} Region at 13.3 cm^{-1} Resolution.

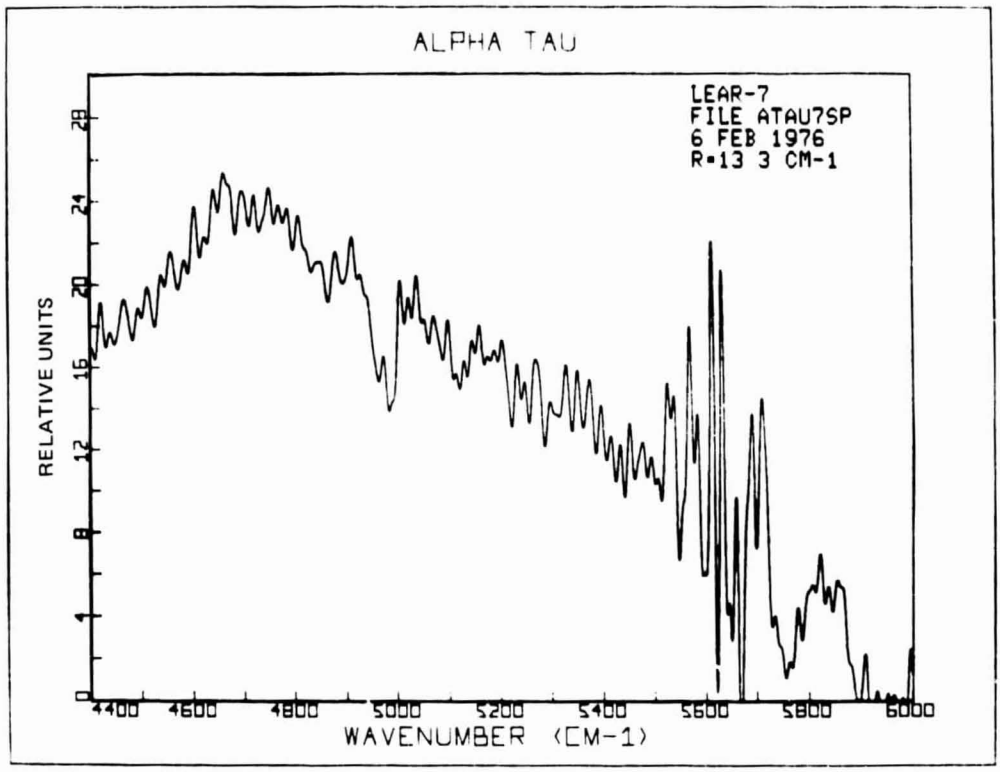

Fig. 14b Spectrum of Alpha Tau on 6 Feb 1976 in 4400-6000 cm^{-1} Region at 13.3 cm^{-1} Resolution.

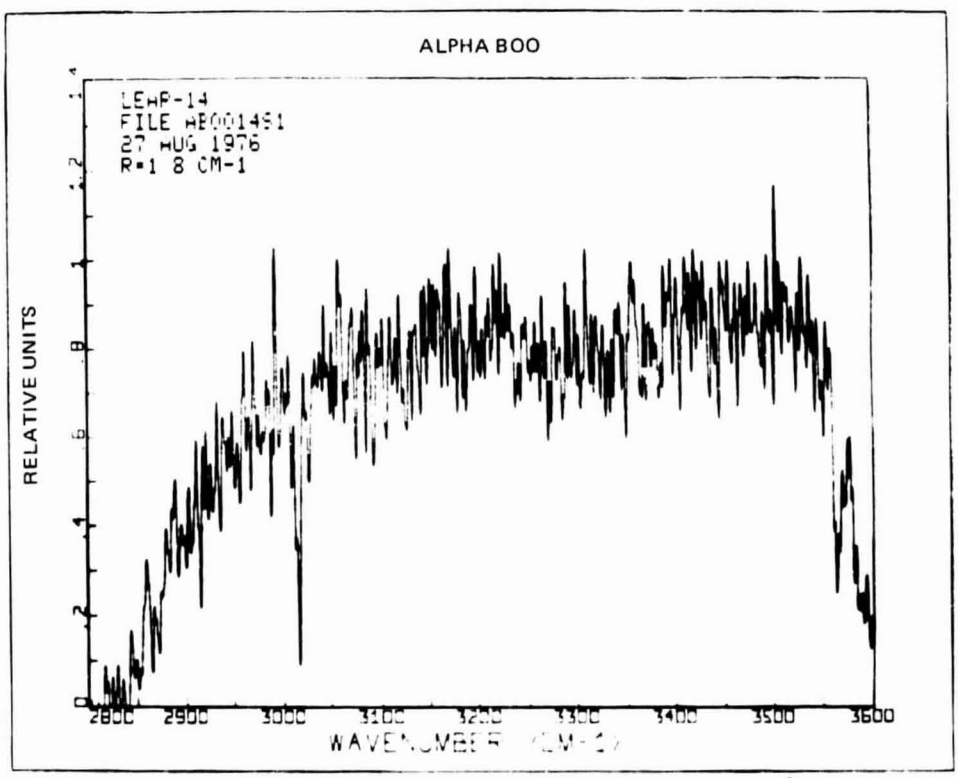

Fig. 15a Spectrum of Alpha Boo on 27 Aug 1976 in 2800-3600 cm^{-1} Region at 1.8 cm^{-1} Resolution.

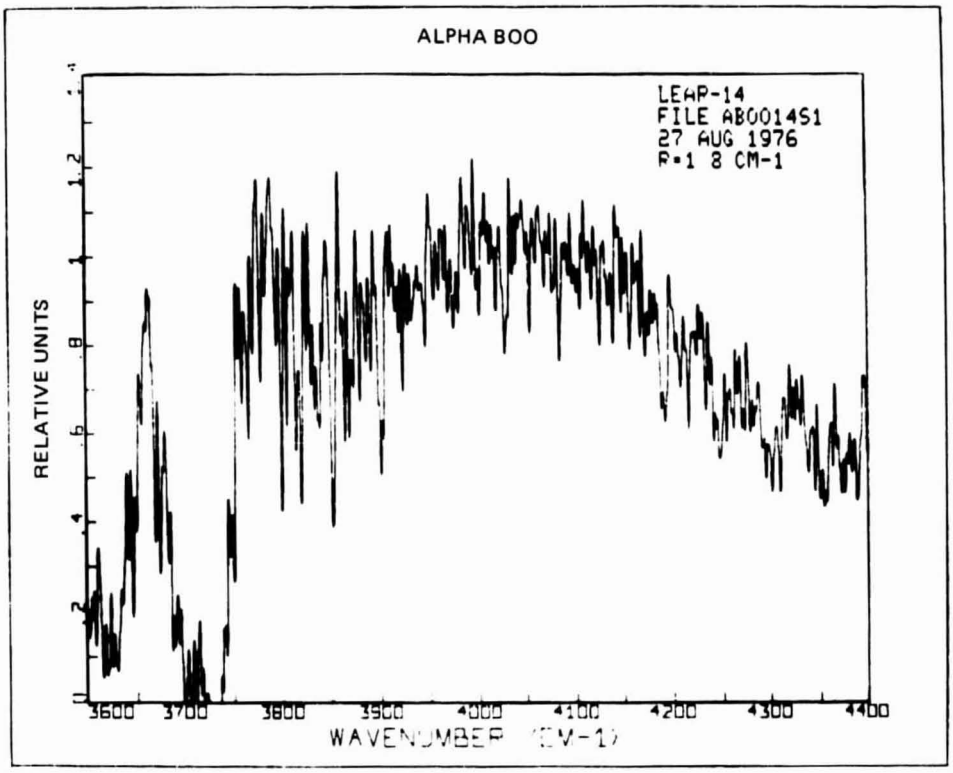

Fig. 15b Spectrum of Alpha Boo on 27 Aug 1976 in 3600-4400 cm^{-1} Region at 1.8 cm^{-1} Resolution.

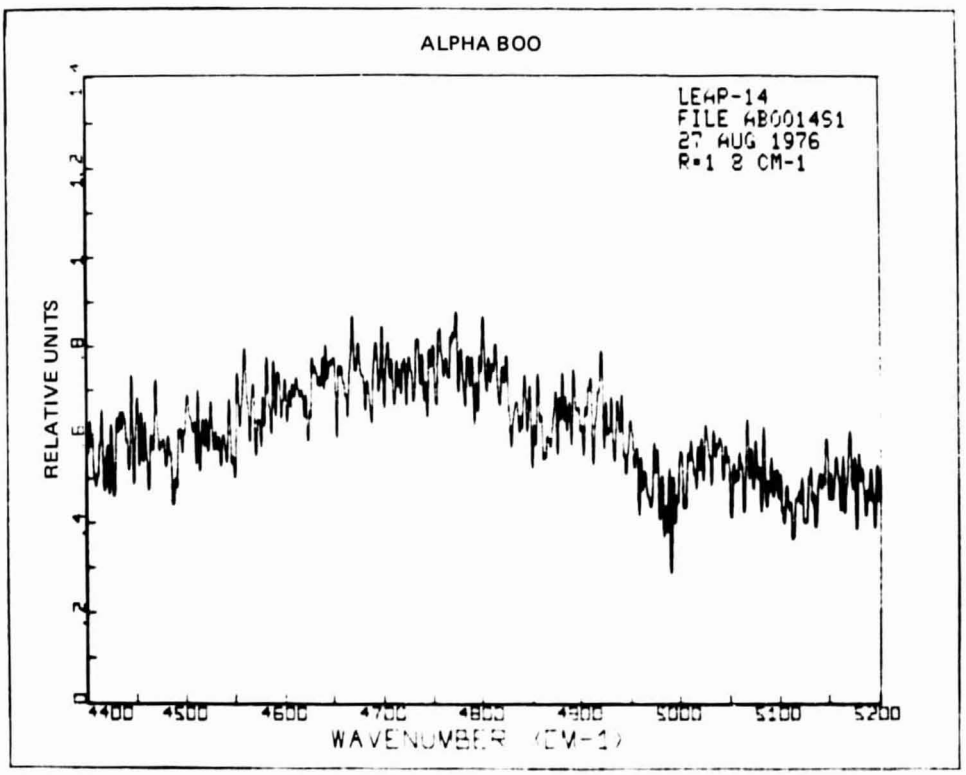

Fig. 15c Spectrum of Alpha Boo on 27 Aug 1976 in 4400-5200 cm^{-1} Region at 1.8 cm^{-1} Resolution.

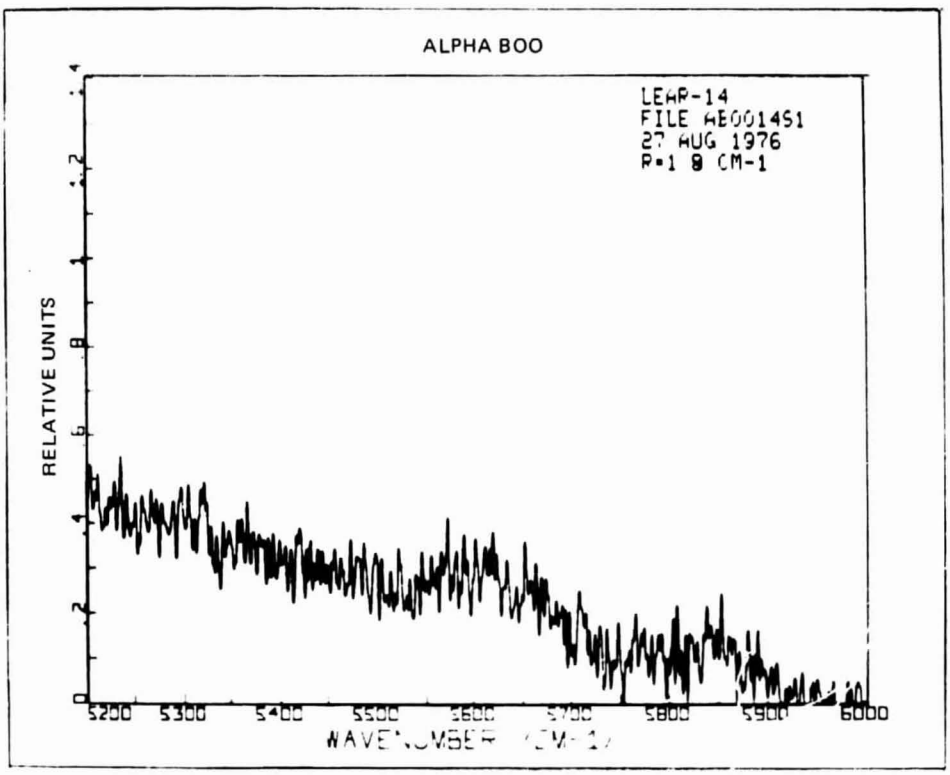

Fig. 15d Spectrum of Alpha Boo on 27 Aug 1976 in 5200-6000 cm^{-1} Region at 1.8 cm^{-1} Resolution.

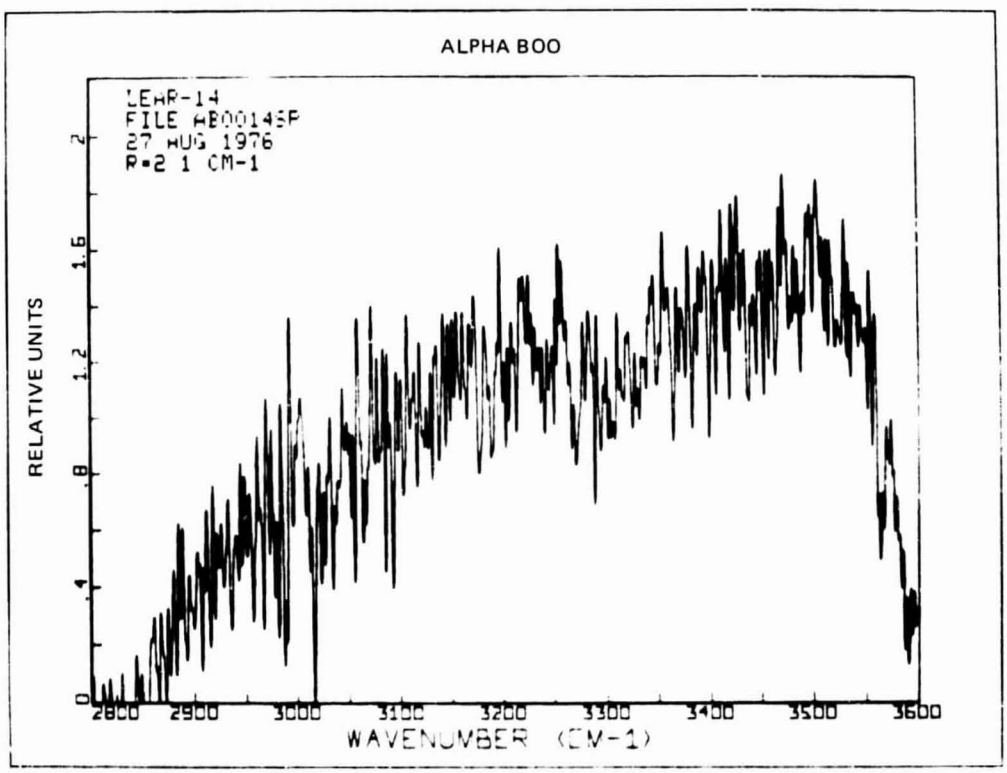

Fig. 16a Spectrum of Alpha Boo on 27 Aug 1976 in 2800-3600 cm^{-1} Region at 2.1 cm^{-1} Resolution.

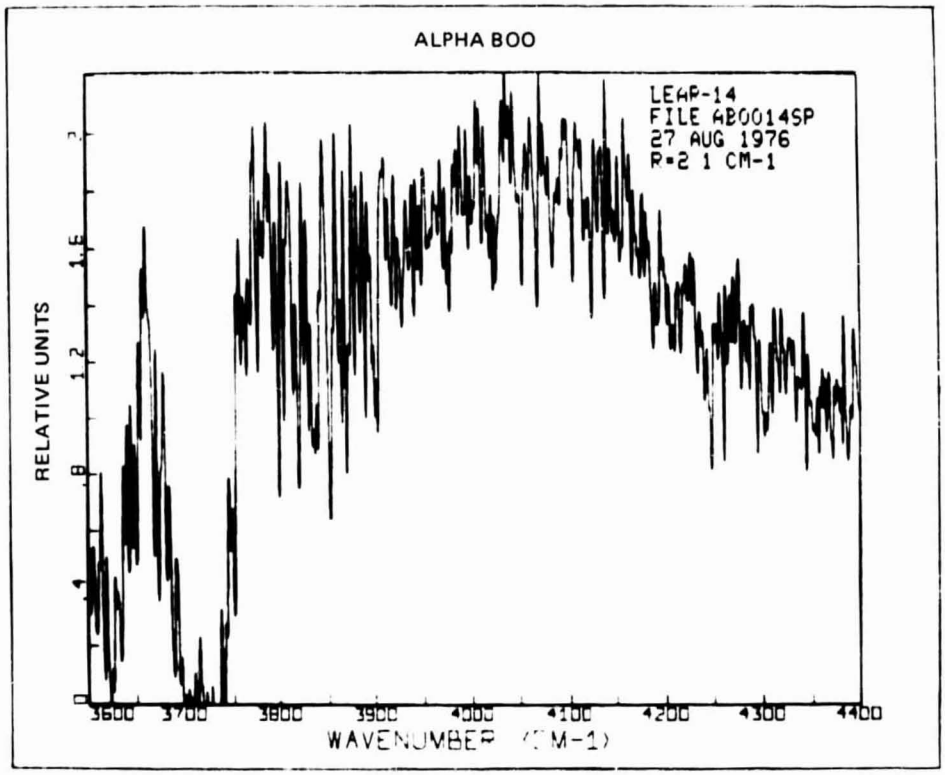

Fig. 16b Spectrum of Alpha Boo on 27 Aug 1976 in 3600-4400 cm^{-1} Region at 2.1 cm^{-1} Resolution.

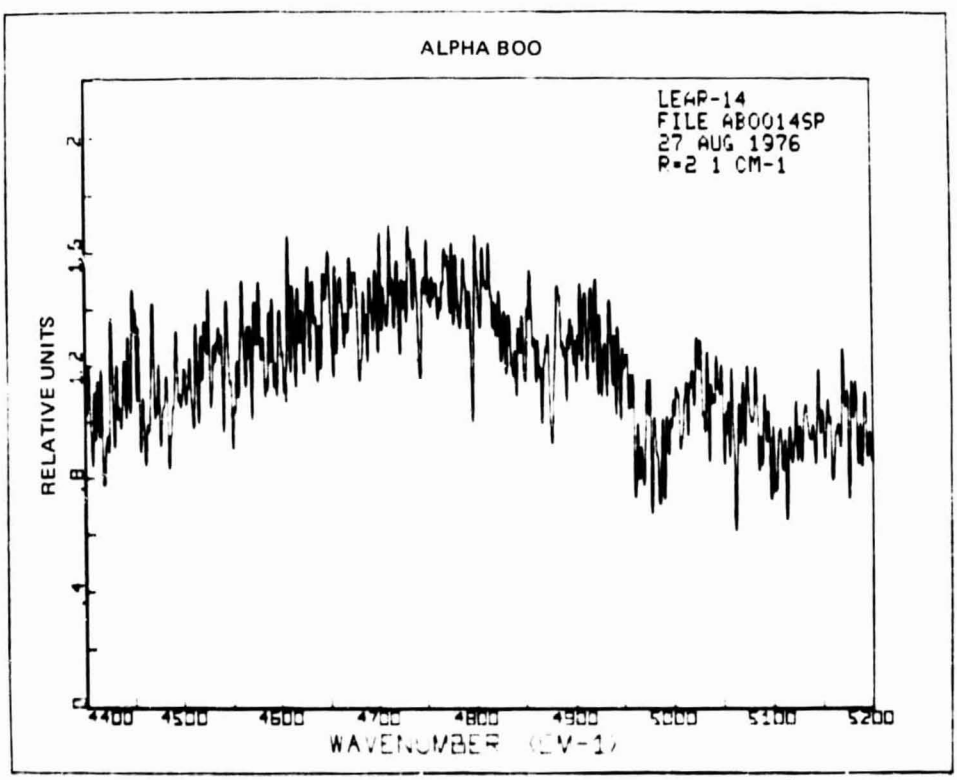

Fig. 16c Spectrum of Alpha Boo on 27 Aug 1976 in 4400-5200 cm^{-1} Region at 2.1 cm^{-1} Resolution.

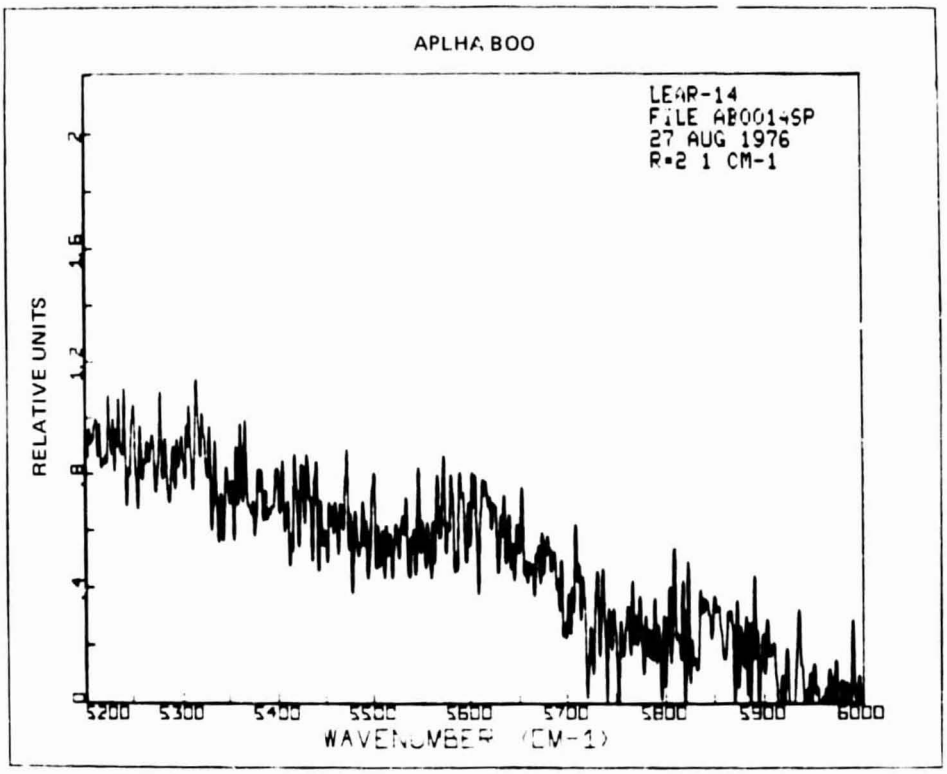

Fig. 16d Spectrum of Alpha Boo on 27 Aug 1976 in 5200-6000 cm^{-1} Region at 2.1 cm^{-1} Resolution.

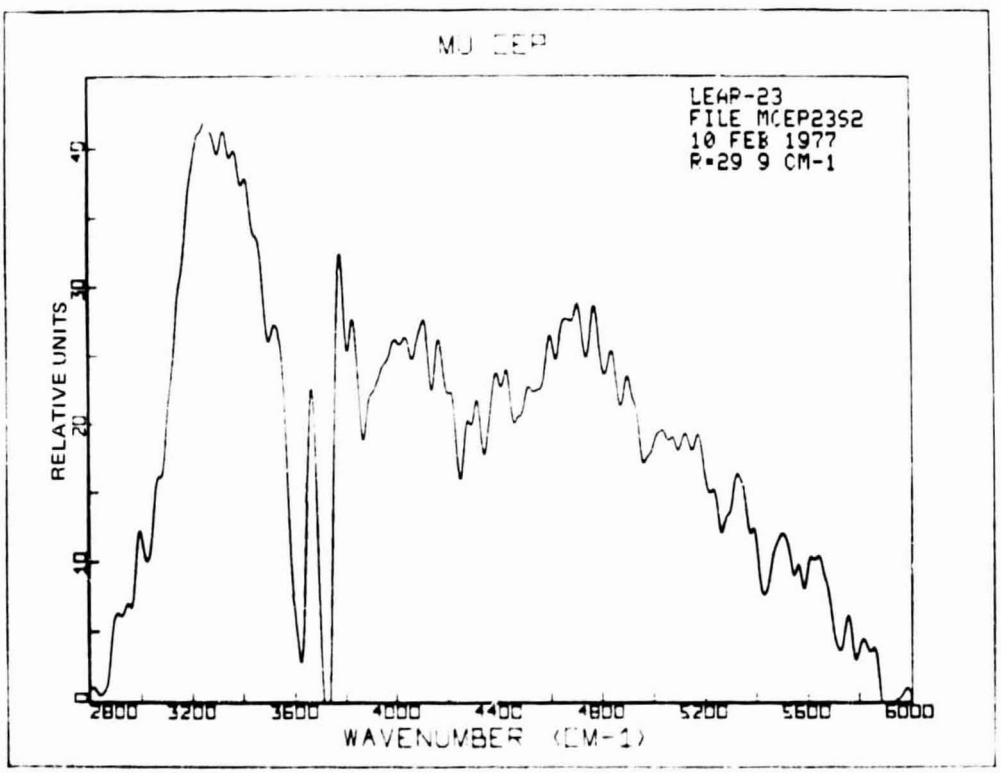

Fig. 17 Spectrum of Mu Cep on 10 Feb 1977 in 2800-6000 cm^{-1} Region at 29.9 cm^{-1} Resolution.

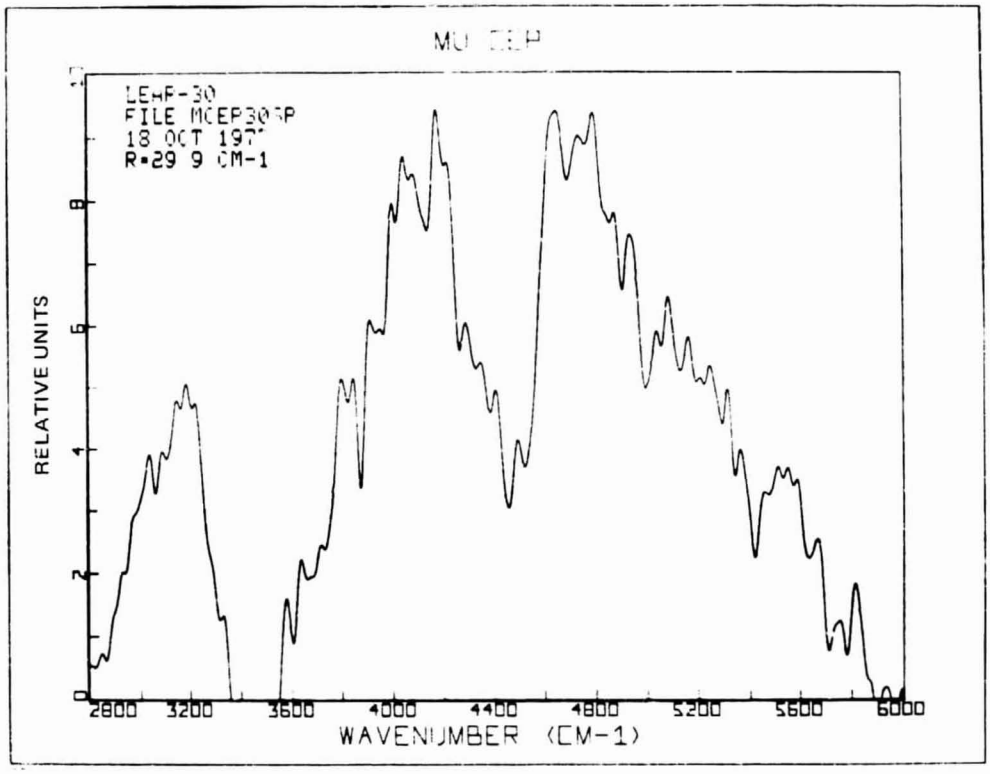

Fig. 18 Spectrum of Mu Cep on 18 Oct 1977 in 2800-6000 cm^{-1} Region at 29.9 cm^{-1} Resolution.

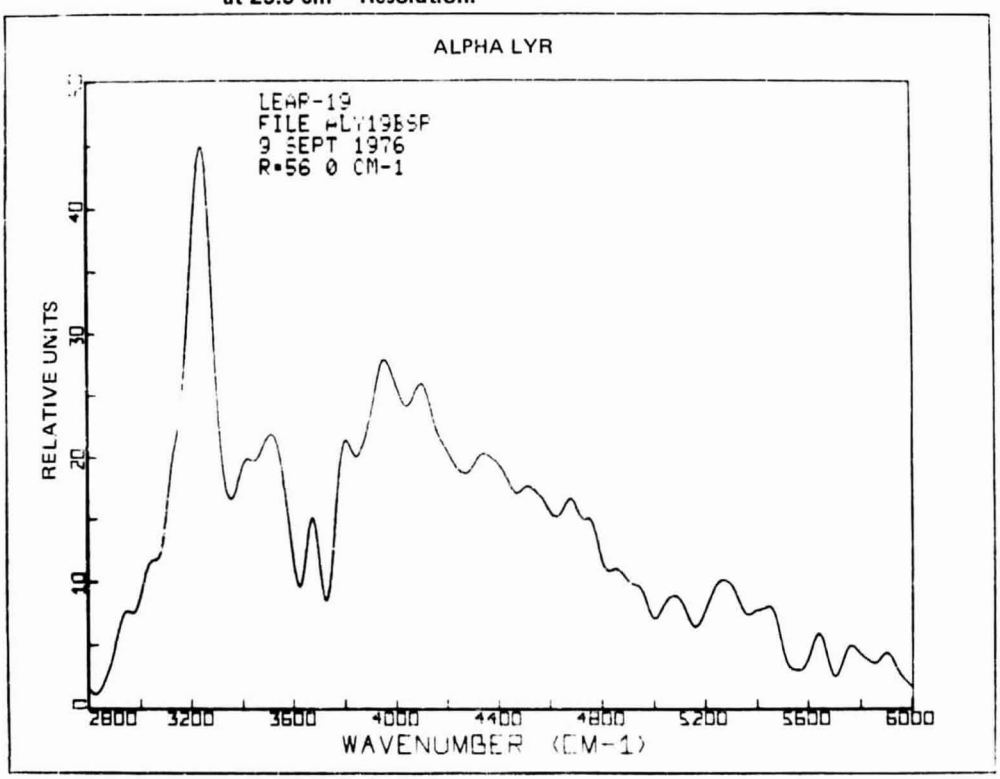

Fig. 19 Spectrum of Alpha Lyr on 9 Sept 1976 in 2800-6000 cm^{-1} Region at 56.0 cm^{-1} Resolution.

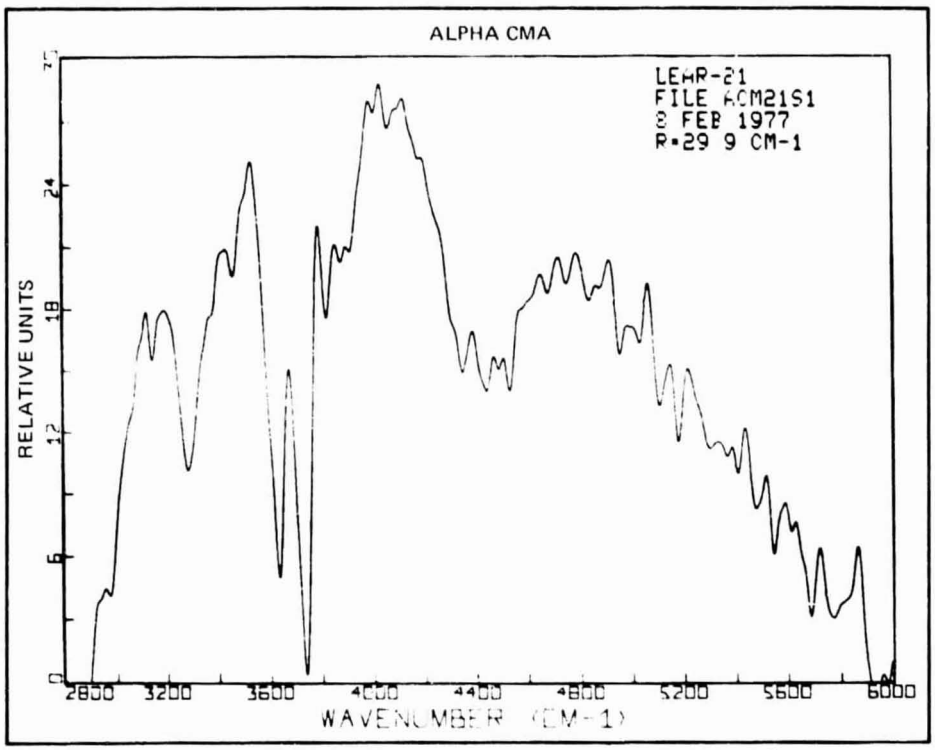

Fig. 20 Spectrum of Alpha CMa on 8 Feb 1977 in 2800-6000 cm^{-1} Region at 29.9 cm^{-1} Resolution.

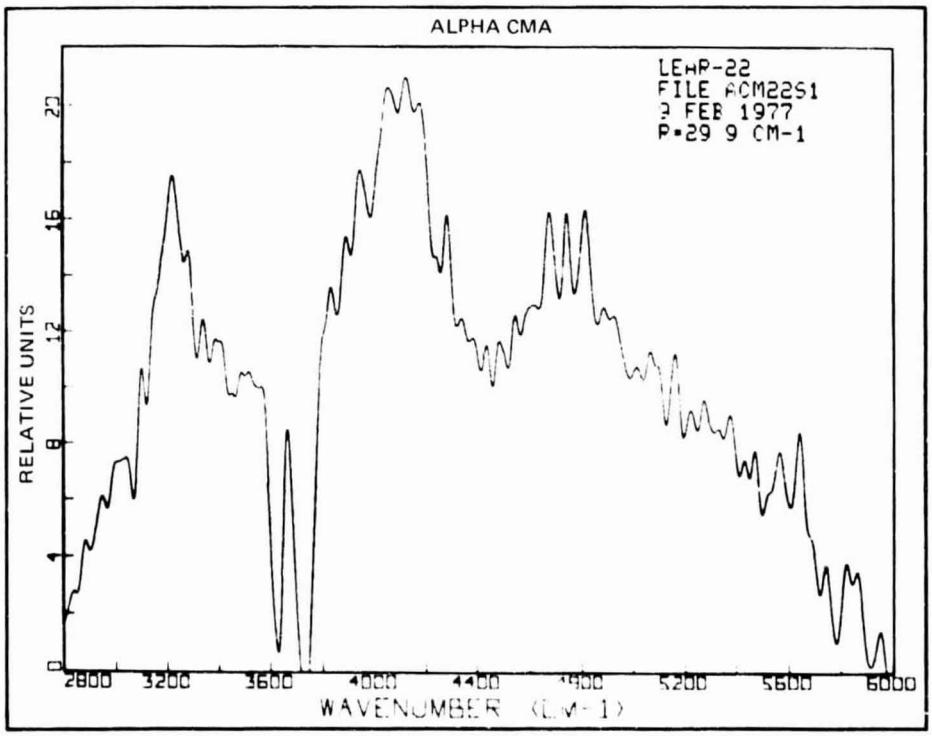

Fig. 21 Spectrum of Alpha CMa on 9 Feb 1977 in 2800-6000 cm^{-1} Region at 29.9 cm^{-1} Resolution.

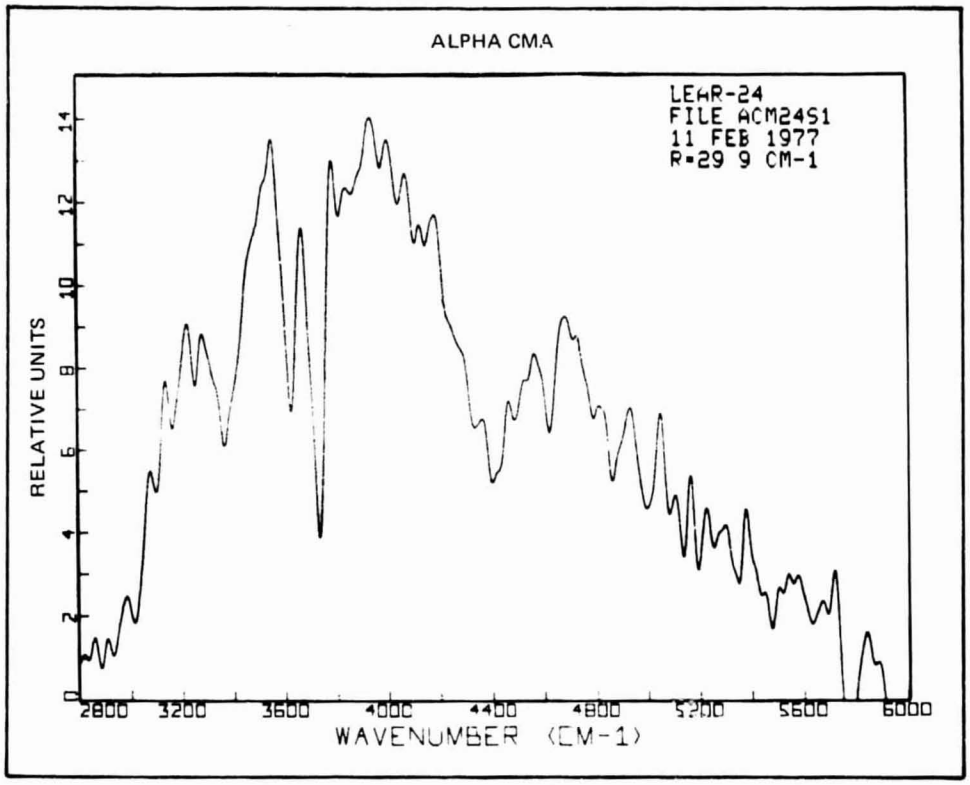

Fig. 22 Spectrum of Alpha CMa on 11 Feb 1977 in 2800-6000 cm^{-1} Region at 29.9 cm^{-1} Resolution.

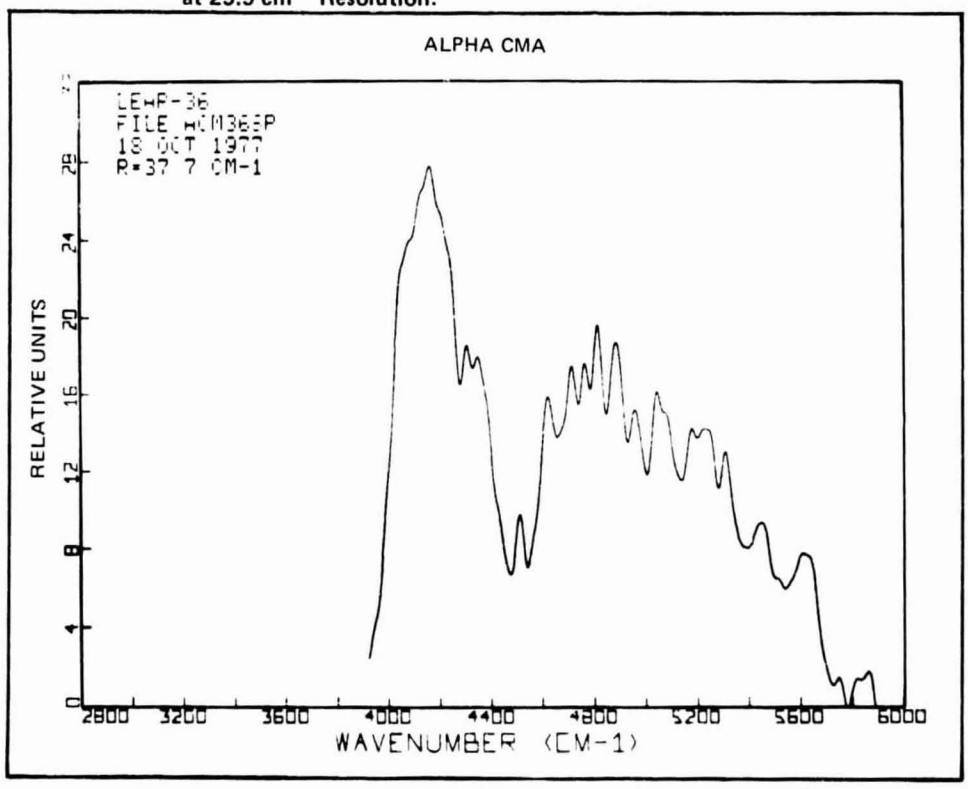

Fig. 23 Spectrum of Alpha CMa on 18 Oct 1977 in 2800-6000 cm^{-1} Region at 37.7 cm^{-1} Resolution.

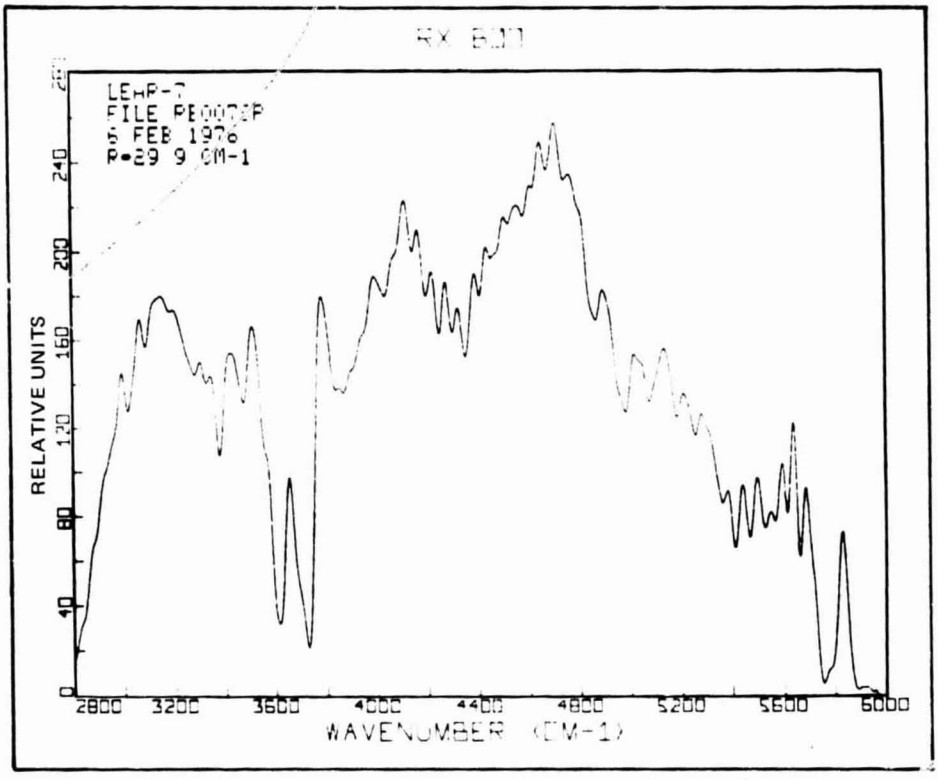

Fig. 24 Spectrum of RX Boo on 6 Feb 1976 in 2800-6000 cm^{-1} Region at 29.9 cm^{-1} Resolution.

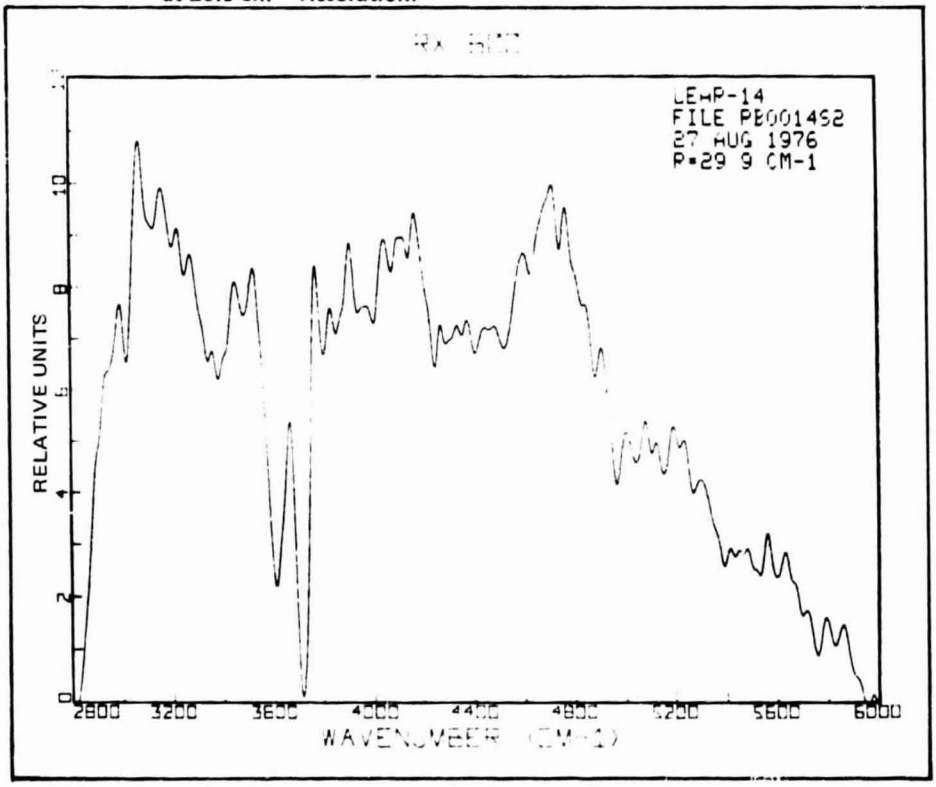

Fig. 25 Spectrum of RX Boo on 27 Aug 1976 in 2800-6000 cm^{-1} Region at 29.9 cm^{-1} Resolution.

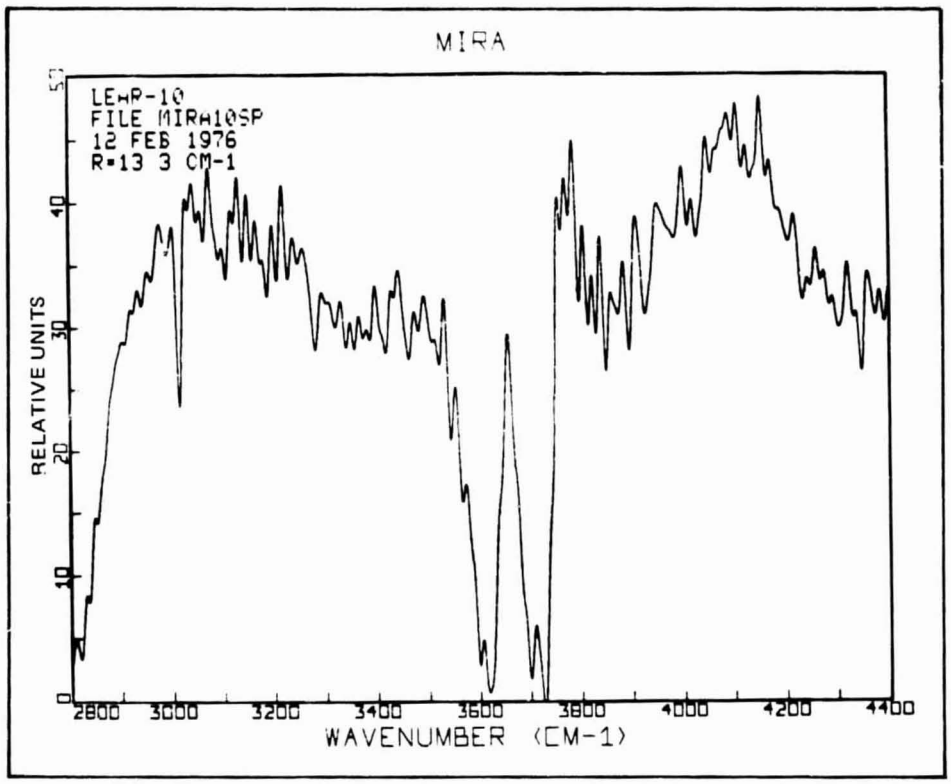

Figure 26a. Spectrum of Mira on 12 Feb 1976 in 2800-4400 cm^{-1} Region at 13.3 cm^{-1} Resolution.

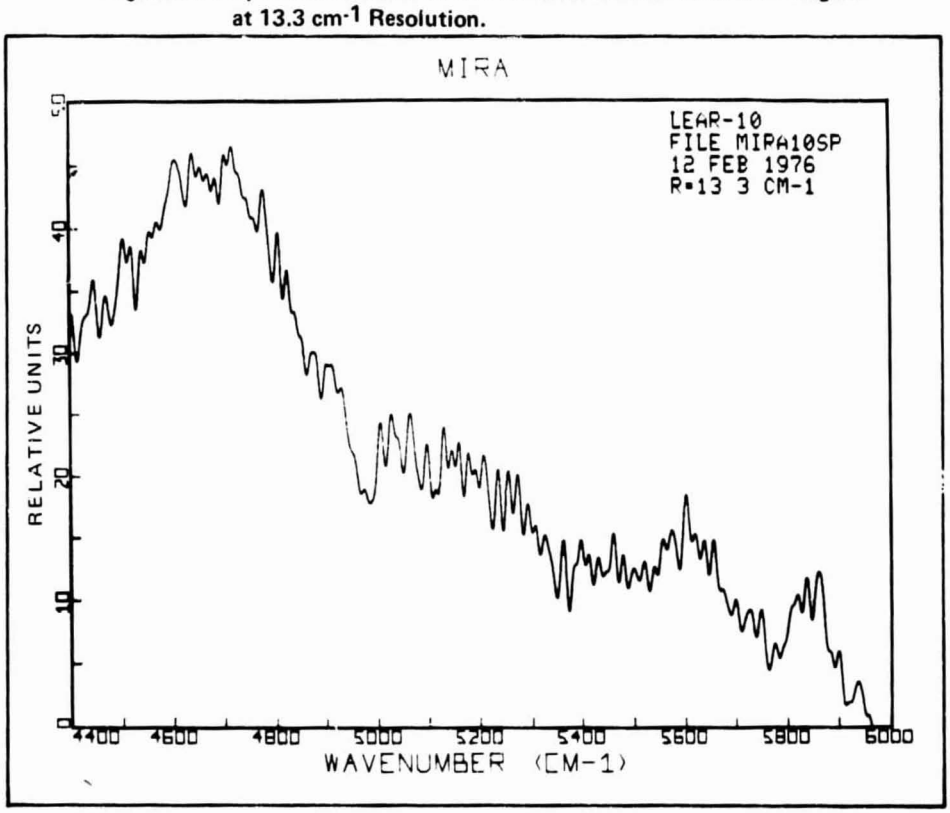

Fig. 26b Spectrum of Mira on 12 Feb 1976 in 4400-6000 cm^{-1} Region at 13.3 cm^{-1} Resolution.

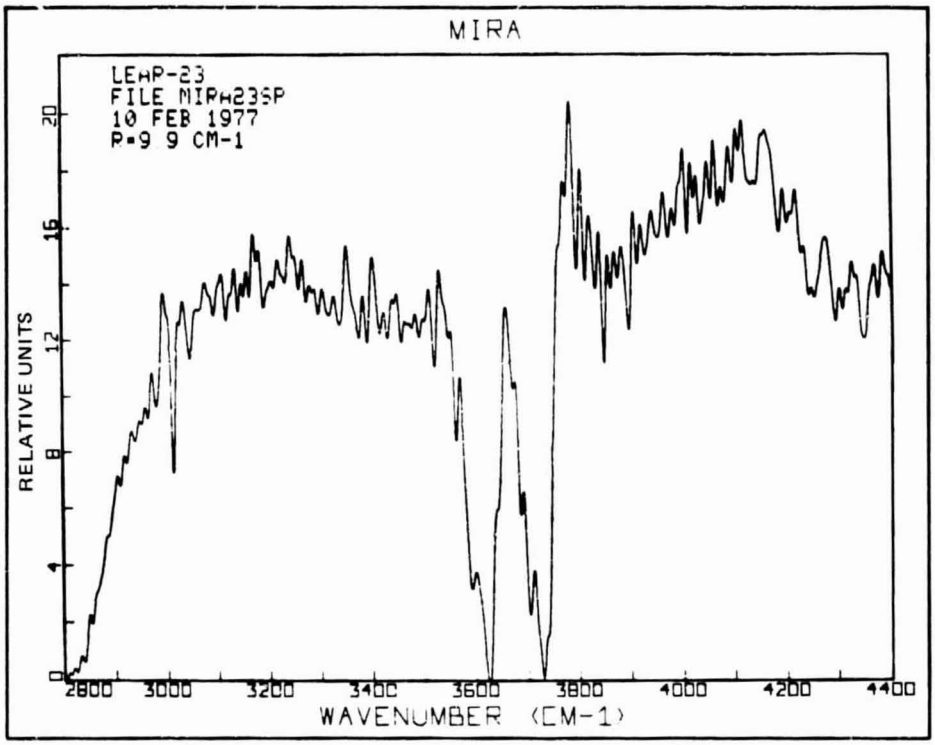

Fig. 27a Spectrum of Mira on 10 Feb 1977 in 2800-4400 cm^{-1} Region at 9.9 cm^{-1} Resolution.

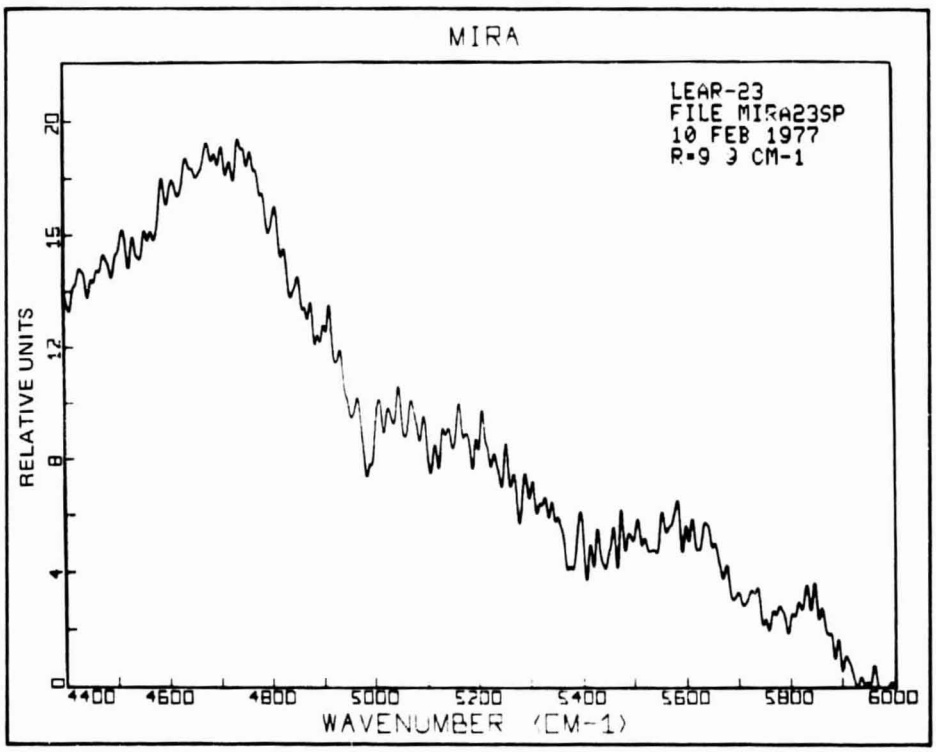

Fig. 27b Spectrum of Mira on 10 Feb 1977 in 4400-6000 cm^{-1} Region at 9.9 cm^{-1} Resolution.

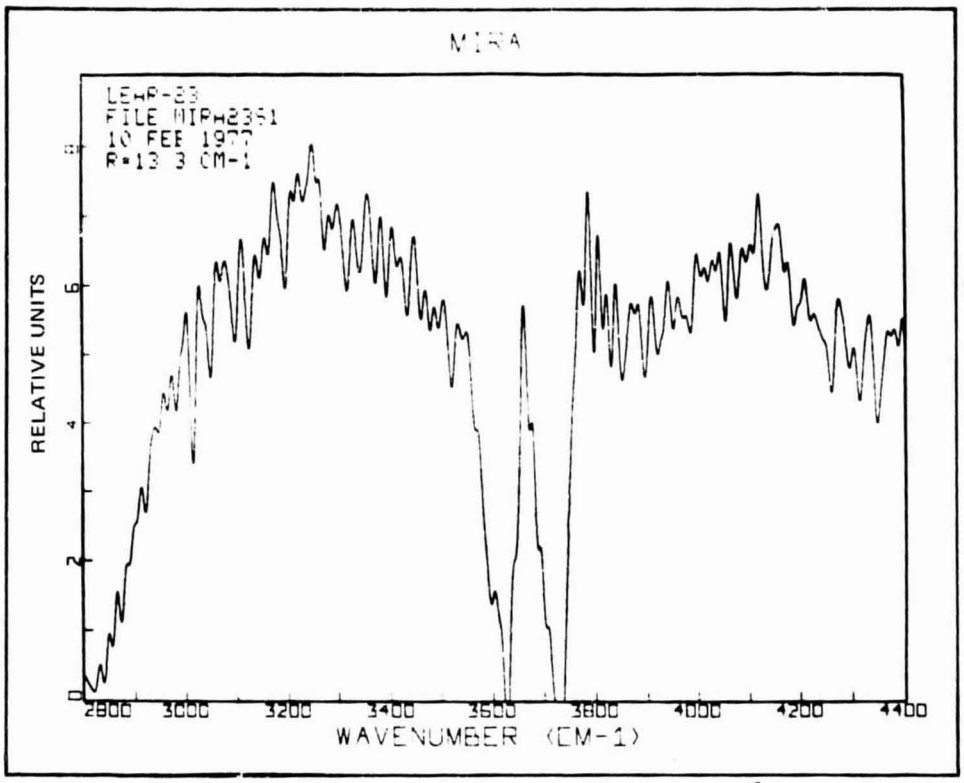

Fig. 28a Spectrum of Mira on 10 Feb 1977 in 2800-4400 cm^{-1} Region at 13.3 cm^{-1} Resolution.

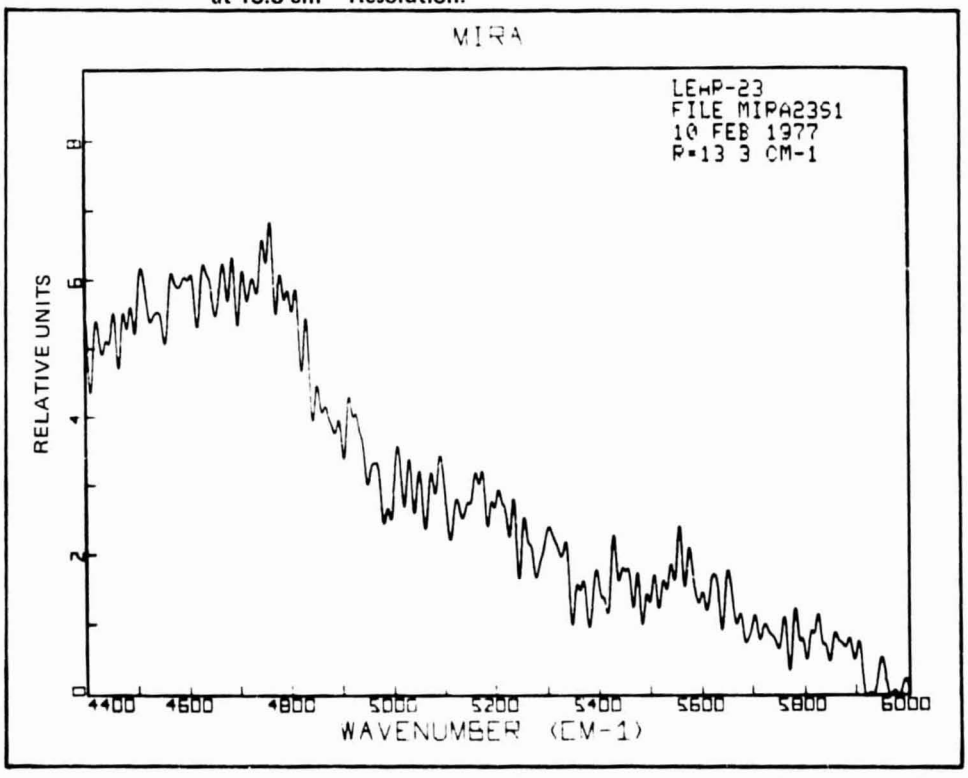

Fig. 28b Spectrum of Mira on 10 Feb 1977 in 4400-6000 cm^{-1} Region at 13.3 cm^{-1} Resolution.

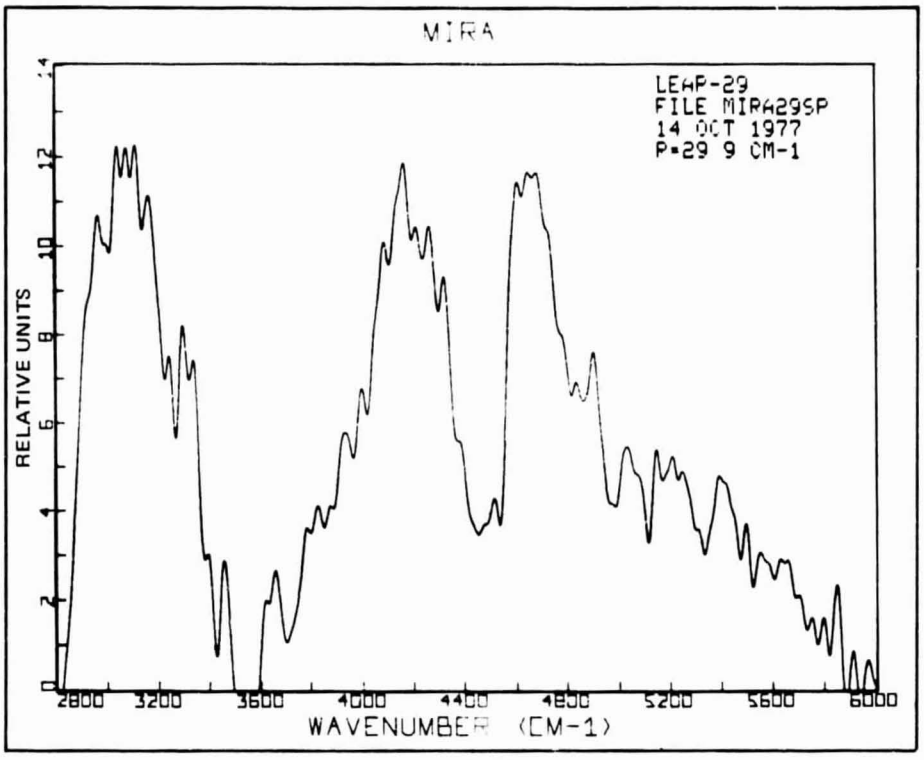

Fig. 29 Spectrum of Mira on 14 Oct 1977 in 2800-6000 cm^{-1} Region at 29.9 cm^{-1} Resolution.

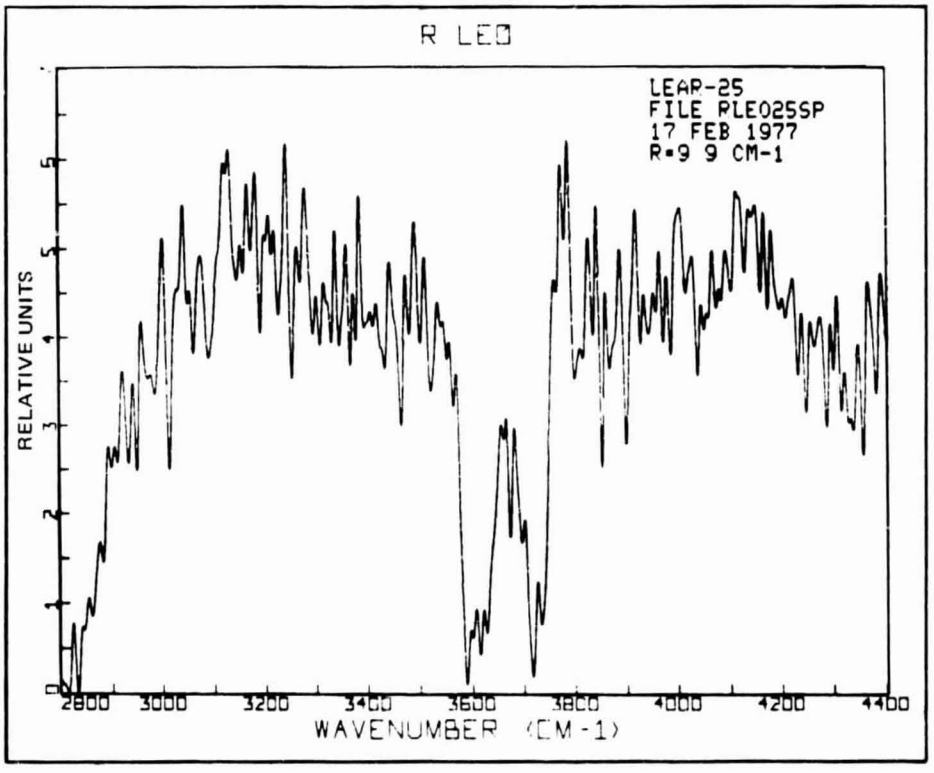

Fig. 30a Spectrum of R Leo on 17 Feb 1977 in 2800-4400 cm^{-1} Region at 9.9 cm^{-1} Resolution.

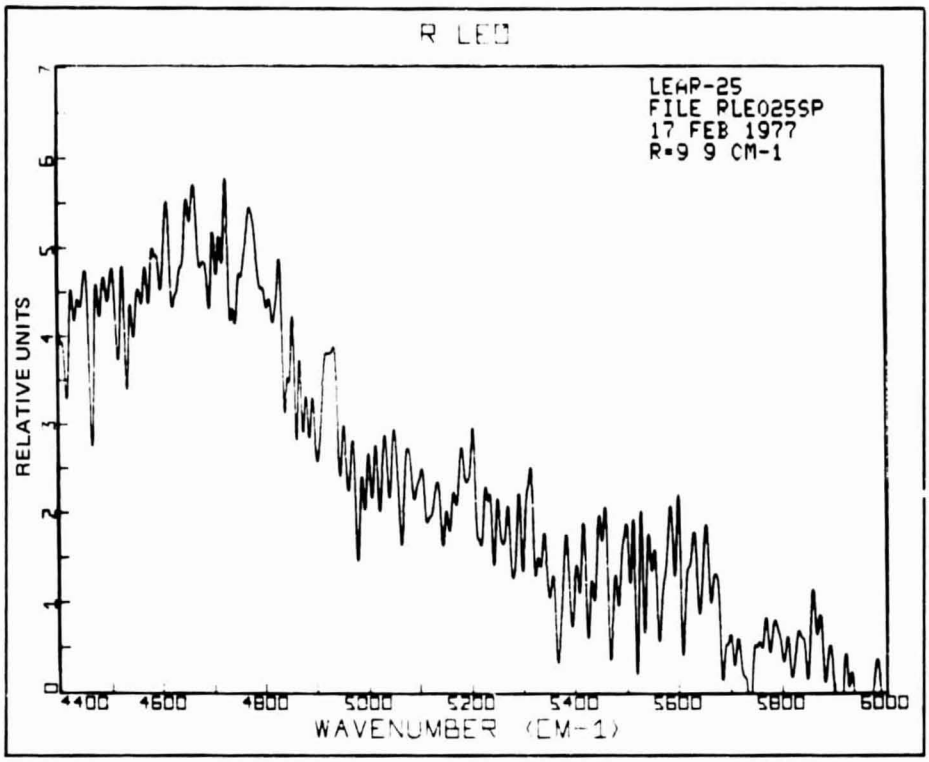

Fig. 30b Spectrum of R Leo on 17 Feb 1977 in 4400-6000 cm^{-1} Region at 9.9 cm^{-1} Resolution.

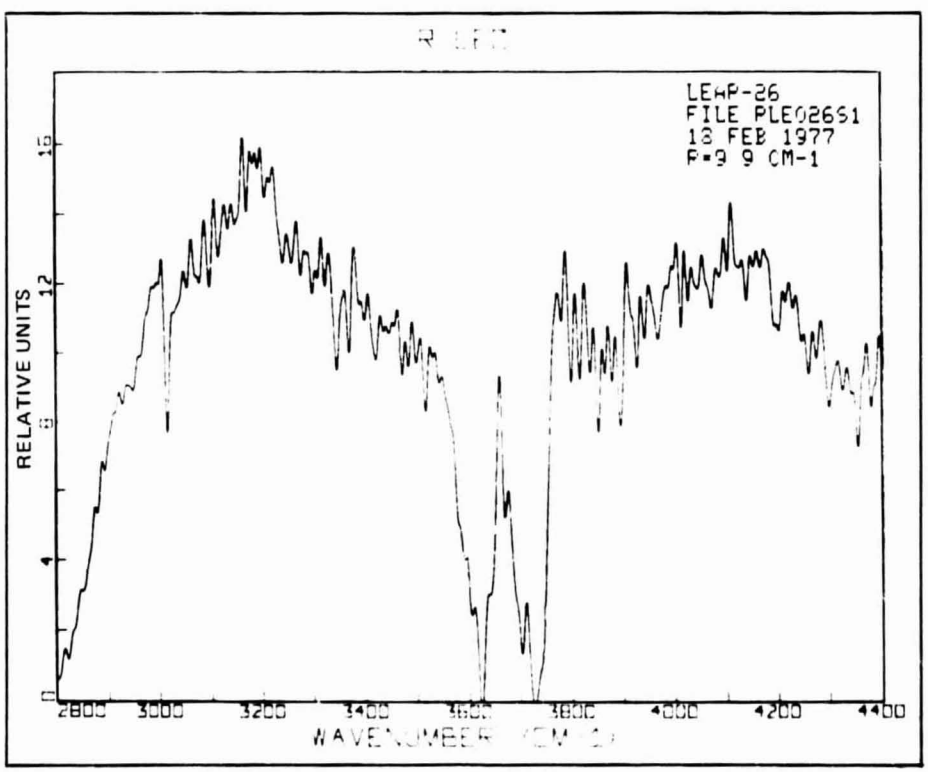

Fig. 31a Spectrum of R Leo on 18 Feb 1977 in 2800-4400 cm^{-1} Region at 9.9 cm^{-1} Resolution.

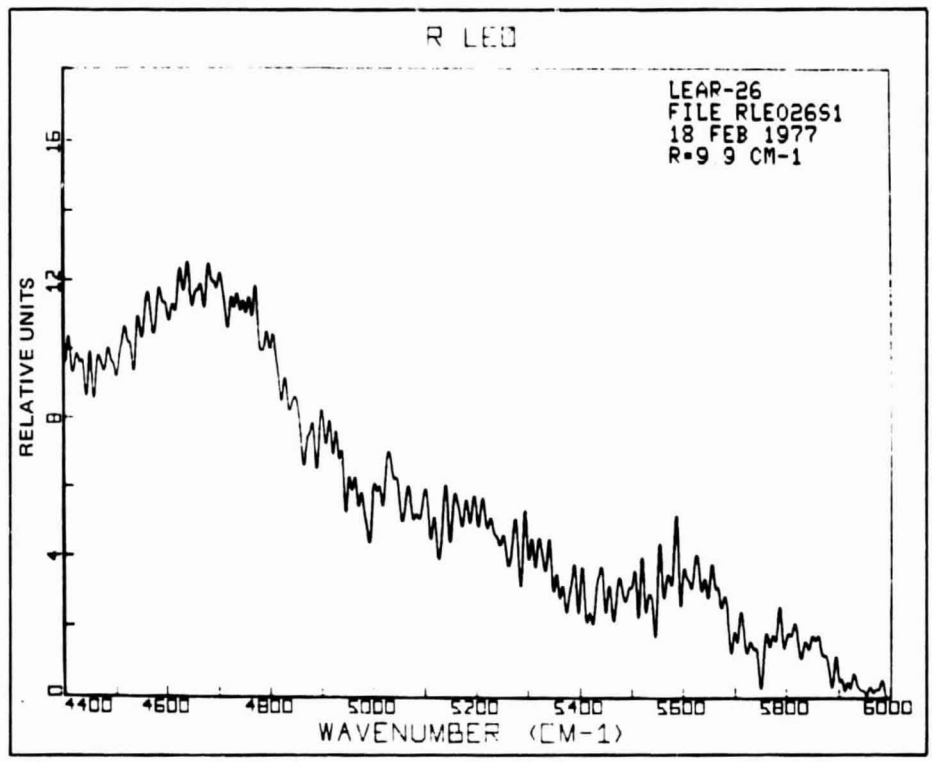

Fig. 31b Spectrum of R Leo on 18 Feb 1977 in 4400-6000 cm^{-1} Region at 9.9 cm^{-1} Resolution.

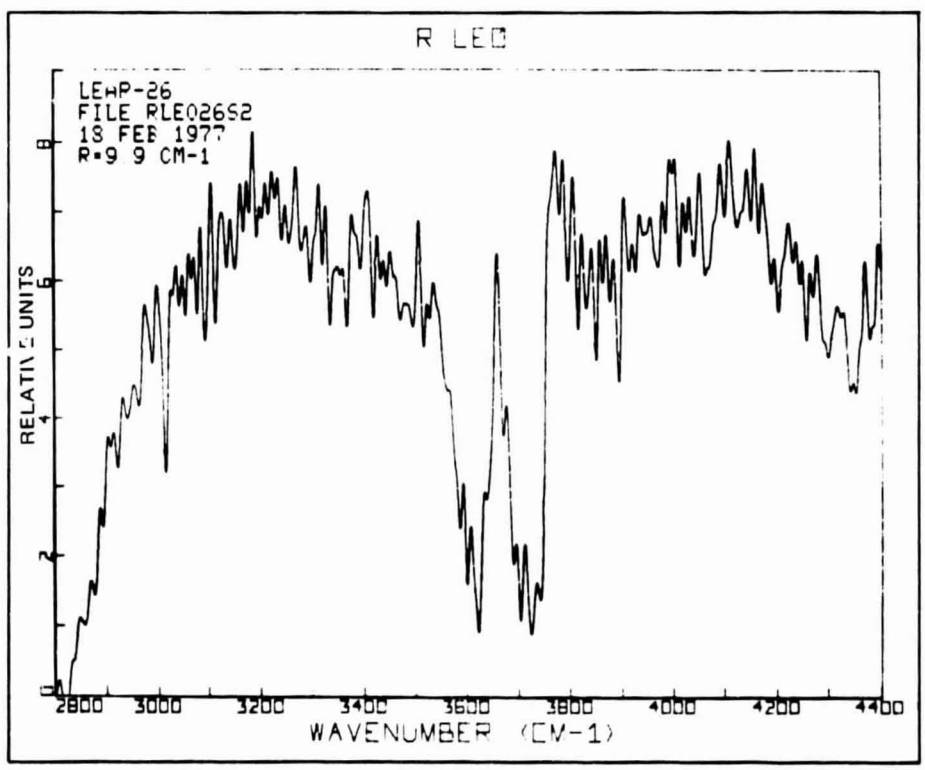

Fig. 32a Spectrum of R Leo on 18 Feb 1977 in 2800-4400 cm^{-1} Region at 9.9 cm^{-1} Resolution.

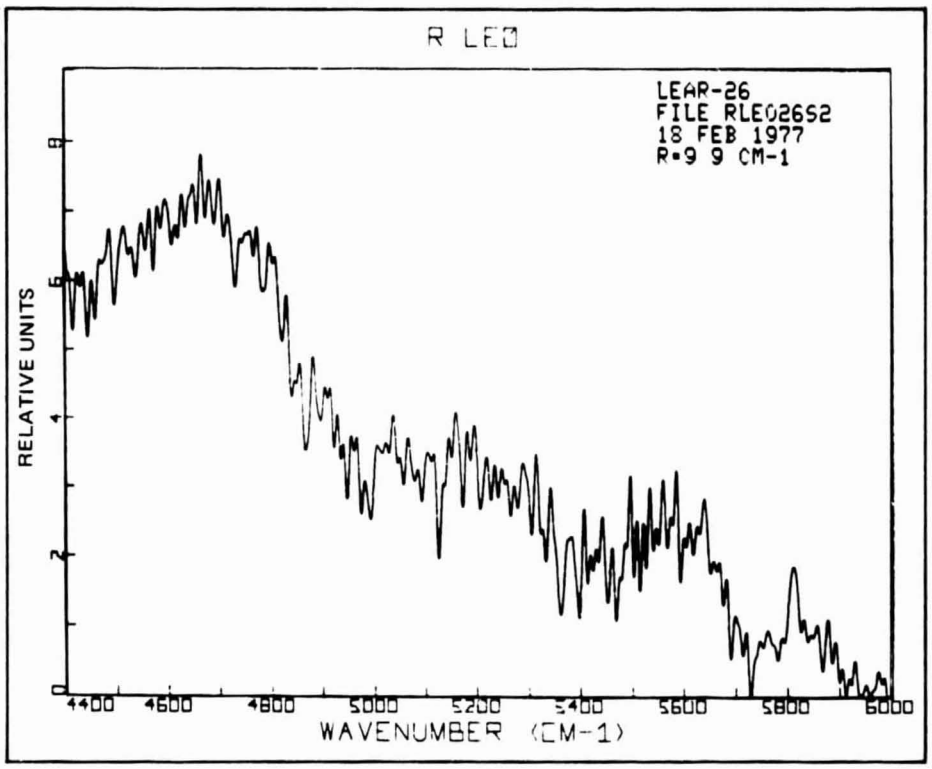

Fig. 32b Spectrum of R Leo on 18 Feb 1977 in 4400-6000 cm^{-1} Region at 9.9 cm^{-1} Resolution.

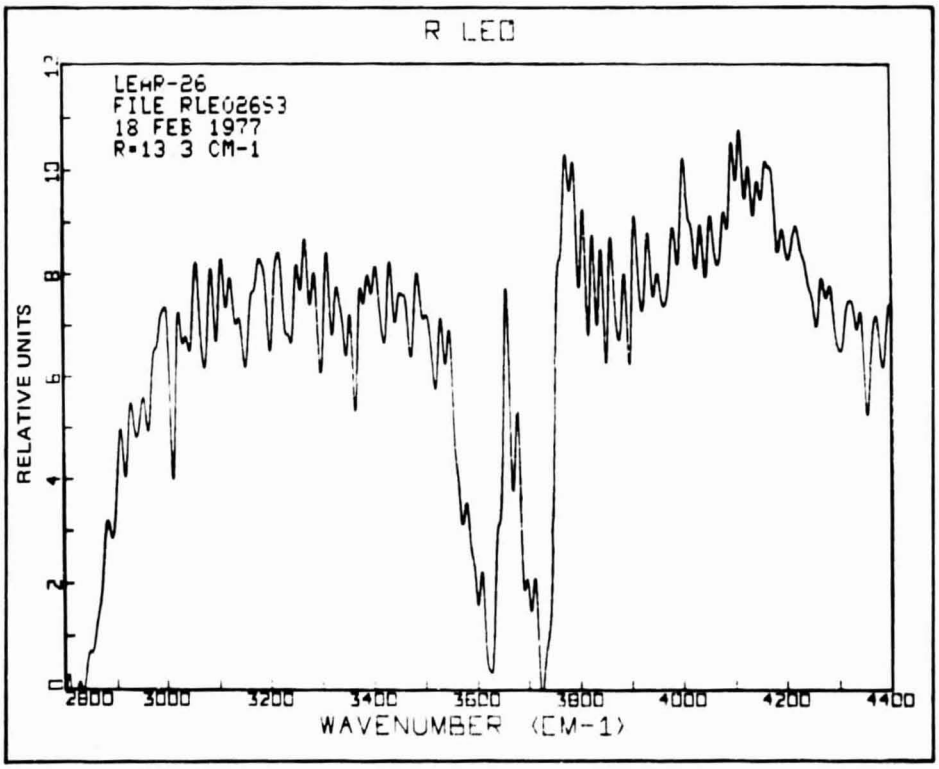

Fig. 33a Spectrum of R Leo on 18 Feb 1977 in 2800-4400 cm^{-1} Region at 13.3 cm^{-1} Resolution.

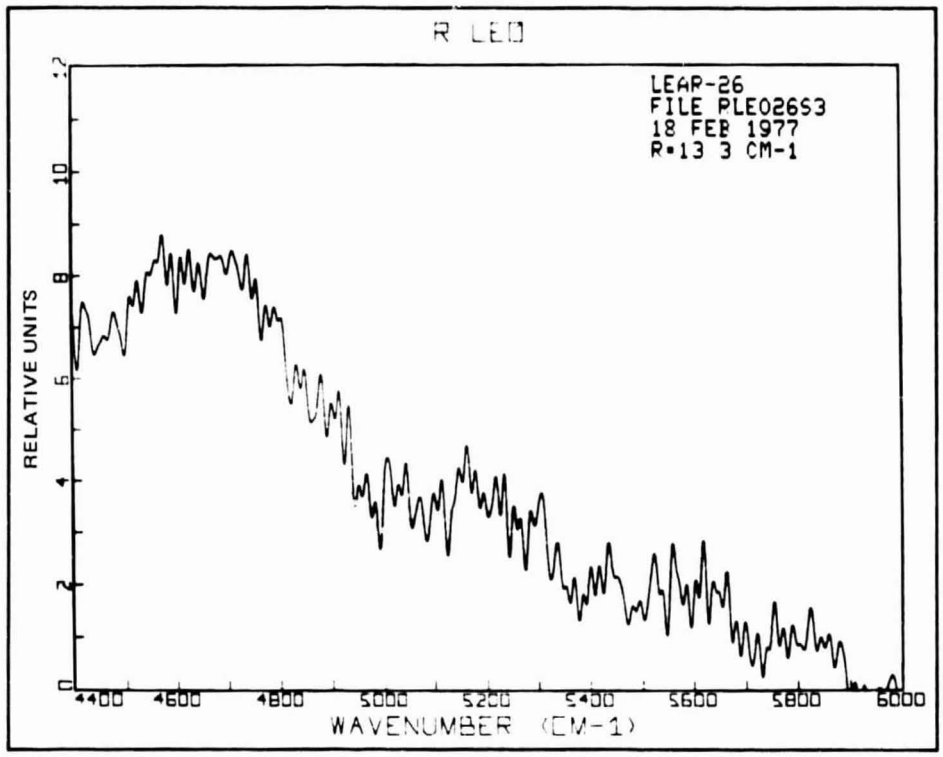

Fig. 33b Spectrum of R Leo on 18 Feb 1977 in 4400-6000 cm^{-1} Region at 13.3 cm^{-1} Resolution.

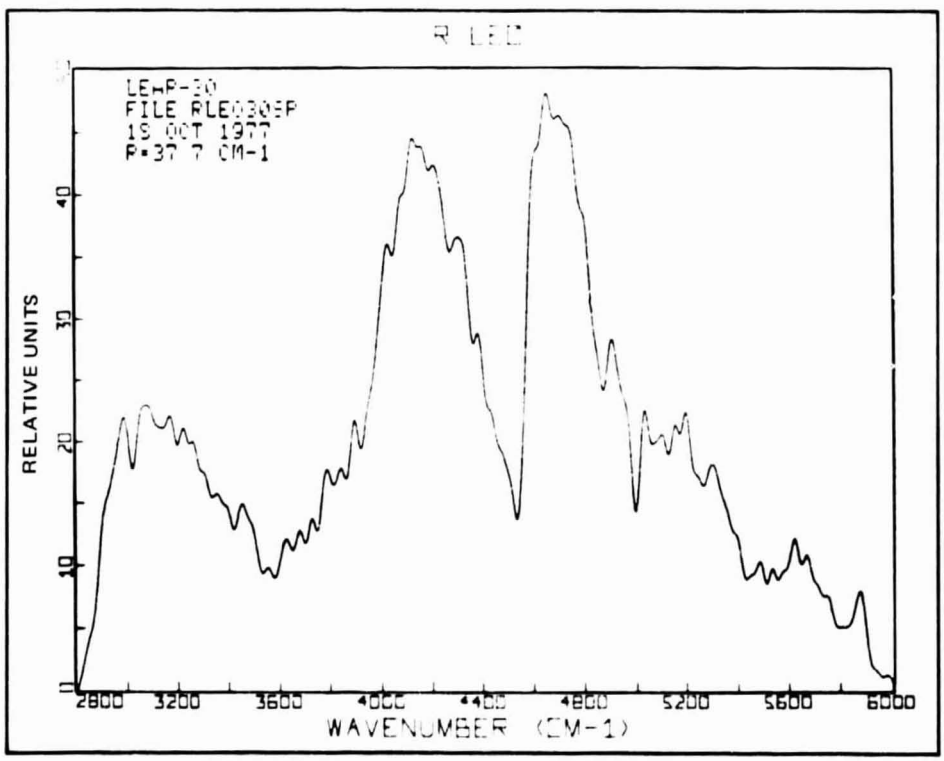

Fig. 34 Spectrum of R Leo on 18 Oct 1977 in 2800-6000 cm^{-1} Region at 37.7 cm^{-1} Resolution.

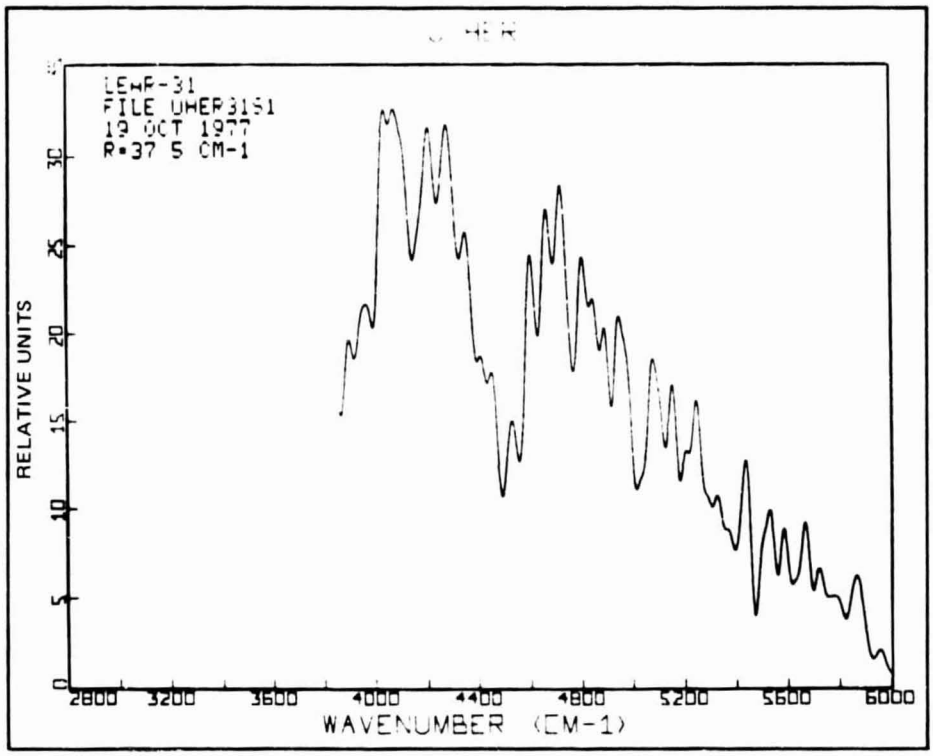

Fig. 35 Spectrum of U Her on 19 Oct 1977 in 2800-6000 cm^{-1} Region at 37.5 cm^{-1} Resolution.

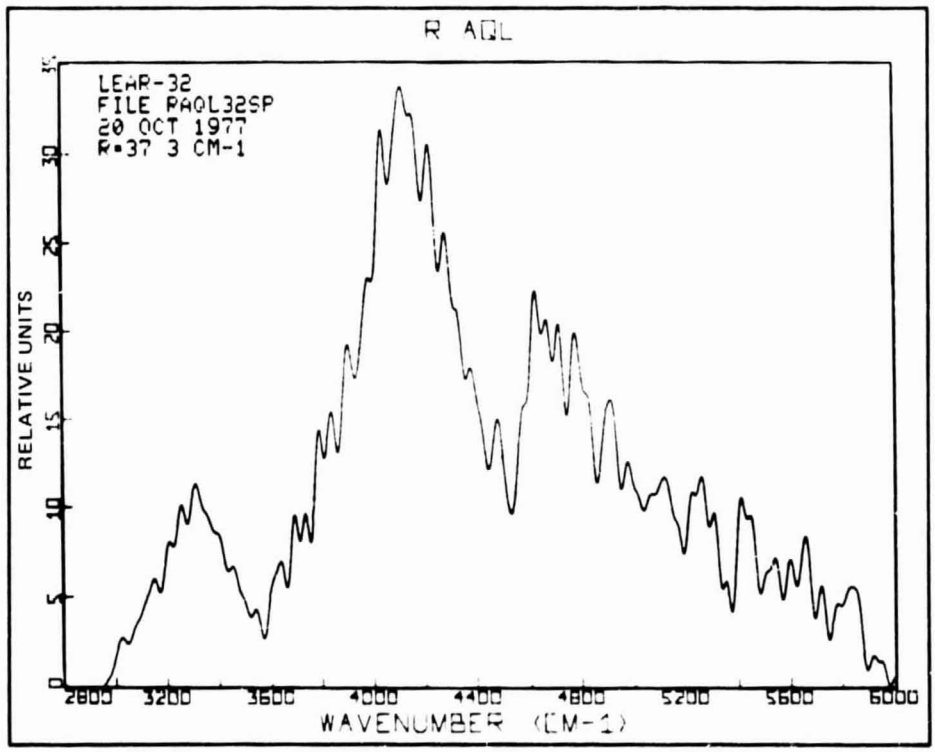

Fig. 36 Spectrum of R Aql on 20 Oct 1977 in 2800-6000 cm^{-1} Region at 37.3 cm^{-1} Resolution.

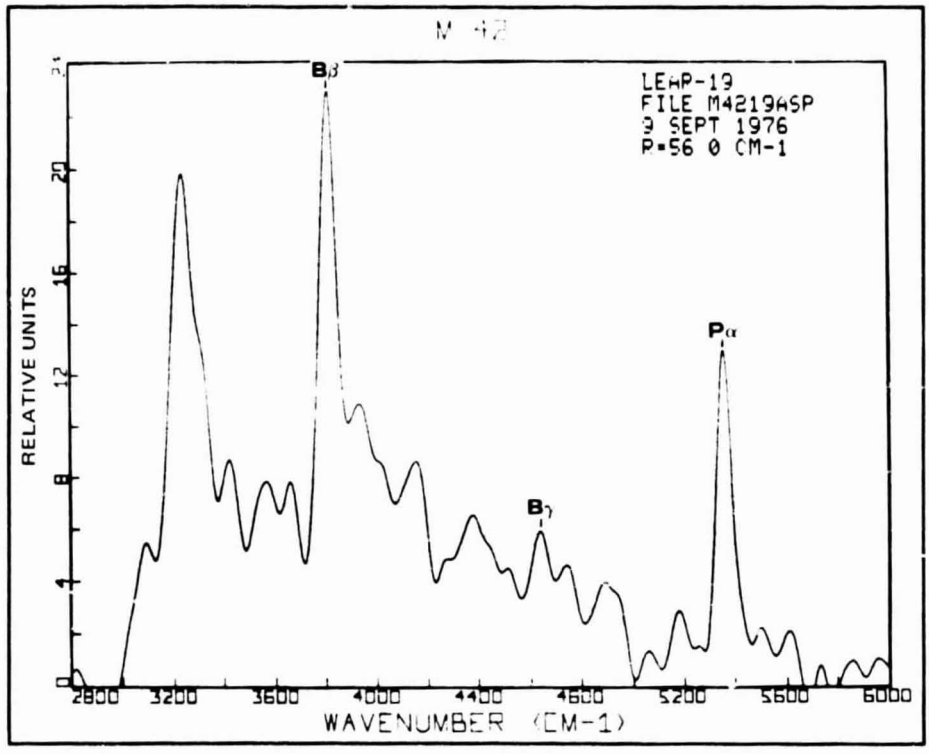

Fig. 37 Spectrum of M 42 on 9 Sept 1976 in 2800-6000 cm^{-1} Region at 56.0 cm^{-1} Resolution. The Hydrogen Emission Lines Paschen α, Brackett β, and Brackett γ are Shown.

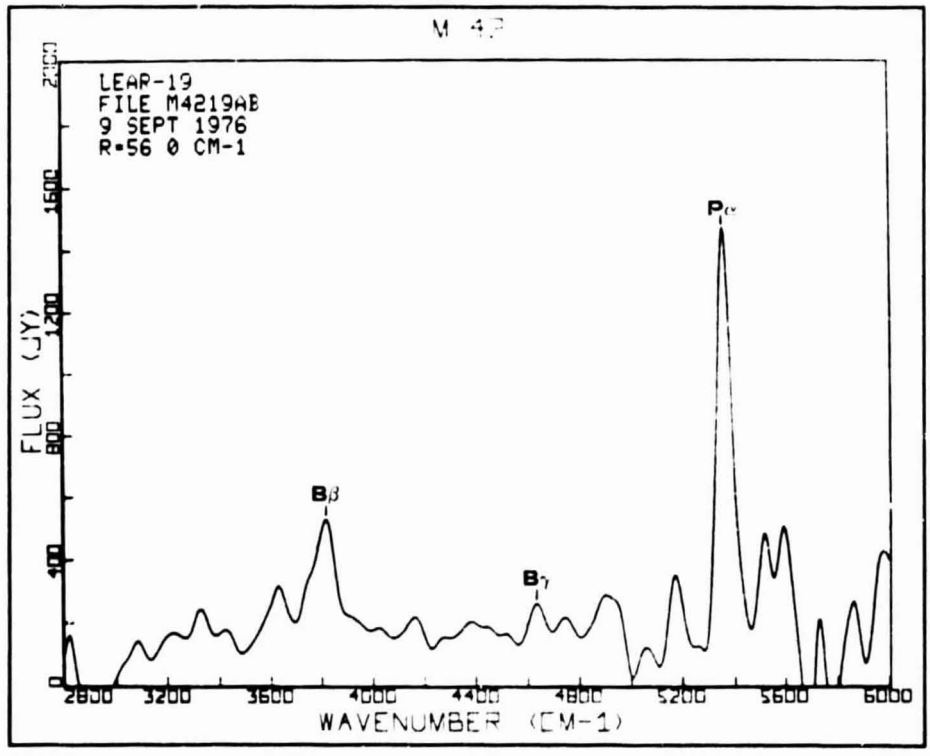

Fig. 38 Spectrum of M 42 on 9 Sept 1976 in 2800-6000 cm^{-1} Region at 56.0 cm^{-1} Resolution in Janskys. The Hydrogen Emission Lines, Pasches α, Brackett β and Brackett γ are Shown.

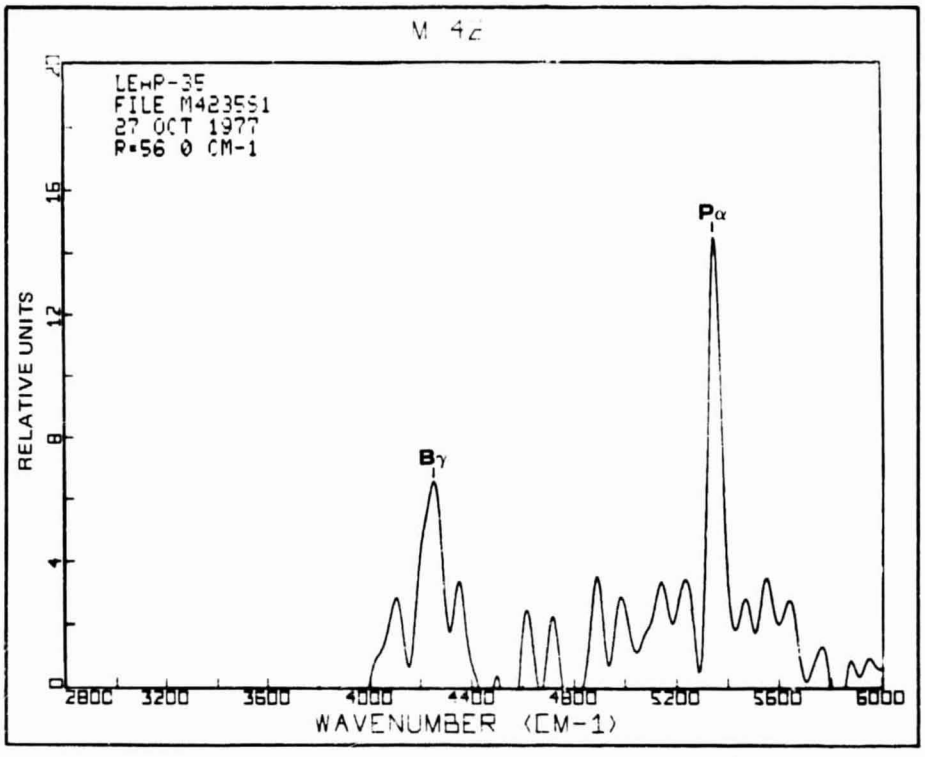

Fig. 39 Spectrum of M 42 on 27 Oct 1977 in 2800-6000 cm^{-1} Region at 56.0 cm^{-1} Resolution. The Hydrogen Emission Lines Paschen α and Brackett γ are Shown.

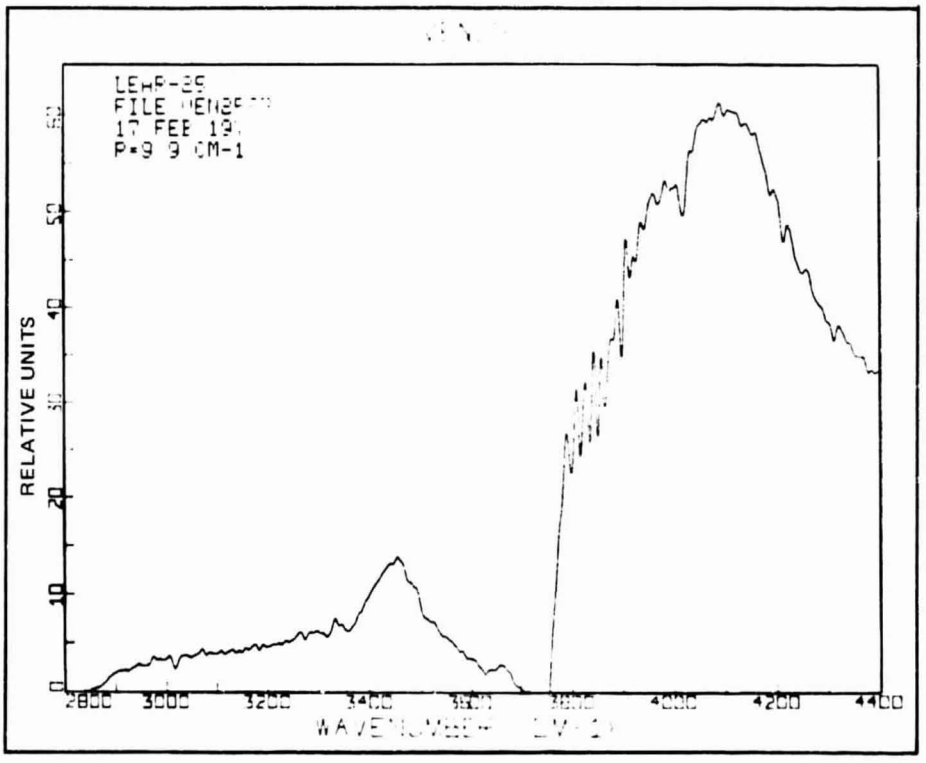

Fig. 40a Spectrum of Venus on 17 Feb 1977 in 2800-4400 cm^{-1} Region at 9.9 cm^{-1} Resolution.

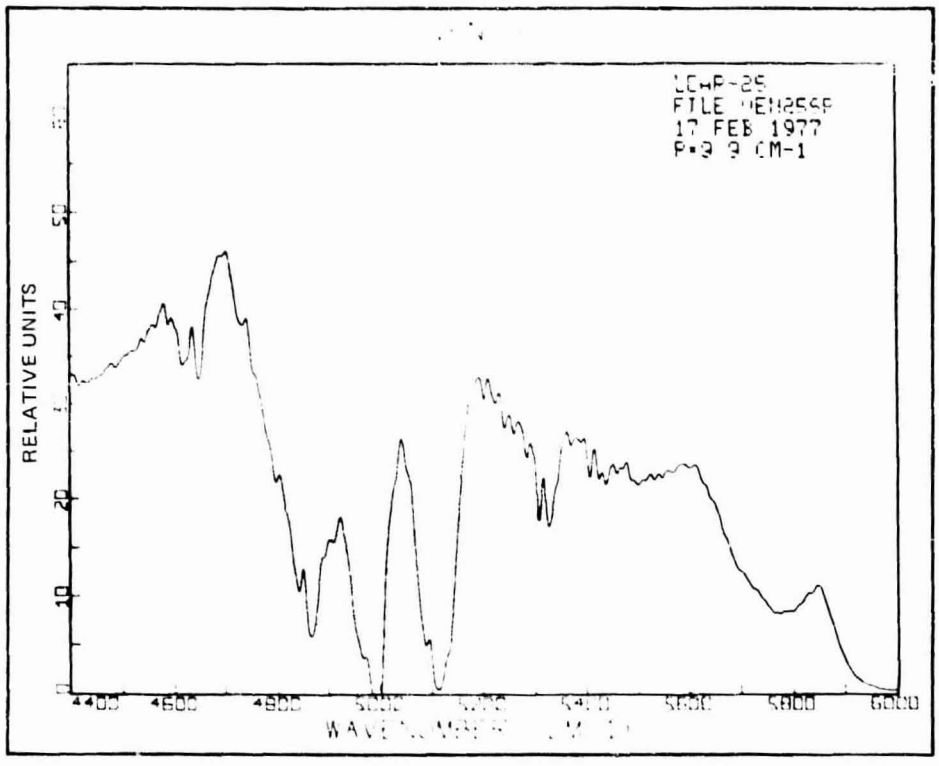

Fig. 40b Spectrum of Venus on 17 Feb 1977 in 4400-6000 cm^{-1} Region at 9.9 cm^{-1} Resolution.

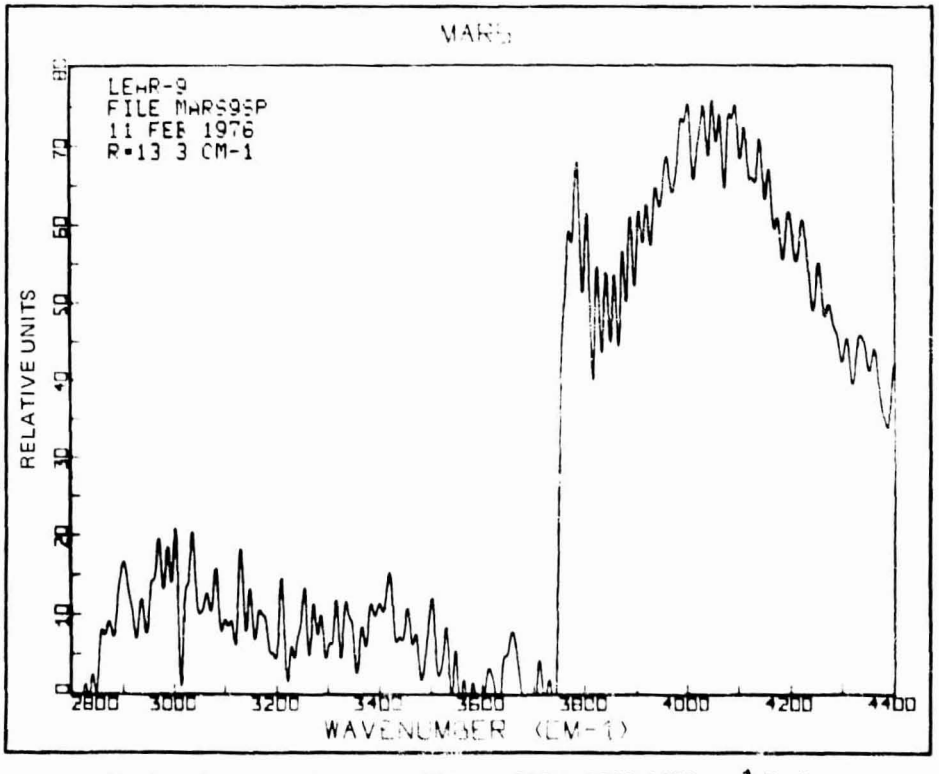

Fig. 41a Spectrum of Mars on 11 Feb 1976 in 2800-4400 cm^{-1} Region at 13.3 cm^{-1} Resolution.

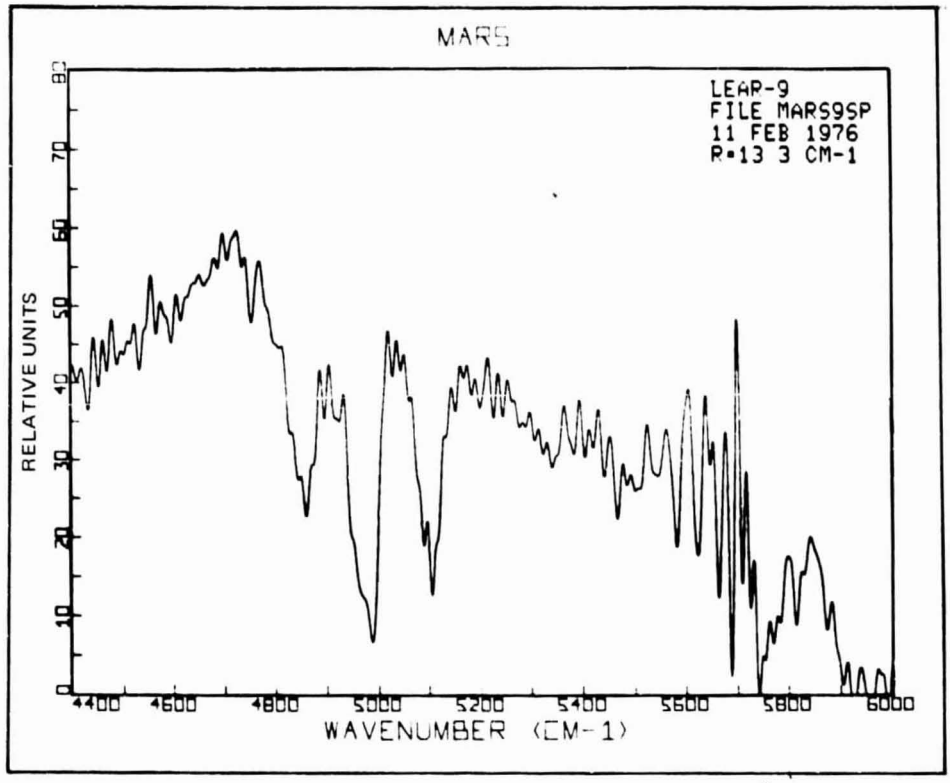

Fig. 41b Spectrum of Mars on 11 Feb 1976 in 4400-6000 cm^{-1} Region at 13.3 cm^{-1} Resolution.

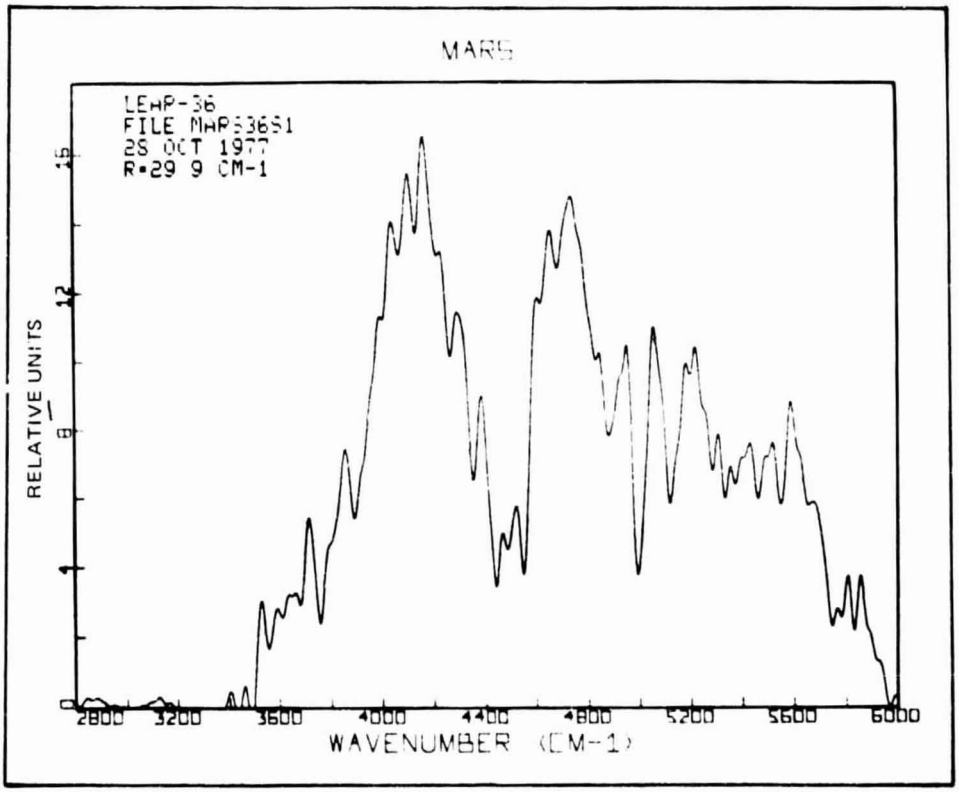

Fig. 42 Spectrum of Mars on 28 Oct 1977 in 2800-6000 cm^{-1} Region at 29.9 cm^{-1} Resolution.

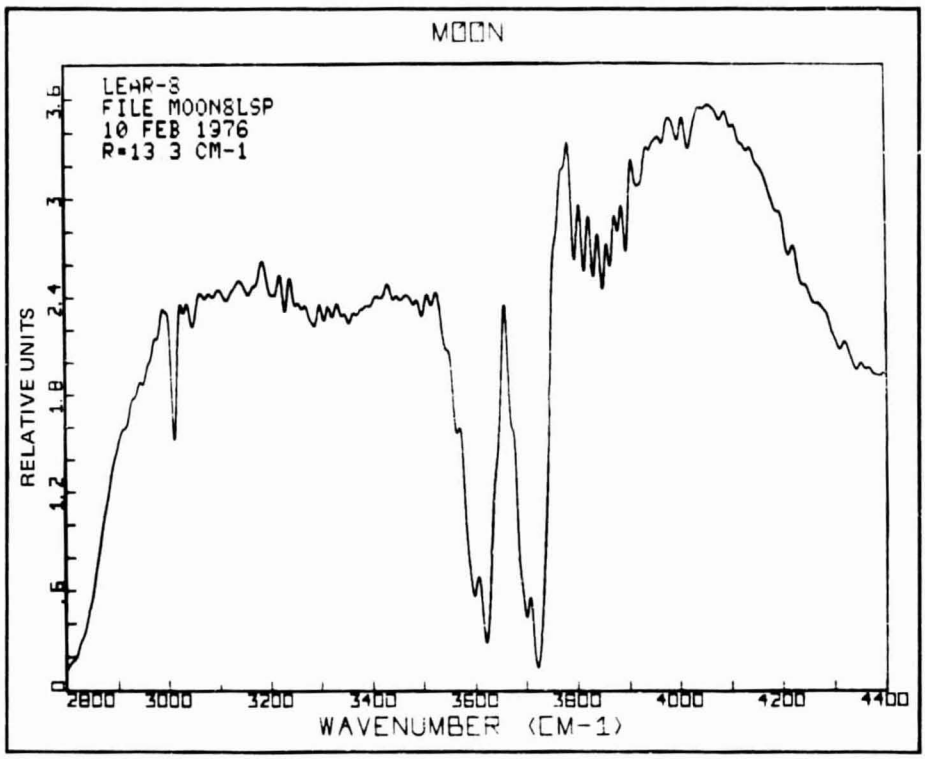

Fig. 43a Spectrum of Moon on 10 Feb 1976 in 2800-4400 cm^{-1} Region at 13.3 cm^{-1} Resolution.

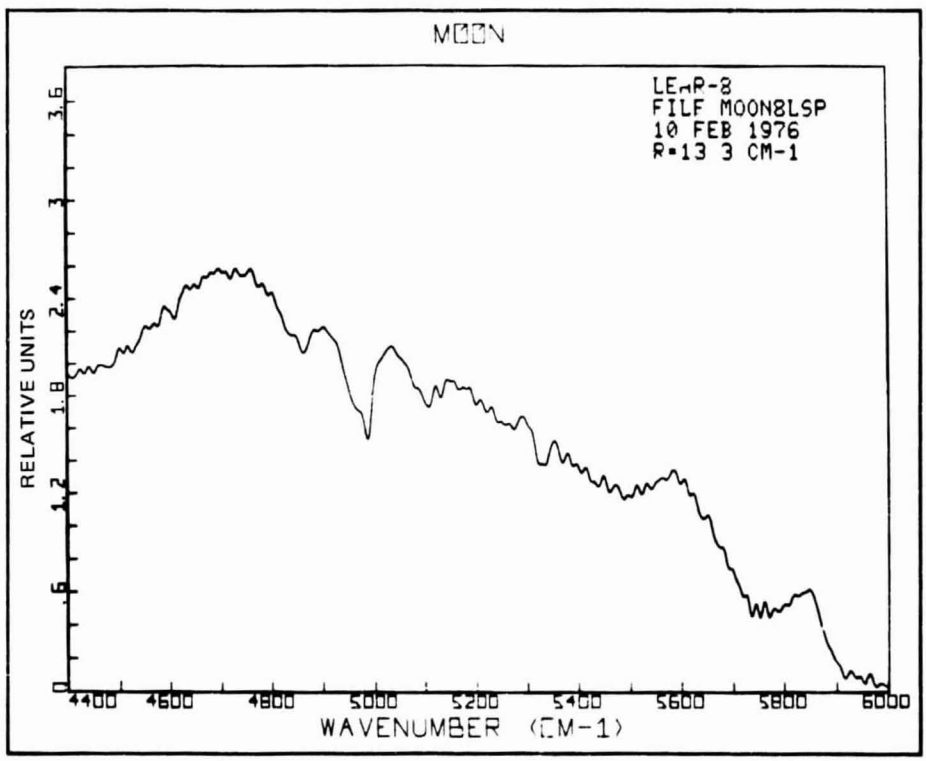

Fig. 43b Spectrum of Moon on 10 Feb 1976 in 4400-6000 cm^{-1} Region at 13.3 cm^{-1} Resolution.

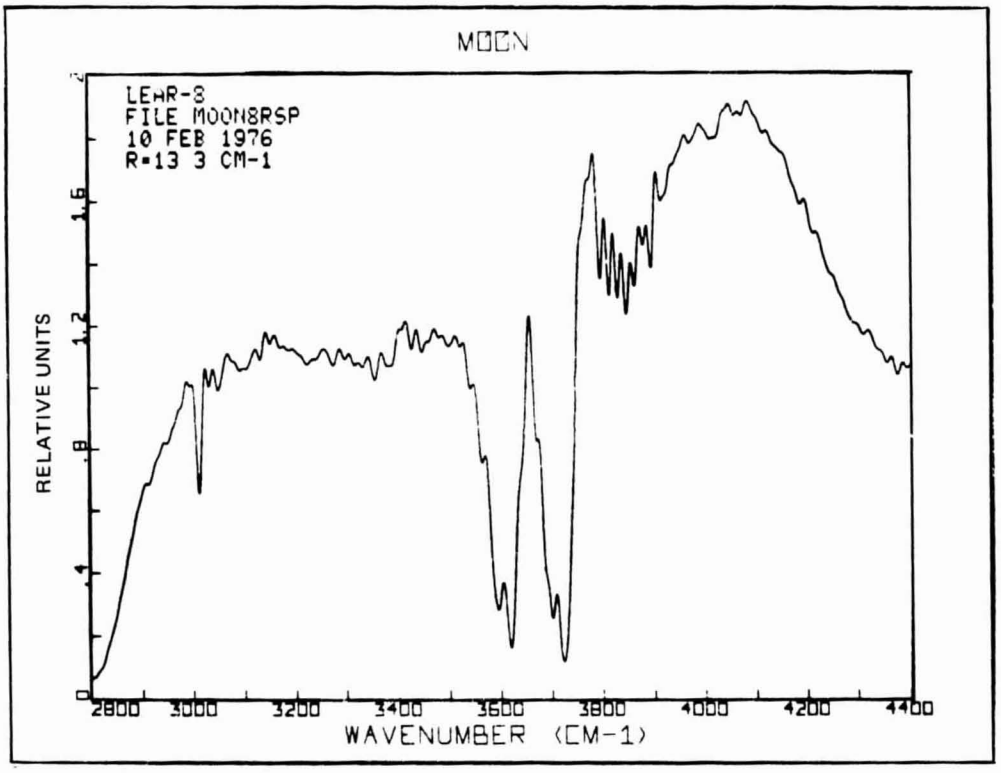

Fig. 44a Spectrum of Moon on 10 Feb 1976 in 2800-4400 cm^{-1} Region at 13.3 cm^{-1} Resolution.

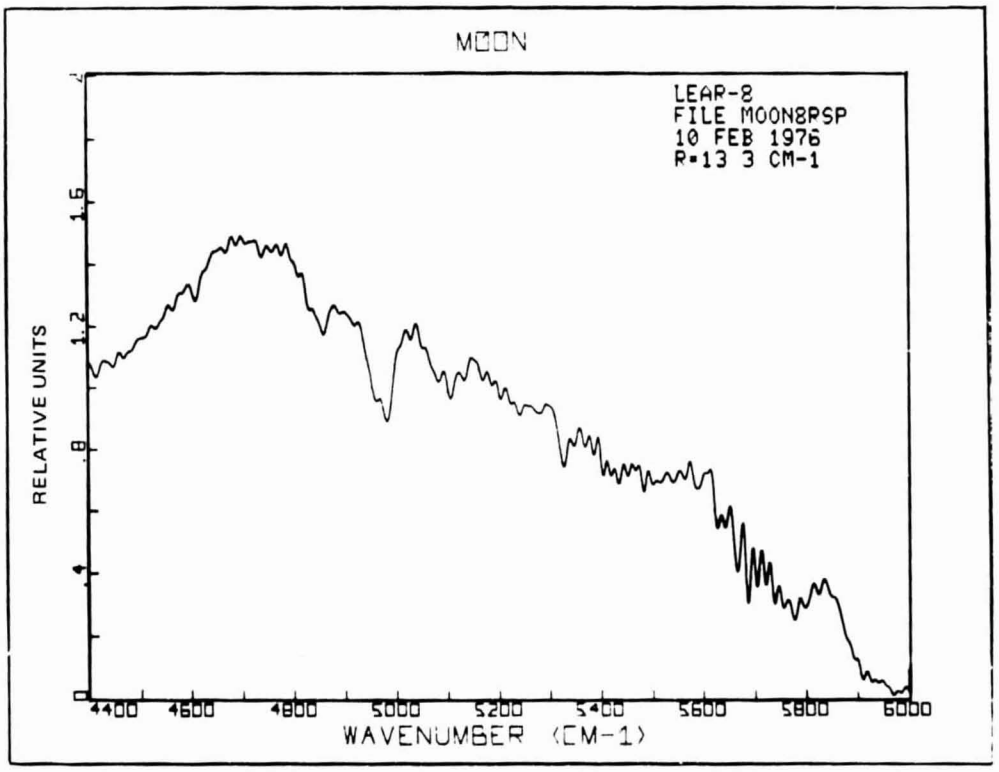

Fig. 44b Spectrum of Moon on 10 Feb 1976 in 4400-6000 cm^{-1} Region at 13.3 cm^{-1} Resolution.

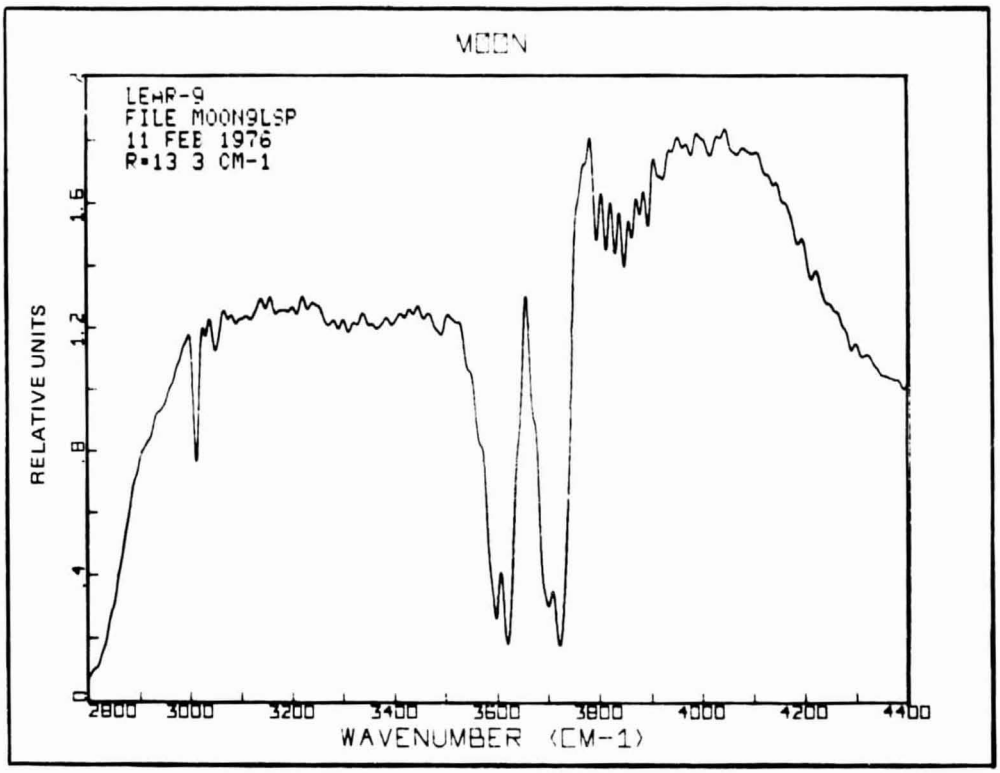

Fig. 45a Spectrum of Moon on 11 Feb 1976 in 2800-4400 Region at 13.3 cm^{-1} Resolution.

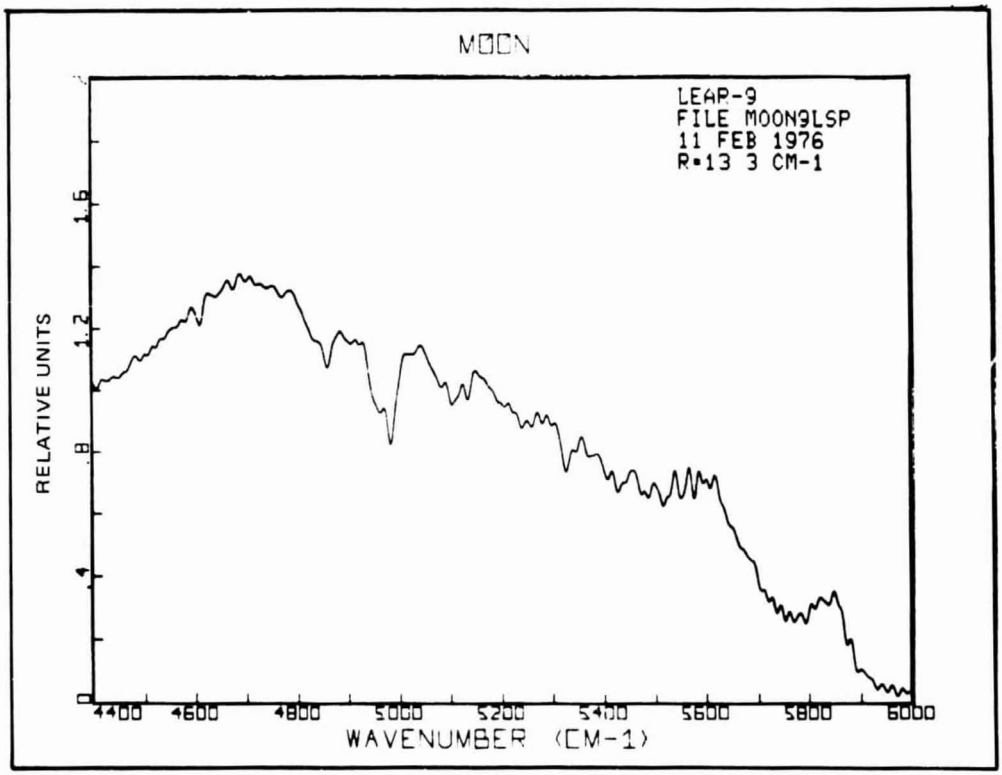

Fig. 45b Spectrum of Moon on 11 Feb 1976 in 4400-6000 Region at 13.3 cm^{-1} Resolution.

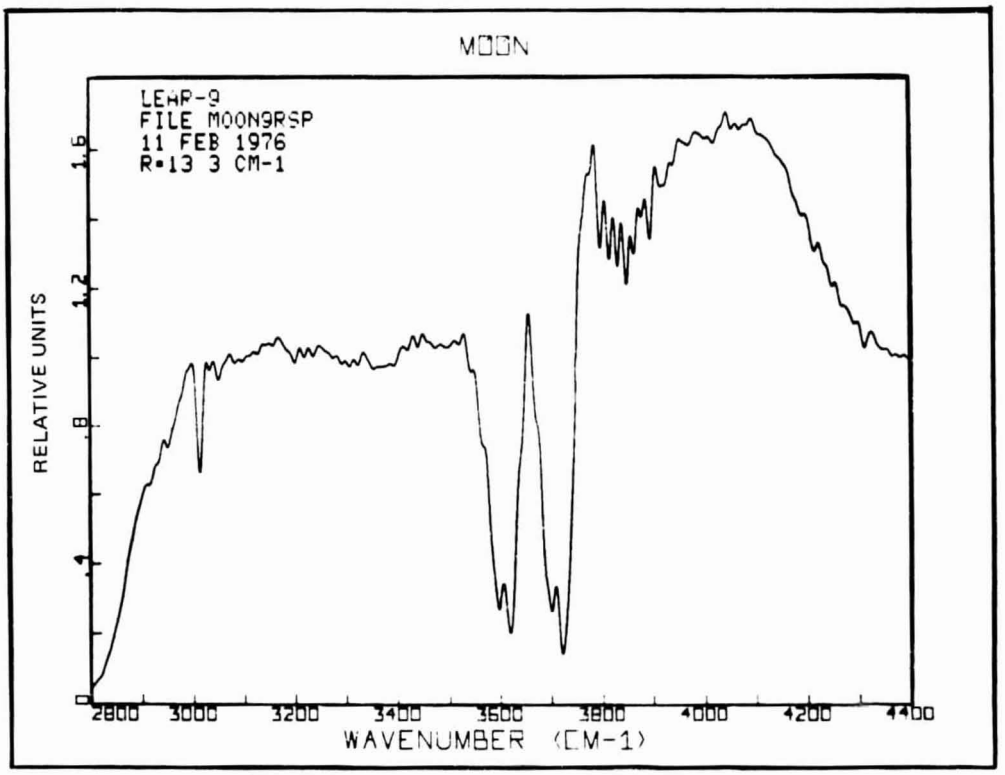

Fig. 46a Spectrum of Moon on 11 Feb 1976 in 2800-4400 cm^{-1} Region at 13.3 cm^{-1} Resolution.

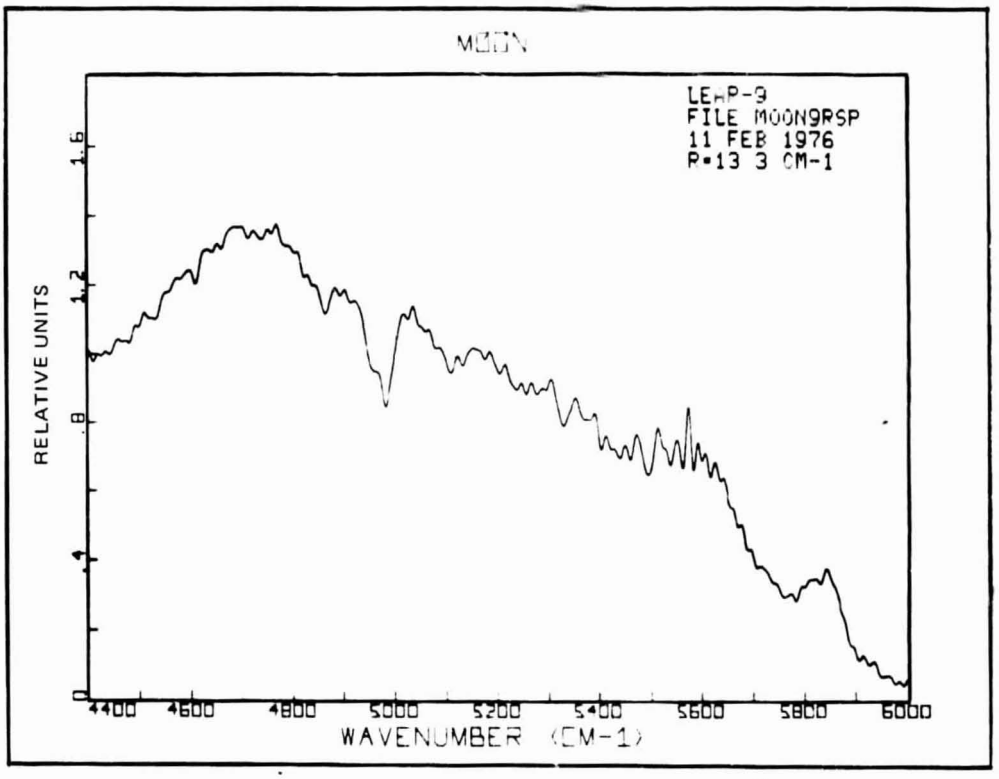

Fig. 46b Spectrum of Moon on 11 Feb 1976 4400-6000 cm^{-1} Region at 13.3 cm^{-1} Resolution.

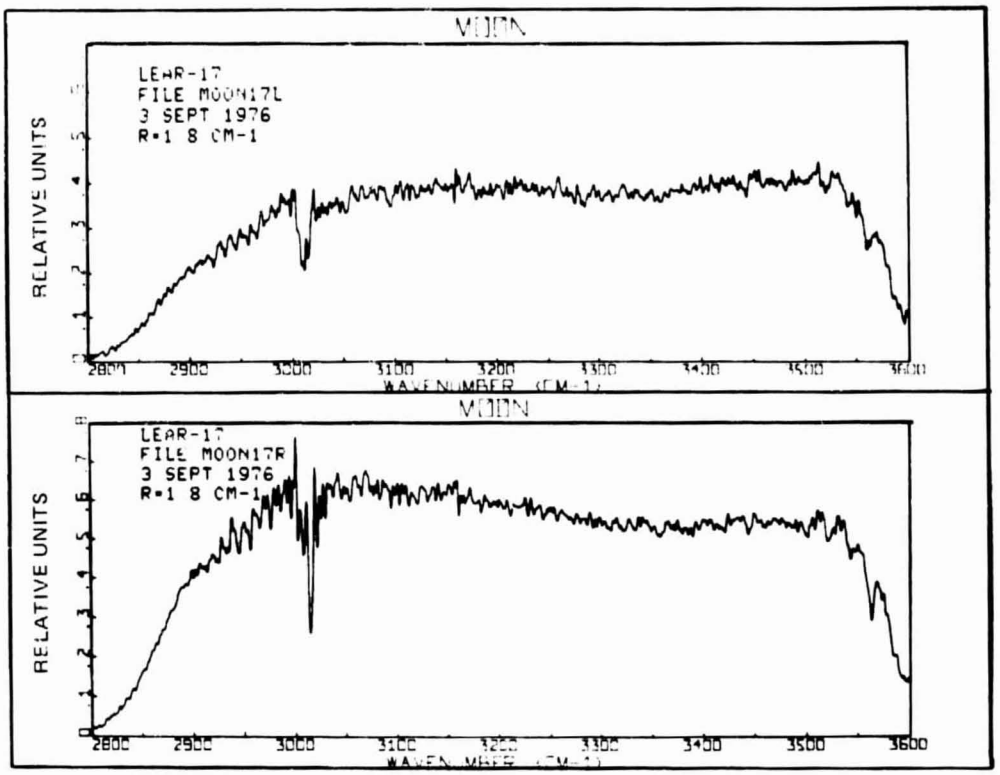

Fig. 47a,b Spectrum of Moon on 3 Sept 1976 in 2800-3600 cm-1 region at 1.8 cm-1 resolution. Upper curve (a) is L aperture and lower curve (b) is R aperture.

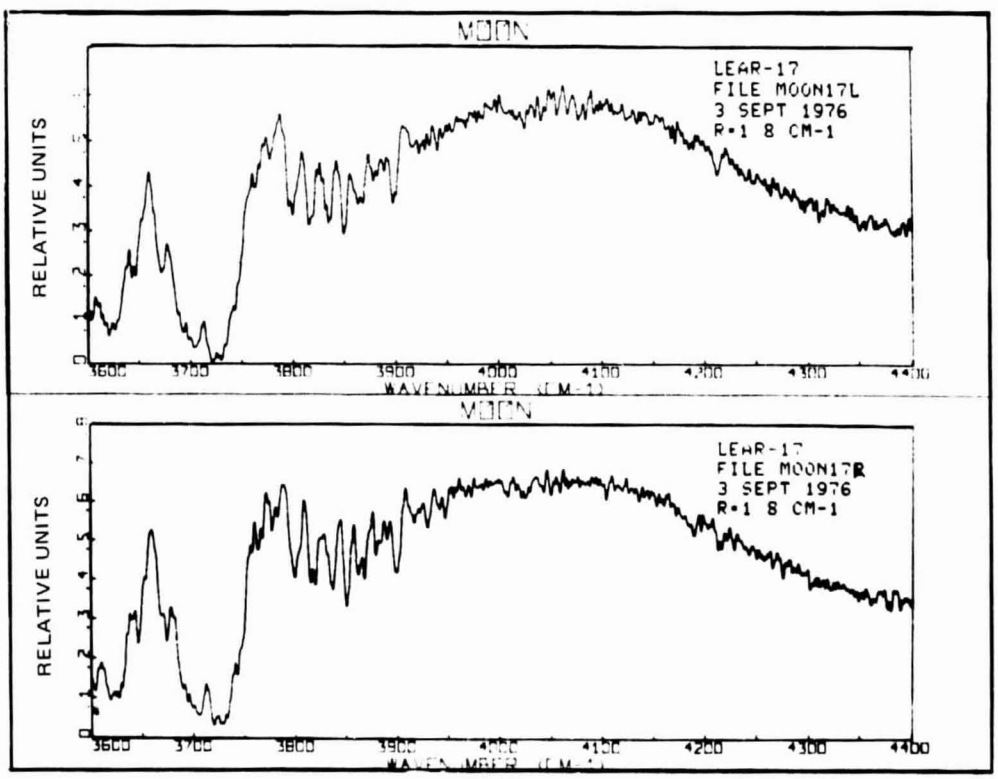

Fig. 47c, d Spectrum of Moon on 3 Sept 1976 in 3600-4400 cm-1 region at 1.8 cm-1 resolution. Upper curve (c) is L aperture and lower curve (d) is R aperture.

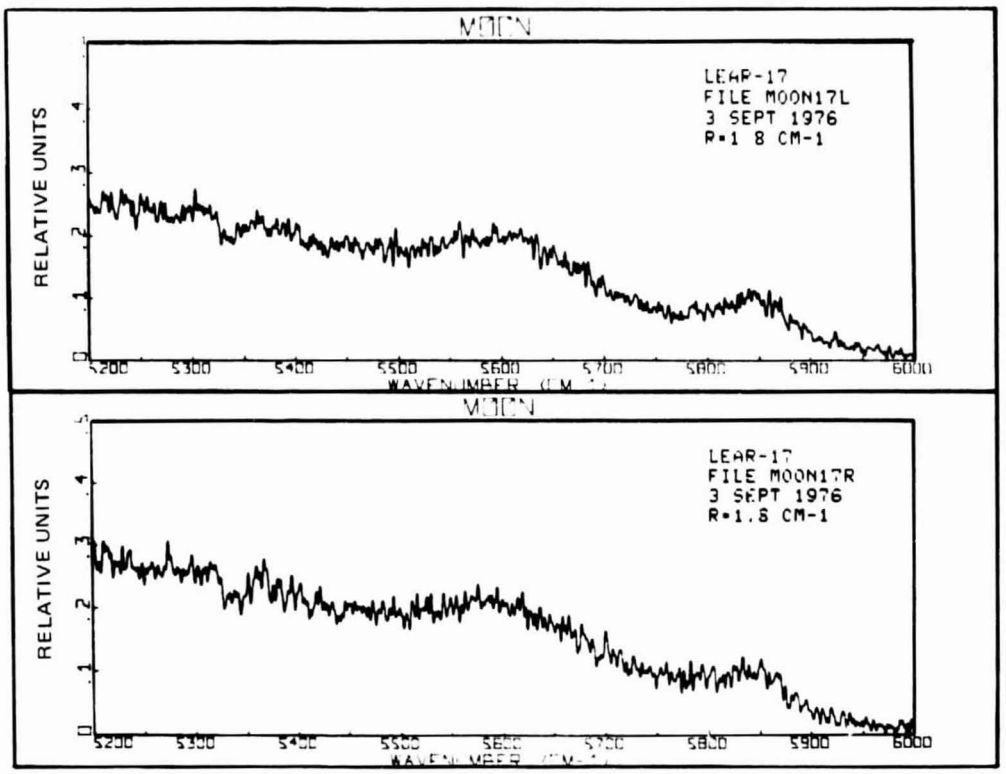

Fig. 47e,f Spectrum of Moon on 3 Sept 1976 in 5200-6000 cm^{-1} region at 1.8 cm-1 resolution. Upper curve (e) is L aperture and lower curve (f) is R aperture.

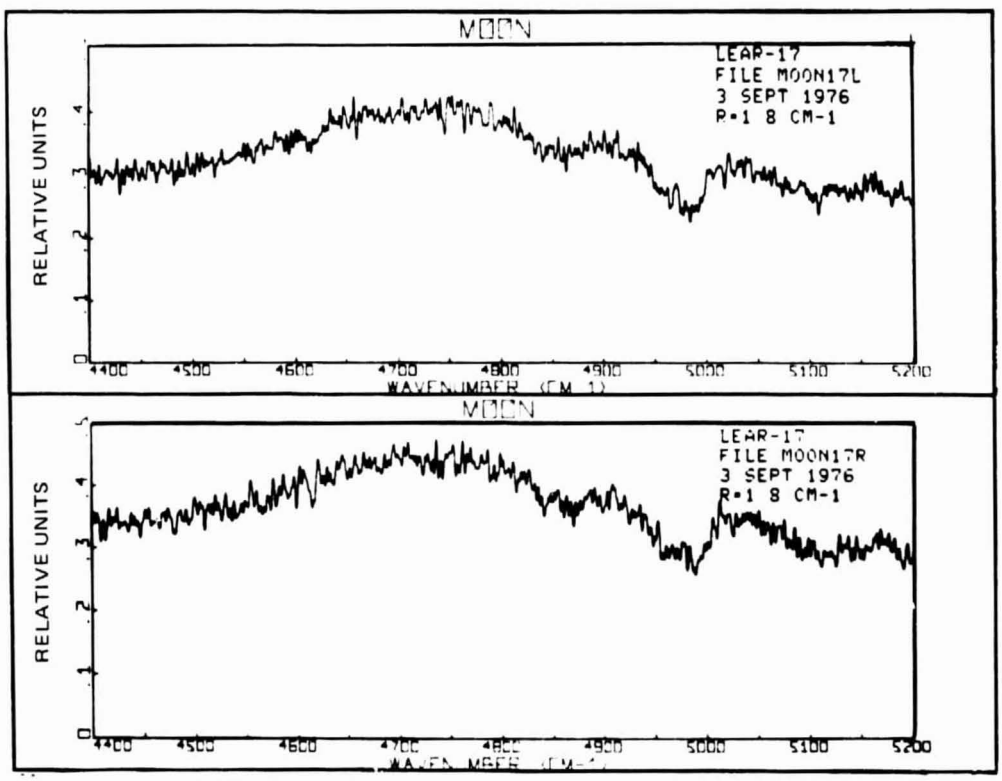

Fig. 47g,h Spectrum of Moon on 3 Sept 1976 in 4400-6000 cm-1 region at 1.8 cm-1 resolution. Upper curve (g) is L aperture and lower curve (h) is R aperture.

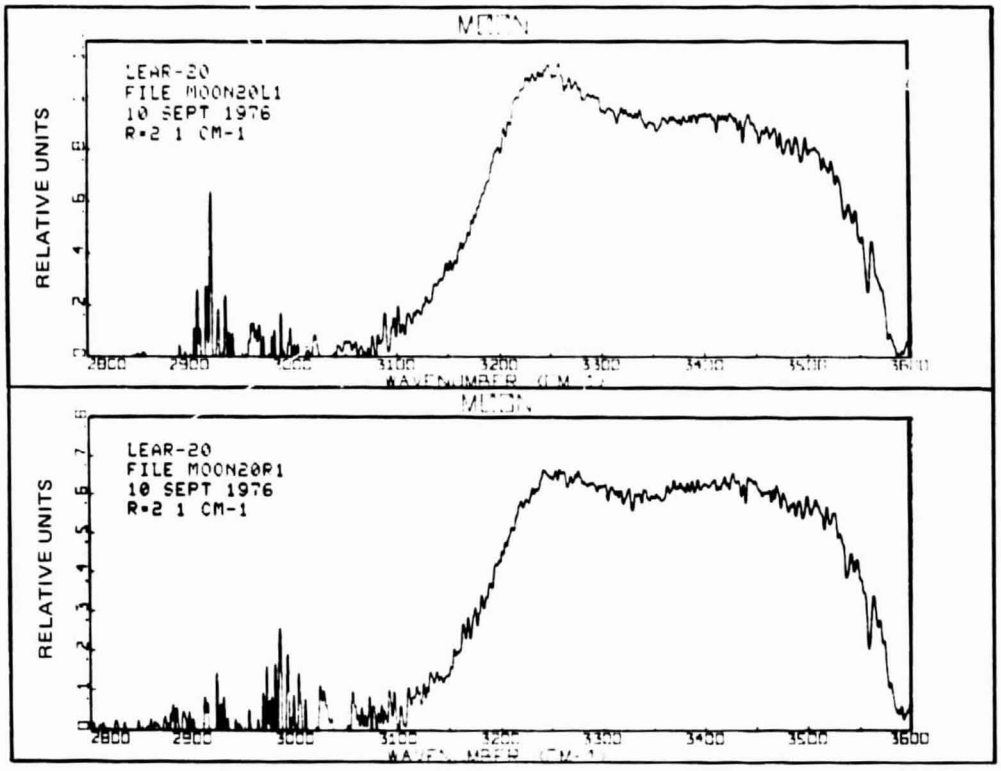

Fig. 48a,b Spectrum of Moon on 10 Sept 1976 in 2800-3600 cm-1 region at 2.1 cm-1 resolution. Upper curve (a) is L aperture and lower curve (b) is R aperture.

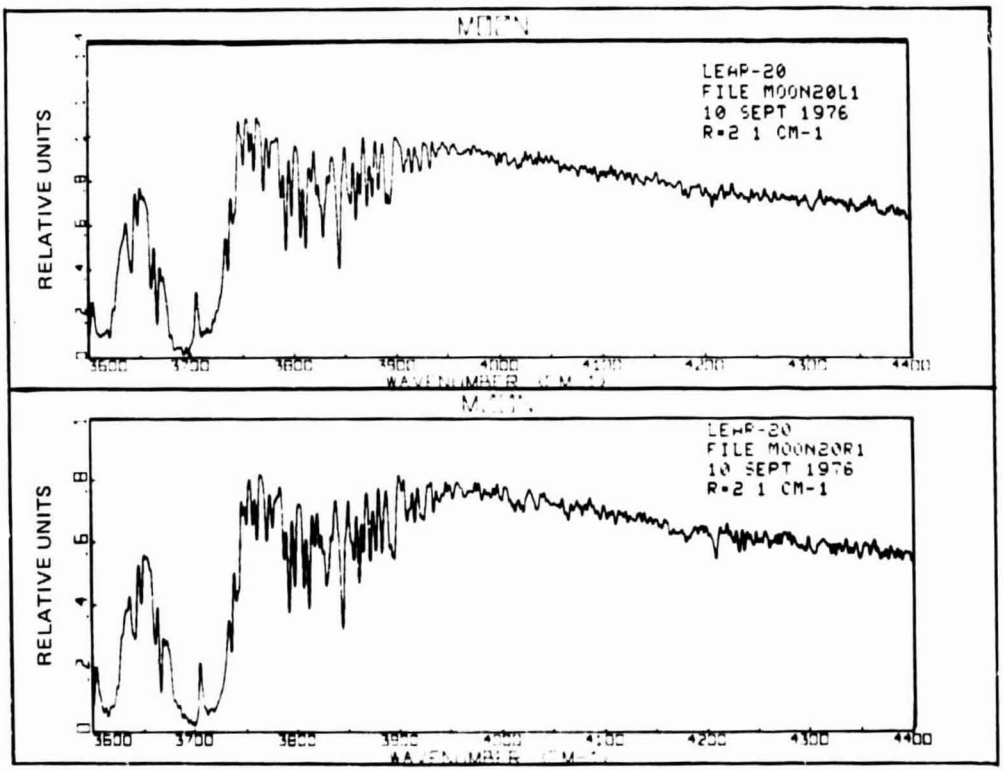

Fig. 48c,d Spectrum of Moon on 10 Sept 1976 in 3600-4400 cm-1 region at 2.1 cm-1 resolution. Upper curve (c) is L aperture and lower curve (d) is R aperture.

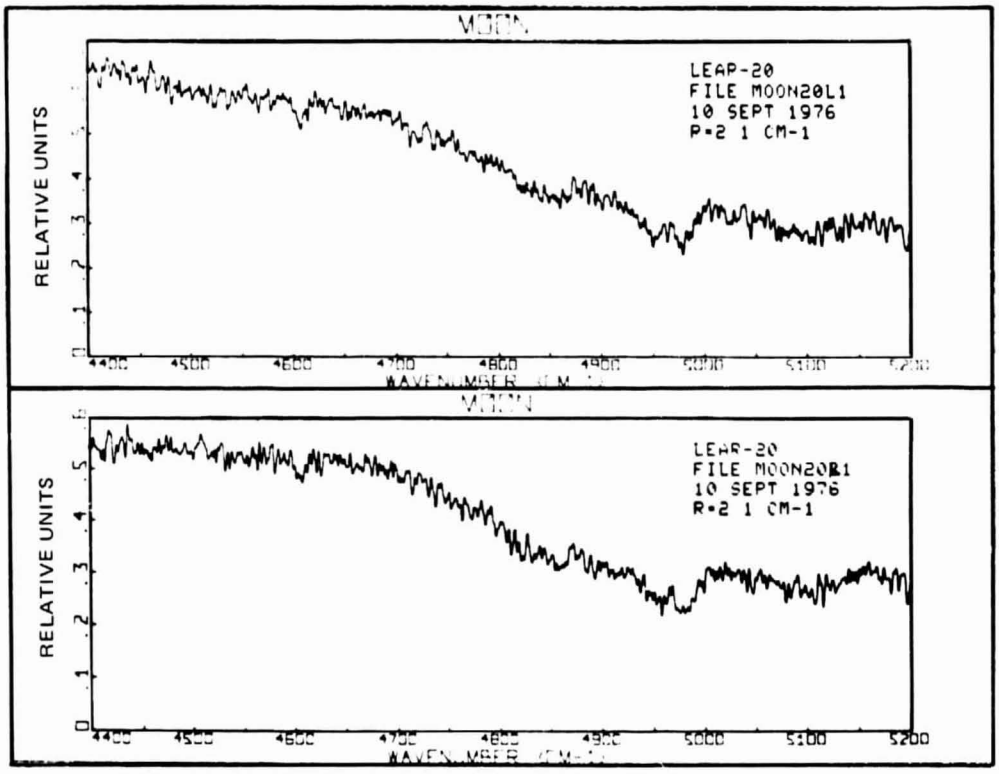

Fig. 48e,f Spectrum of Moon on 10 Sept 1976 in 4400-5200 cm-1 region at 2.1 cm-1 resolution. Upper curve (e) is L aperture and lower curve (f) is R aperture.

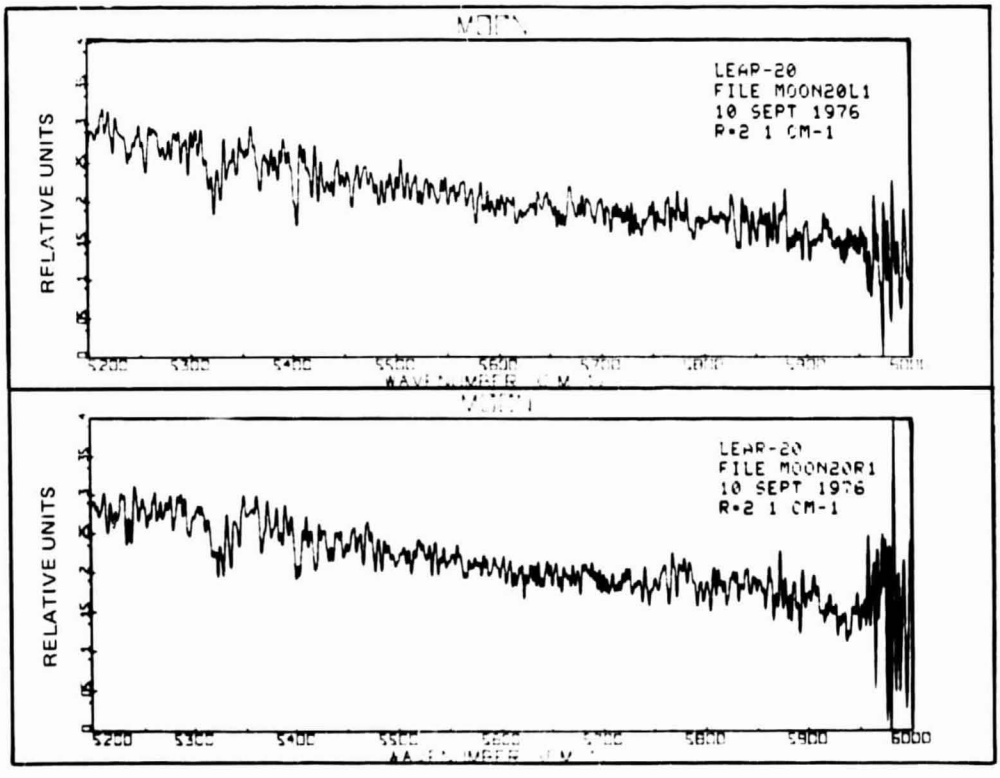

Fig. 48g,h Spectrum of Moon on 10 Sept 1976 in 5200-6000 cm-1 region at 2.1 cm-1 resolution. Upper curve (g) is L aperture and lower curve (h) is R aperture.

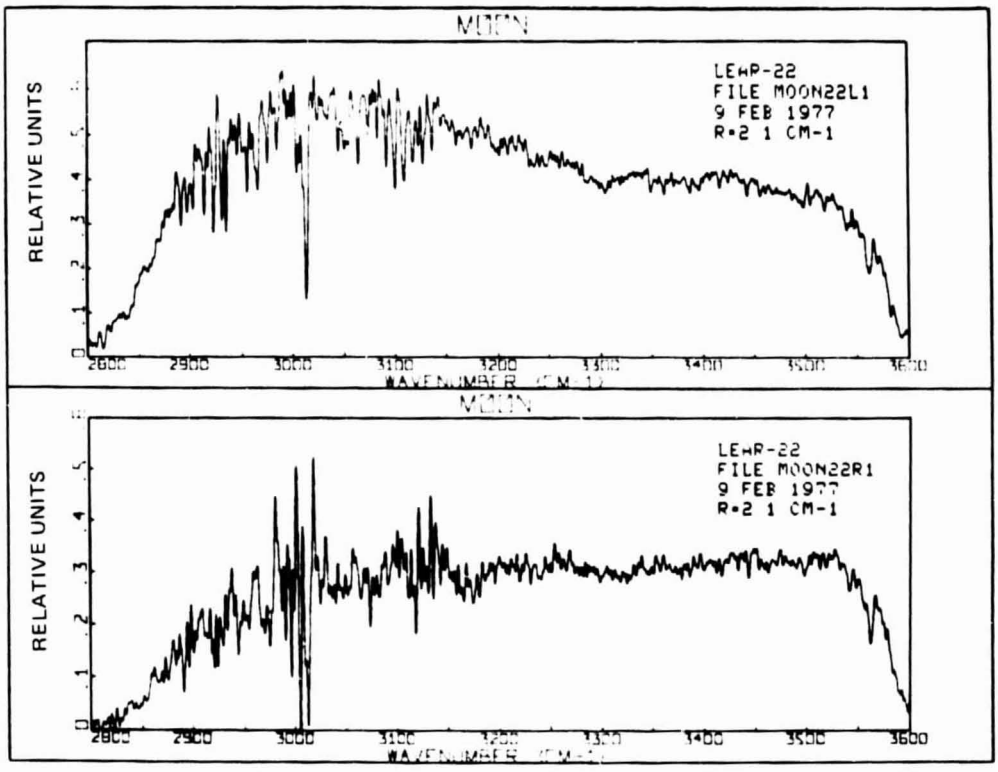

Fig. 49a,b Spectrum of Moon on 9 Feb 1977 in 2800-3600 cm-1 region at 2.1 cm-1 resolution. Upper (a) is L aperture and lower curve (b) is R aperture.

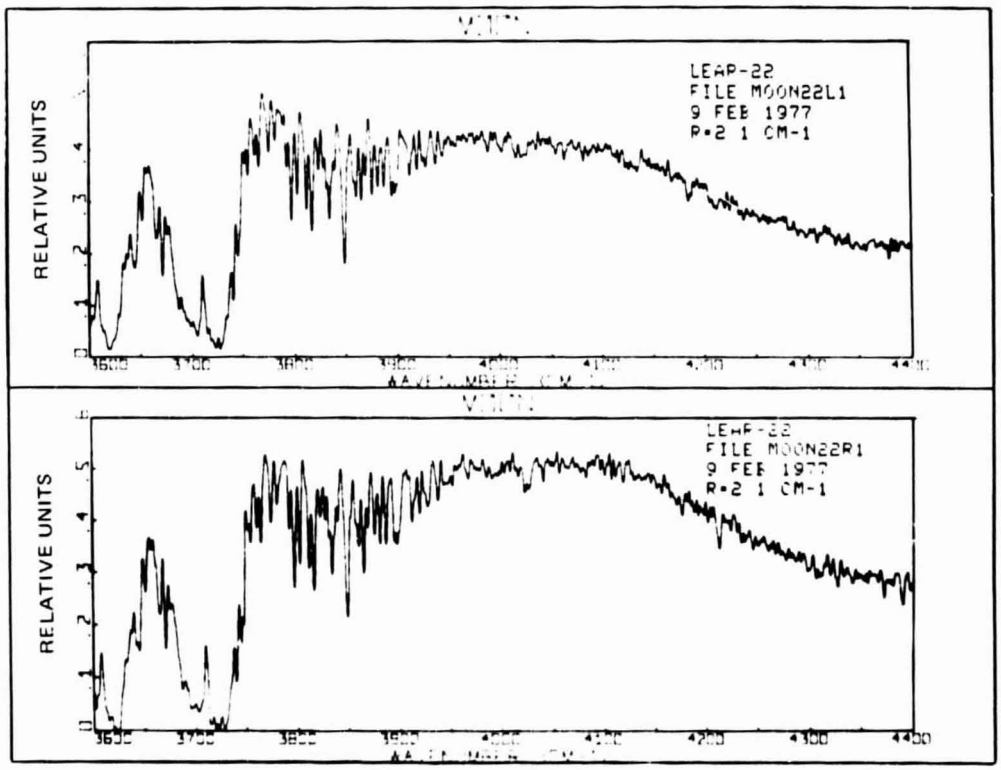

Fig. 49c,d Spectrum of Moon on 9 Feb 1977 in 3600-4400 cm-1 region at 2.1 cm-1 resolution. Upper curve (c) is L aperture and lower curve (d) is R aperture.

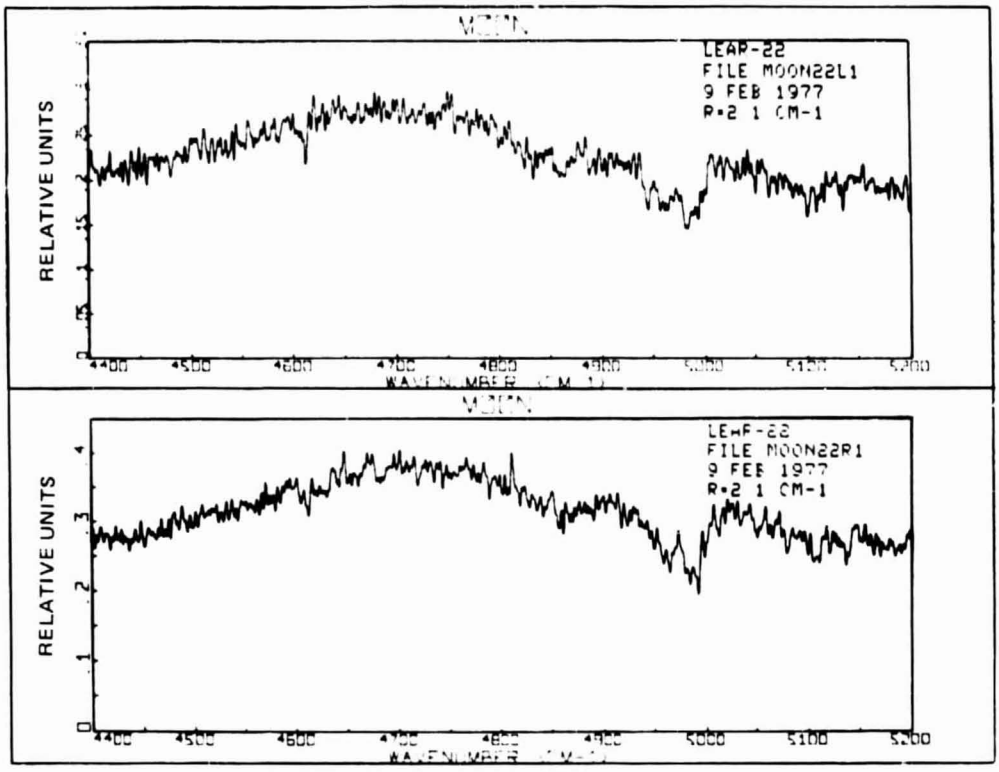

Fig. 49e,f Spectrum of Moon on 9 Feb 1977 in 4400-5200 cm-1 region at 2.1 cm-1 resolution. Upper curve (e) is L aperture and lower curve (f) is R aperture.

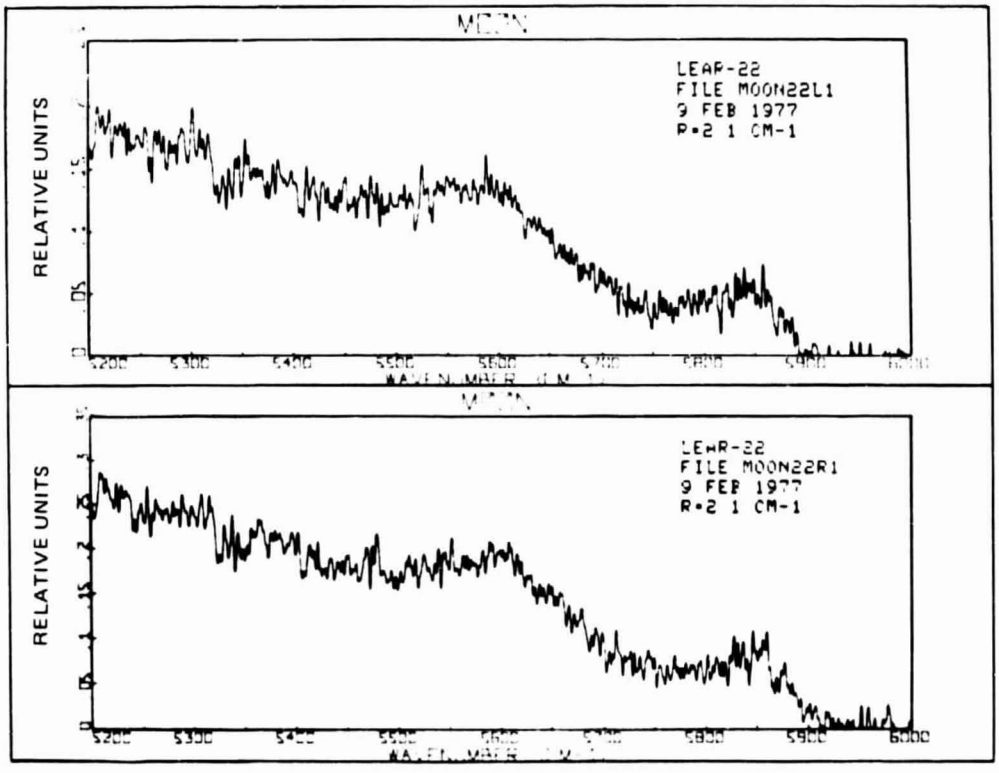

Fig. 49g,h Spectrum of Moon on 9 Feb 1977 in 5200-6000 cm-1 region at 2.1 cm-1 resolution. Upper curve (g) is L aperture and lower curve (h) is R aperture.

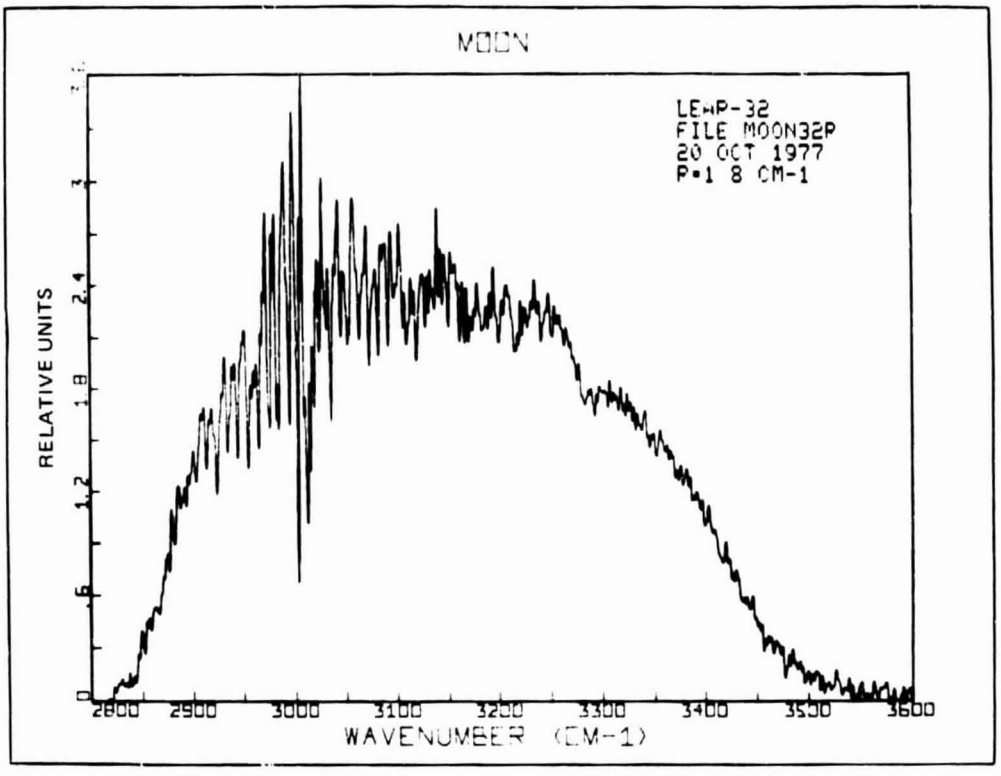

Fig. 50a Spectrum of Moon on 20 Oct 1977 in 2800-3600 cm-1 region at 1.8 cm-1 resolution

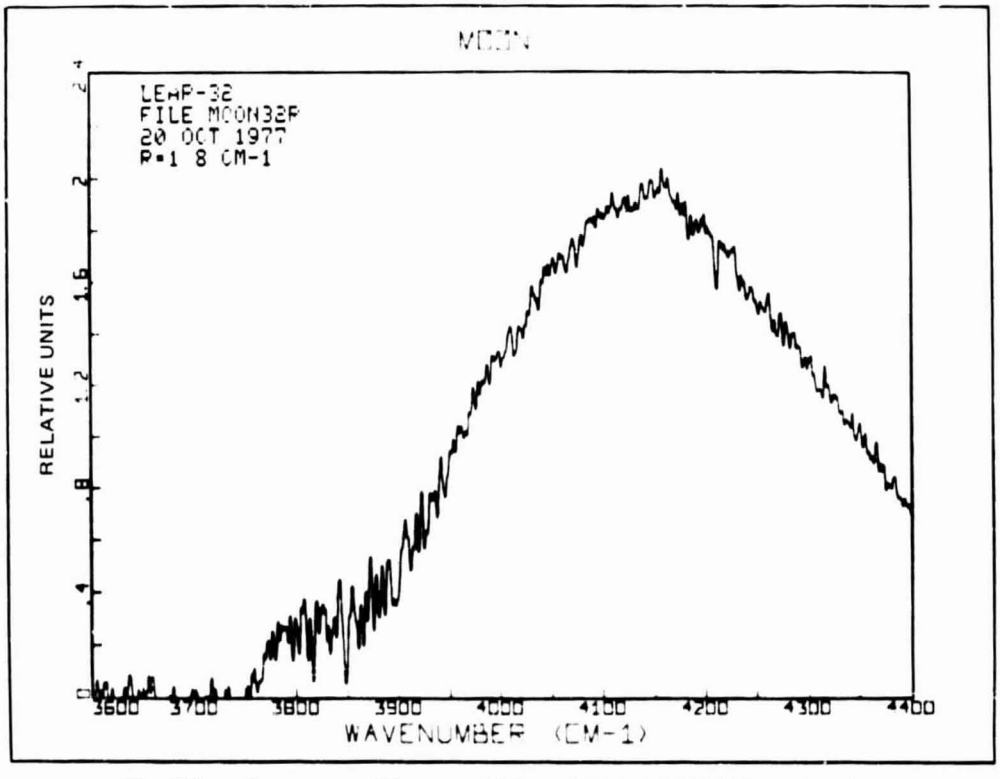

Fig. 50b Spectrum of Moon on 20 Oct 1977 in 3600-4400 cm-1 region at 1.8 cm-1 resolution

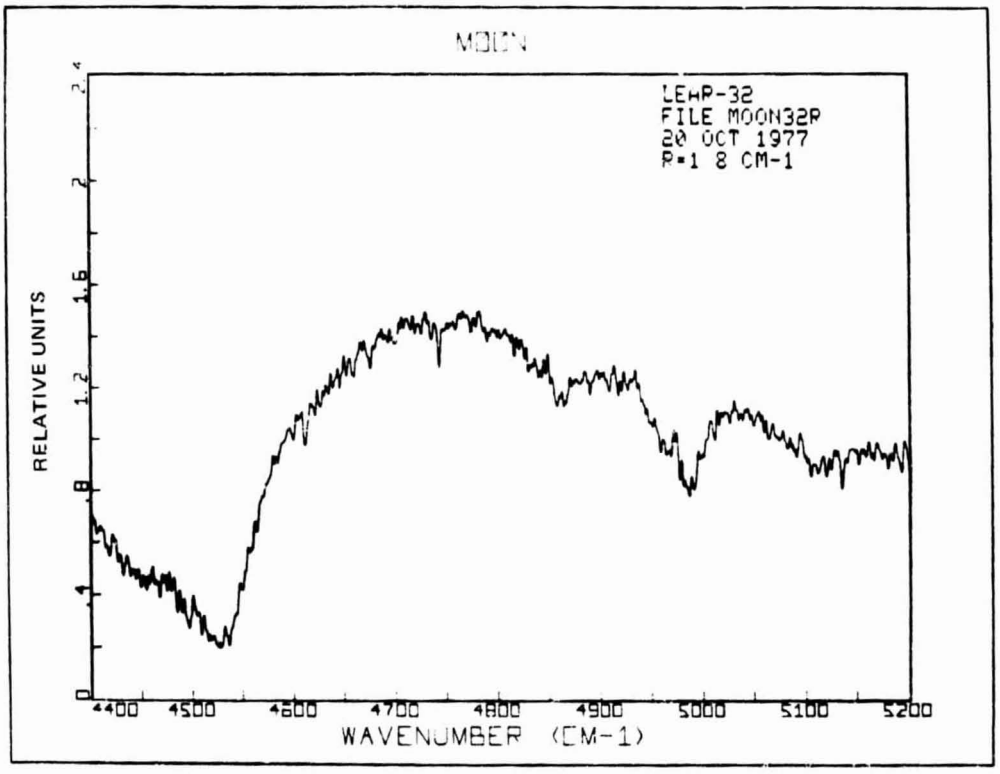

Fig. 50c Spectrum of Moon on 20 Oct 1977 in 4400-5200 cm-1 region at 1.8 cm-1 resolution.

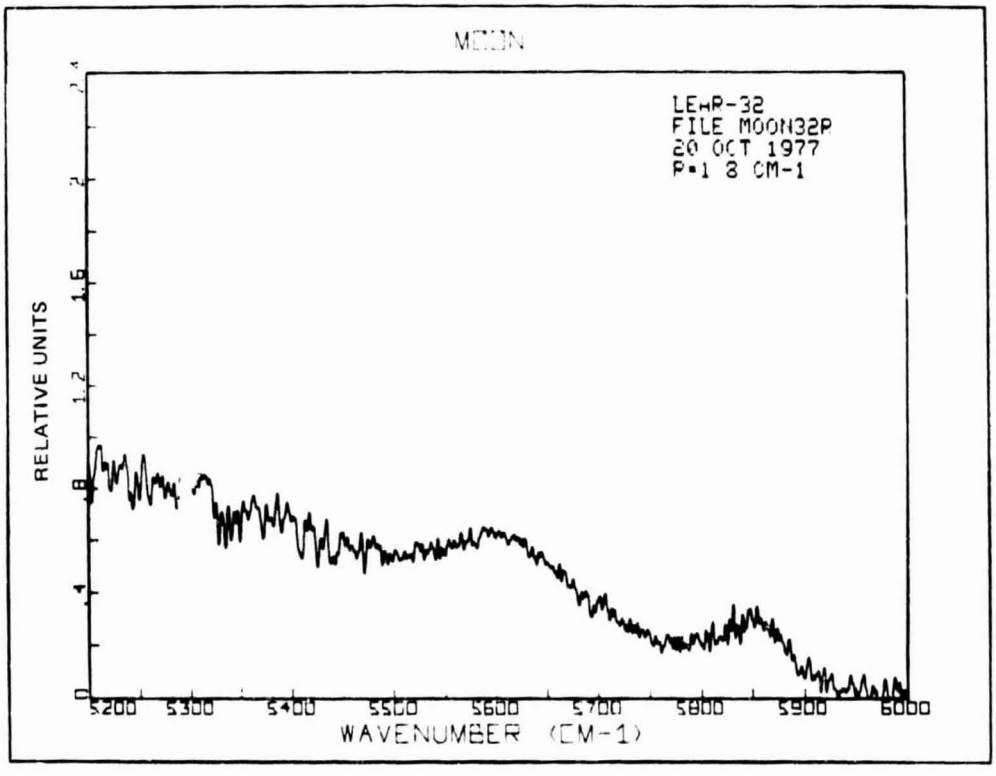

Fig. 50d Spectrum of Moon on 20 Oct 1977 in 5200-6000 cm-1 region at 1.8 cm-1 resolution.

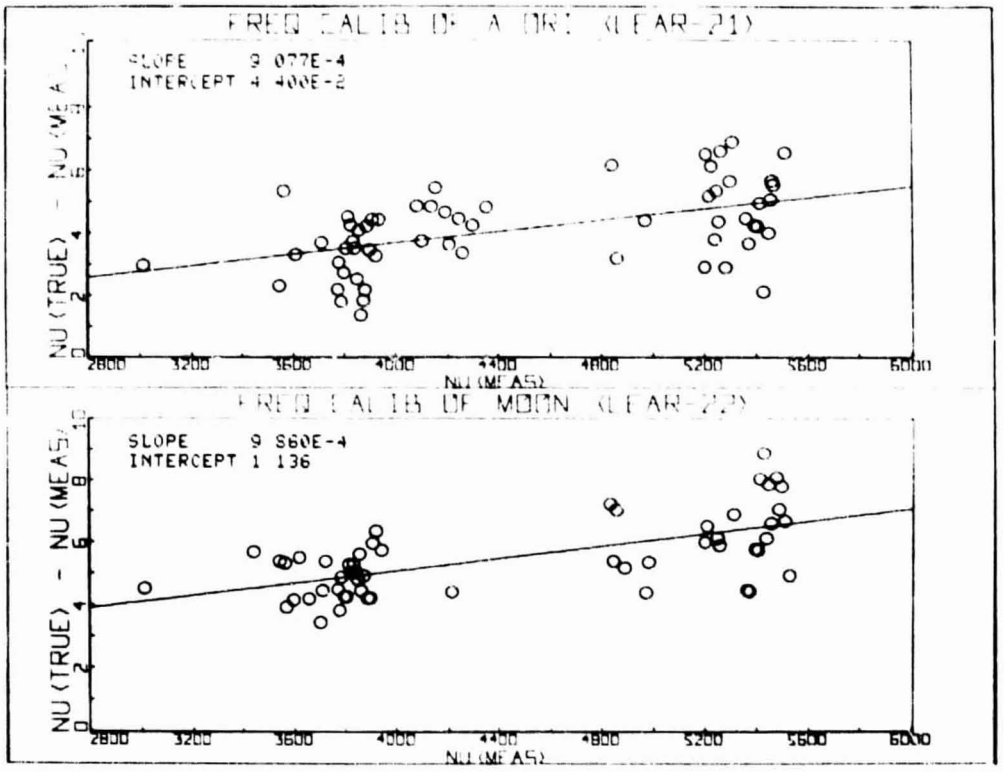

Fig. 51 Frequency Calibration of Alpha Ori and Moon. A Least Squares Straight Line Has Been Fit to the Data Which is Used to Correct the Measured Frequencies in the Spectra ν (Meas) to Laboratory Frequencies ν (True).

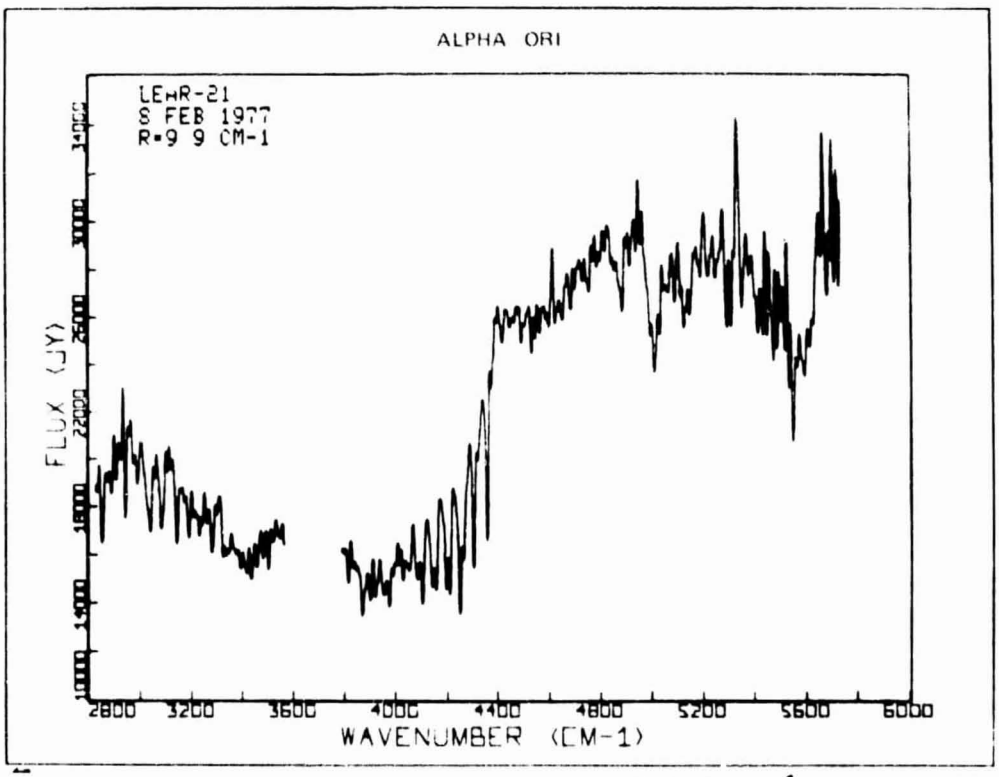

Fig. 52 Spectrum of Alpha Ori on 8 Feb 1977 in 2800-6000 cm^{-1} Region at 9.9 cm^{-1} Resolution in Janskys (10^{-26} $W/m^2/Hz$). The CO Lines at 4000-4360 cm^{-1} Are Shown.

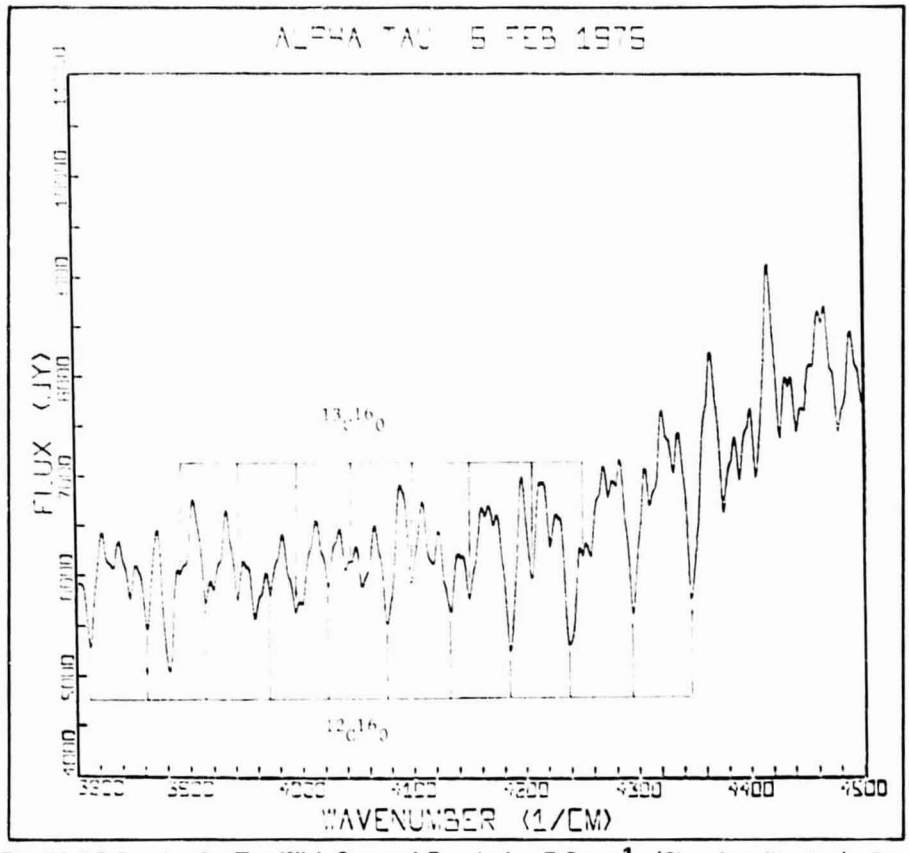

Fig. 53 CO Bands of α Tau With Spectral Resolution 7.3 cm^{-1} (Sinc Apodization). The First Overtone Bands of ^{12}C ^{16}O And ^{13}C ^{16}O Are Shown

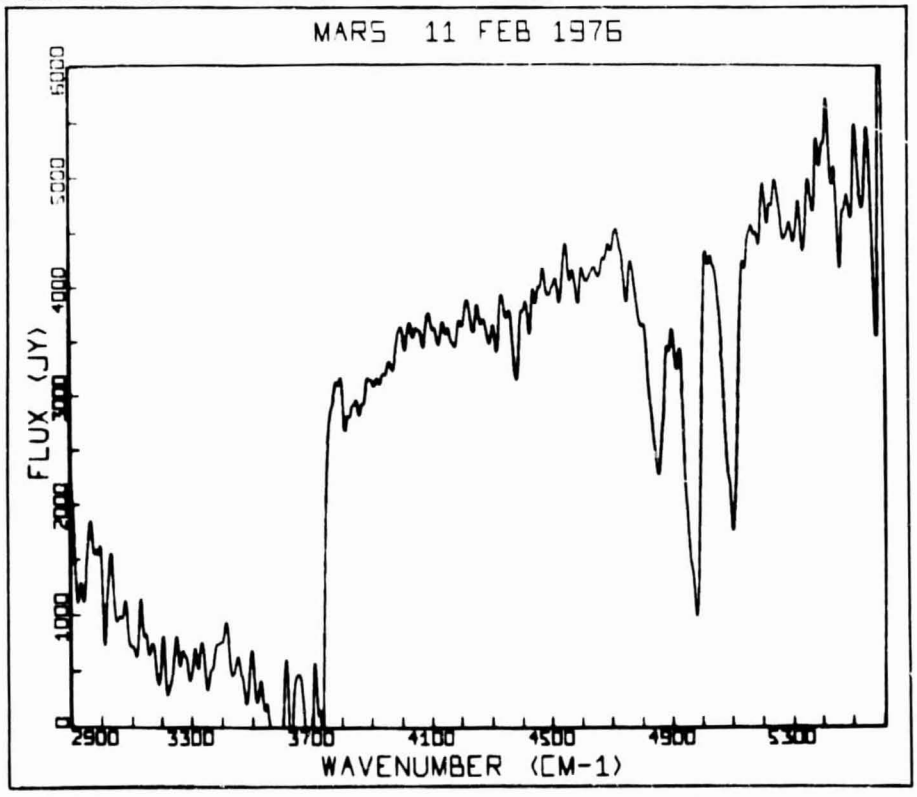

Fig. 54 Spectrum Of Mars, 11 Feb 1976 With Spectral Resolution 1 3.3cm^{-1}. CO_2 Bands At 4800-5100 cm^{-1}, H_2O Bands At 3800-4000 cm^{-1}, And Water Of Hydration Bands 2900-3750 cm^{-1} Are Shown

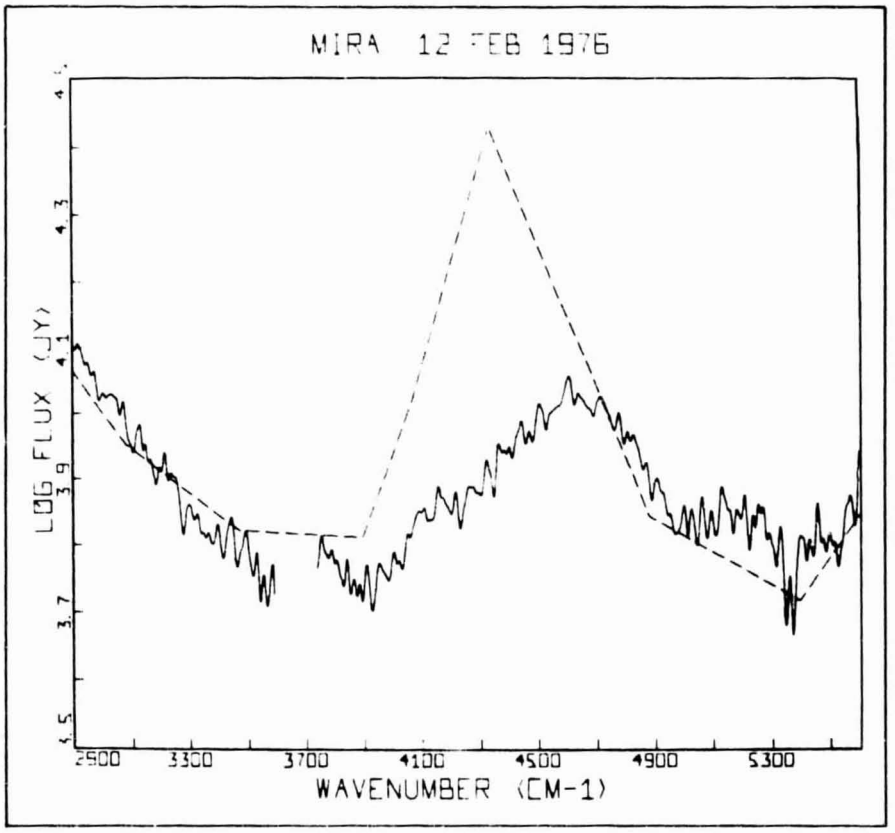

Fig. 55 Mira (o Cet), 12 Feb. 1976 With Spectral Resolution 13.3 cm^{-1} (Solid Line). A Theoretical Model Of Auman, 1969 (Dashed Curve) Has Been Fit To Observed Data And Shows Good Agreement With Hot Water Bands Centered at 3700 and 5300 cm^{-1}, But The Model Predicts Too Much Flux In Region Of 3900-4500 cm^{-1}. This is To Be expected as No CO Band Absorption Was Included In Model

APPENDIX

BASIC programs, PHASE, and HFFT used in the data reduction procedure are listed. Some comments are included.

```
PHASE
  10 REM N1 IS NO. OF POINTS IN INTERFEROGRAM (MAX = 7100)
  20 REM N IS NO. OF POINTS USED TO GENERATE PHASES
  30 REM N9 IS POSITION OF SYMMETRY POINT OF INTERFEROGRAM
  40 REM K9 IS NO. OF PHASE CORR. DESIRED
  50 REM N7 IS LENGTH OF CONVOLVING FCTN.
  60 DIM X[7100],I[26],S[52],R[52],Q[50]
  70 DIM A$[8],B$[8]
  80 N=50
  90 N7=51
 100 K9=3
 110 FILES *,*
 120 INPUT "INPUT INTERFEROGRAM FILE NAME  ",A$
 130 PRINT
 140 ASSIGN A$,1,S0
 150 IF S0=0 THEN 180
 160 PRINT "SOMETHING WRONG WITH FILE NAME "
 170 STOP
 180 INPUT "INPUT NO. OF POINTS IN INTERFEROGRAM ",N1
 190 PRINT
 200 INPUT "OUTPUT PHASE CORRECTED FILE NAME (NO NEED TO CREATE)  ",B$
 210 PRINT
 220 ASSIGN B$,2,R0
 230 IF R0=0 THEN 270
 240 IF R0<>3 THEN 160
 250 CREATE R1,3%,S%,256
 260 IF R1=0 THEN 220
 270 INPUT "INPUT INTERFEROGRAM SYMMETRY POINT ",N9
 280 PRINT
 290 ON END #1 THEN 310
 300 MAT READ #1;X
 310 K=K9+1
 320 N9=N1-N7+1
 330 N2=(N/2)+1
 340 N3=N/2
 350 N5=9
 360 FOR K1=1 TO K9
 370   FOR I=1 TO N
 380     S[I]=(6.28318/N)*(I-1)
 390   NEXT I
 400   N8=N9-1
 410   FOR I=1 TO N3
 420     Q[I]=X[N8+I]
 430     Q[N+1-I]=X[N9-I]
 440   NEXT I
 450   PRINT Q[1]
 460   PRINT
 470   FOR J=N5 TO N2
 480     R[J]=I[J]=0
 490     FOR K=1 TO N
 500       B=(J-1)*S[K]
 510       R[J]=R[J]+Q[K]*COS(B)
 520       I[J]=I[J]-Q[K]*SIN(B)
 530     NEXT K
 540   NEXT J
 550   F=7901.14*2/N
 560   FOR L=N5+1 TO N2-1
 570     D=.54*R[L]+.23*(R[L-1]+R[L+1])
 590     E=.54*I[L]+.23*(I[L-1]+I[L+1])
 590     P=(ATN(E/D))*57.2958
```

```
600     IF D<0 THEN 620
610     GOTO 630
620     P=P+180
630     IF P>180 THEN 650
640     GOTO 660
650     P=P-360
660     Q[L]=P
670   NEXT L
680   Q[N2]=0
690   PRINT "          INPUT PHASES"
700   PRINT
710   Q5=0
720   FOR I=N5+1 TO N2
730     G=F*(I-1)
740     PRINT I,G,Q[I]
750     Q5=Q5+ABS(Q[I])
760     Q[I]=Q[I]/57.2958
770     S[2*I-1]=COS(Q[I])
780     S[2*I]=SIN(Q[I])
790   NEXT I
800   PRINT
810   PRINT "AVERAGE ABSOLUTE DIFFERENCE = ";Q5/(N2-N5)
820   PRINT
830   A1=6.28318/N
840   FOR J=1 TO N7
850     M1=J-((N7-1)/2)-1
860     M2=M1*3.14159/((N7-1)/2)
870     S1=S2=0
880     FOR I=N5+1 TO N2
890       A2=A1*(I-1)*M1
900       S1=S1+S[2*I-1]*COS(A2)
910       S2=S2+S[2*I]*SIN(A2)
920     NEXT I
930     Q1=S1-S2
940     R[J]=Q1*(.54+.46*COS(M2))
950     R[J]=R[J]/N2
960   NEXT J
970   PRINT
980   PRINT "          CONVOLVED INTERFEROGRAM"
990   PRINT
000   FOR J=1 TO M9
010     A=0
020     FOR I=1 TO N7
030       A=A+R[I]*X[I+J-1]
040     NEXT I
050     X[J]=A
060     IF K1=K9 THEN 1080
070     GOTO 1090
080     PRINT #2,X[J]
090   NEXT J
100   PRINT
110   PRINT "  DIFFERENCE (LEFT - RIGHT)"
120   PRINT
130   M8=N9-((N7-1)/2)
140   FOR J=1 TO 11
150     K=J-1
160     L=X[M8-K]
170     R=X[M8+K]
180     C=L-R
190     Q[J]=ABS(C)
```

```
1200      PRINT K,L,R,C
1210    NEXT J
1220    D=0
1230    FOR J=1 TO 11
1240      D=D+Q[J]
1250    NEXT J
1260    D=D/10
1270    PRINT
1280    PRINT "AVERAGE ABSOLUTE DIFFERENCE = ";D
1290    PRINT
1300    PRINT
1310    N9=M8
1320    M9=M9-N7+1
1330  NEXT K1
1340  PRINT "POSITION OF SYMMETRY POINT = ";M8
1350  PRINT
1360  PRINT "CPU SECONDS = ";CPU(0)
```

```
HFFT
  10 REM FFT DOES COSINE TRANSFORM ONLY
  20 REM USING HAMMING APODIZATION FCTN
  30 REM N7 IS TOTAL NO. OF DATA PTS FROM INTERF SYMM PT
  40 REM N9 IS INTERFEROGRAM SYMMETRY POINT
  50 REM G DETERMINES NO. OF PTS TO BE TRANSFORMED (N = 2^G)
  60 REM W1 AND W1 ARE WAVENUMBER LIMITS DESIRED (MIN,MAX = 2800,6000)
  70 DIM X[4100],Y[4100],A[4,60]
  80 FILES *,*
  90 DIM A$[8],B$[8]
 100 INPUT "INPUT PHASE CORR. INTERFEROGRAM FILE NAME  ",A$
 110 PRINT
 120 ASSIGN A$,1,S0
 130 IF S0=0 THEN 150
 140 IF S0<>3 THEN 100
 150 INPUT "INPUT TOTAL NO. OF DATA PTS FROM INTERF SYMM PT  ",N7
 160 PRINT
 170 INPUT "INPUT INTERF SYMMETRY PT  ",N9
 180 PRINT
 190 INPUT "OUTPUT SPECTRUM FILE NAME (NO NEED TO CREATE)  ",B$
 200 PRINT
 210 ASSIGN B$,2,R0
 220 IF R0=0 THEN 270
 230 IF R0<>3 THEN 190
 240 CREATE R1,B$,130,256
 250 IF R1=0 THEN 210
 260 STOP
 270 INPUT "INPUT VALUE OF G (NO. OF PTS TO BE TRANSF = 2^G)  ",G
 280 PRINT
 290 N=2**G
 300 R6=1.815*7901.14/N7
 310 INPUT "INPUT WAVENUMBER LIMITS (W1,W2) ",W1,W2
 320 PRINT
 330 F=7901.14/N
 340 J3=INT((W1/F)+1)
 350 J4=INT((W2/F)+1)
 360 MAT X=ZER
 370 MAT Y=ZER
 380 FOR I=1 TO N9-1
 390   READ #1;A
 400 NEXT I
 410 FOR I=1 TO N7/2
 420   READ #1;X[I+2],Y[I+2]
 430 NEXT I
 440 READ #1;X[N/2+3]
 450 Y[N/2+3]=0
 460 S1=S2=0
 470 FOR I=1 TO N/2+1
 480   S1=S1+X[I+2]
 490   S2=S2+Y[I+2]
 500 NEXT I
 510 S1=2*S1-X[3]-X[N/2+3]
 520 S2=2*S2
 530 X[1]=X[3]
 540 Y[1]=0
 550 FOR I=2 TO N/2+1
 560   X[I]=X[I+2]
 570   Y[I]=(Y[I+2]-Y[I+1])/2
 580 NEXT I
 590 Y[N/2+1]=0
```

```
600 T=2*3.14159/N
610 N2=N/2+2
620 N3=N/2+3
630 FOR J=1 TO N/4+1
640   J1=J
650   FOR L=1 TO 2
660     T1=T*(J-1)
670     K=N/2+2-J
680     L1=N/2+1+L
690     S=SIN(T1)
700     C=COS(T1)
710     X1=X[J]+X[K]
720     X2=X[J]-X[K]
730     Y1=Y[J]+Y[K]
740     Y2=Y[J]-Y[K]
750     X[L1]=(X1+X2*S-Y1*C)/2
760     Y[L1]=(Y2+Y1*S+X2*C)/2
770     J=K
780   NEXT L
790   J=J1
800   K=N2-J
810   X[J]=X[N2]
820   Y[J]=Y[N2]
830   X[K]=X[N3]
840   Y[K]=Y[N3]
850 NEXT J
860 G=G-1
870 LET N=2**G
880 LET P=8*ATN(1)/N
890 FOR I=1 TO N
900   LET X[I]=X[I]/N
910   LET Y[I]=Y[I]/N
920 NEXT I
930 FOR L=0 TO G-1
940   LET G1=2**(G-L-1)
950   LET M=0
960   FOR I=1 TO 2**L
970     LET K1=INT(M/G1)
980     GOSUB 1690
990     LET Y1=COS(P*K2)
1000    LET Y2=-SIN(P*K2)
1010    FOR J=1 TO G1
1020      M1=M+G1+1
1030      M2=M+1
1040      Y3=X[M1]*Y1-Y[M1]*Y2
1050      Y4=X[M1]*Y2+Y[M1]*Y1
1060      X[M1]=X[M2]-Y3
1070      Y[M1]=Y[M2]-Y4
1080      X[M2]=X[M2]+Y3
1090      Y[M2]=Y[M2]+Y4
1100      LET M=M+1
1110    NEXT J
1120    LET M=M+G1
1130  NEXT I
1140 NEXT L
1150 FOR I=0 TO N-1
1160   LET K1=I
1170   GOSUB 1690
1180   IF K2>=I THEN 1270
1190   I1=I+1
```

```
1200    K4=K2+1
1210    K3=X[I1]
1220    X[I1]=X[K4]
1230    X[K4]=K3
1240    K3=Y[I1]
1250    Y[I1]=Y[K4]
1260    Y[K4]=K3
1270  NEXT I
1280  X[1]=(S1+S2)/(4*N)
1290  T1=3.14159/(2*N)
1300  N1=N+1
1310  N2=N+2
1320  FOR J=1 TO N/2
1330    J2=J
1340    FOR L=1 TO 2
1350      J1=J+2-L
1360      K=N1-J
1370      K1=N2-J1
1380      L1=N+L
1390      A1=X[J1]+X[K1]
1400      A=Y[J]+Y[K]
1410      B1=(X[J1]-X[K1])/SIN(T1*(2*J1-2))
1420      B=(Y[J]-Y[K])/SIN(T1*(2*J-1))
1430      X[L1]=(A1-B1)/4
1440      Y[L1]=(A-B)/4
1450      J=K
1460    NEXT L
1470    J=J2
1480    K=N+1-J
1490    X[J+1]=X[N1]
1500    Y[J]=Y[N1]
1510    X[K]=X[N2]
1520    Y[K]=Y[N2]
1530  NEXT J
1540  M1=11
1550  I1=INT(J3/2)+1
1560  I2=INT(J4/2)+1
1570  L1=I2-I1+1+2*M1
1580  FOR I=1 TO L1
1590    X[4101-I]=X[I2+1-I+M1]
1600  NEXT I
1610  FOR I=I1-M1 TO I2+M1
1620    K=2*(I-I1+M1)+1
1630    X[K]=X[4100-I2+I-M1]
1640    X[K+1]=Y[I]
1650  NEXT I
1660  K=1
1670  J5=2*(I1-M1)-1
1680  GOTO 1770
1690  LET K2=0
1700  FOR K=1 TO G
1710    LET K3=INT(K1/2)
1720    LET K2=2*(K2-K3)+K1
1730    LET K1=K3
1740  NEXT K
1750  RETURN
1760  REM FOLLOWING INTERPOLATES AND SMOOTHS FOR COSINE TRANSFORM ONLY
1770  N8=20
1780  M=2*N8
1790  FOR K=1 TO 4
```

```
1800    FOR I=1 TO M
1810       A=3.14159*(N[ I+.25)
1820      C=(3.14159/A6)**2
1830      A[K,I]=(SIN(A6)/A6)*(.5+.46/(1-C))
1840    NEXT I
1850  NEXT K
1860  J3=J3-J5+1
1870  J4=J4-J5+1
1880  FOR J=J3 TO J4
1890    Y[1]=.54*X[ ]+.23*(X[J-1]+X[J+1])
1900    Y[2]=Y[3]=Y[ ]=Y[5]=0
1910    FOR K=1 TO 4
1920      FOR I=1 TO M
1930        Y[ +1]=Y[K+1]+X[J+[ -K]*A[K,I]
1940      NEXT I
1950    NEXT K
1960    FOR I=1 TO 5
1970      PRINT #2,Y[I]
1980    NEXT I
1990  NEXT J
2000  PRINT "CALC. WAVENUMBER RANGE ";F*(J3+J5-2);"TO";F*(J4+J5-6/5)
2010  PRINT
2020  PRINT "WAVENUMBER INTERVAL ";F/5
2030  PRINT
2040  PRINT "RESOLU TION = ";R6;"CM-1"
2050  PRINT
2060  PRINT "CPU SECONDS = ";CPU(0)
```